Physical, Hydraulic, and Transport Properties of Sediments and Engineered Materials Associated with Hanford Immobilized Low-Activity Waste

ML Rockhold
ZF Zhang
PD Meyer
JN Thomle

February 2015

Pacific Northwest
NATIONAL LABORATORY

Proudly Operated by **Battelle** *Since 1965*

DISCLAIMER

This report was prepared as an account of work sponsored by an agency of the United States Government. Neither the United States Government nor any agency thereof, nor Battelle Memorial Institute, nor any of their employees, makes **any warranty, express or implied, or assumes any legal liability or responsibility for the accuracy, completeness, or usefulness of any information, apparatus, product, or process disclosed, or represents that its use would not infringe privately owned rights**. Reference herein to any specific commercial product, process, or service by trade name, trademark, manufacturer, or otherwise does not necessarily constitute or imply its endorsement, recommendation, or favoring by the United States Government or any agency thereof, or Battelle Memorial Institute. The views and opinions of authors expressed herein do not necessarily state or reflect those of the United States Government or any agency thereof.

PACIFIC NORTHWEST NATIONAL LABORATORY
operated by
BATTELLE
for the
UNITED STATES DEPARTMENT OF ENERGY
under Contract DE-AC05-76RL01830

Printed in the United States of America

**Available to DOE and DOE contractors from the
Office of Scientific and Technical Information,
P.O. Box 62, Oak Ridge, TN 37831-0062;
ph: (865) 576-8401
fax: (865) 576-5728
email: reports@adonis.osti.gov**

**Available to the public from the National Technical Information Service,
U.S. Department of Commerce, 5285 Port Royal Rd., Springfield, VA 22161
ph: (800) 553-6847
fax: (703) 605-6900
email: orders@ntis.fedworld.gov
online ordering: http://www.ntis.gov/ordering.htm**

This document was printed on recycled paper.
(9/2003)

Physical, Hydraulic, and Transport Properties of Sediments and Engineered Materials Associated with Hanford Immobilized Low-Activity Waste

ML Rockhold
ZF Zhang
PD Meyer
JN Thomle

February 2015

Pacific Northwest National Laboratory
Richland, Washington 99352

Executive Summary

Current plans for treatment and disposal of immobilized low-activity waste (ILAW) from Hanford's underground waste storage tanks include vitrification and storage of the glass waste form in a near-surface disposal facility. This Integrated Disposal Facility (IDF) is located in the 200 East Area of the Hanford Central Plateau. Performance assessment (PA) of the IDF requires numerical modeling of subsurface flow and reactive transport processes over very long periods (thousands of years). The models used to predict facility performance require parameters describing various physical, hydraulic, and transport properties. This report provides updated estimates of physical, hydraulic, and transport properties and parameters for both near- and far-field materials, intended for use in future IDF PA modeling efforts.

Previous work on physical and hydraulic property characterization for earlier IDF PA analyses is reviewed and summarized. For near-field materials, portions of this document and parameter estimates are taken from an earlier data package. For far-field materials, a critical review is provided of methodologies used in previous data packages. Alternative methods are described and associated parameters are provided.

For far-field materials, consisting of both sand- and gravel-dominated facies underlying the IDF, a particular model has been used in previous PA modeling efforts to represent the saturation-dependent anisotropy of unsaturated hydraulic conductivity. We recommend that this model be replaced with a more recent and general tensorial pore-connectivity-tortuosity (TCT) model for saturation-dependent anisotropy. Simulation results from both the TCT and the earlier anisotropy model have been compared with observed data from a controlled vadose zone field injection experiment performed just south of the 200 East Area. The TCT model was shown to predict observed flow behavior at this site as well as or better than the model used in previous PA efforts, and with many fewer added model parameters (one versus eight). Recommended parameter estimates for the TCT model are presented.

Previous estimates of dispersivities for vadose zone sediments were based on stochastic theory developed for saturated aquifer materials. An extensive literature review is presented that suggests these estimates may not be appropriate for unsaturated conditions. An alternative approach based on more fundamental physical property information is described and updated parameter estimates are presented.

Acknowledgments

Acronyms and Abbreviations

ADE	advection-dispersion equation
ALARA	as low as reasonably achievable
CDE	convection-dispersion equation
CDN	composite drainage network
DOE	U.S. Department of Energy
EHM	equivalent homogeneous medium
GCL	geosynthetic clay liner
HA	high anisotropy
HDPE	high density polyethylene
HLW	high-level waste
IA	intermediate anisotropy
IDF	Integrated Disposal Facility
ILAW	immobilized low-activity waste
ISO	isotropic
LA	low anisotropy
LAW	low-activity waste
LLW	low-level waste
MIM	mobile-immobile
MLLW	mixed low-level waste
PA	performance assessment
PA-TCT	power-averaging and tensorial connectivity-tortuosity
PFBA	pentafluorobenzoate
PNNL	Pacific Northwest National Laboratory
PSD	particle size distribution
QA	quality assurance
R&D	research and development
RCRA	Resource Conservation and Recovery Act
STOMP	Subsurface Transport Over Multiple Phases
TCT	tensorial pore-connectivity-tortuosity
USGAO	U.S. General Accounting Office (now U.S. Government Accountability Office)
VHT	vapor hydration test
WRPS	Washington River Protection Solutions
WTP	Hanford Tank Waste Treatment and Immobilization Plant
WWFTP	WRPS Waste Form Testing Program

Contents

Figures

Tables

1.0   Introduction

The Hanford Site was established in 1944 as a U.S. Government nuclear materials production facility. Historical site missions included nuclear reactor operation, storage and reprocessing of spent nuclear fuel, and management of radioactive and hazardous wastes. Today, activities on the site involve environmental restoration, energy-related research, and technology development. Over 50 years of operations have resulted in the accumulation of significant quantities of radioactive and hazardous wastes as well as their release to the environment. Figure 1.1 shows the location of the Hanford Site within Washington State, the boundaries of the Hanford Site, and the locations of the major facilities. The 100 Areas are the sites of reactor facilities. The major processing facilities, waste storage facilities, and waste disposal areas are located in the 200 Areas. Descriptions of the disposal facility and several other features of the site are from Meyer et al. (2004).

1.1   Integrated Disposal Facility

As part of its environmental restoration mission, the U.S. Department of Energy (DOE) is proceeding with plans to permanently dispose of a variety of wastes on the Hanford Site. As part of the Hanford Site Solid Waste Program Environmental Impact Statement (DOE 2004), DOE identified its preferred alternative for onsite disposal of solid (radioactive and hazardous) wastes. The preferred alternative involves disposal in a new facility, located in the south-central part of the 200 East Area, referred to as the Integrated Disposal Facility (IDF). Figure 1.2 illustrates the location of the IDF.

Several categories of waste are planned to be disposed in the IDF:

- Immobilized low-activity waste (ILAW) – This is Hanford tank waste that has undergone separations treatment to remove the bulk of the radionuclides as a high-level waste stream. The remaining low-activity waste stream will be solidified at the Hanford Tank Waste Treatment and Immobilization Plant (WTP) using a vitrification process. Alternative processes to immobilize the low-activity waste (supplemental to the baseline vitrification process) are being considered (CHG 2003a; Mann et al. 2003b).

- Failed or decommissioned WTP melters.

- Low-level waste (LLW) – This is waste that contains man-made radionuclides, but which is not classified as high-level waste (HLW) or transuranic waste. Some LLW disposed of at the IDF may originate off-site.

- Mixed low-level waste (MLLW) – This is LLW that also contains hazardous materials regulated under the Resource Conservation and Recovery Act (RCRA) or the corresponding dangerous waste management laws of the State of Washington.

The IDF is to be constructed as a double-lined trench with two initial disposal cells and room for future expansion of the cells. A protective surface cover will be constructed over the trench prior to closure. Additional details on disposal facility design are given in Section 2.2 and in Puigh (2004).
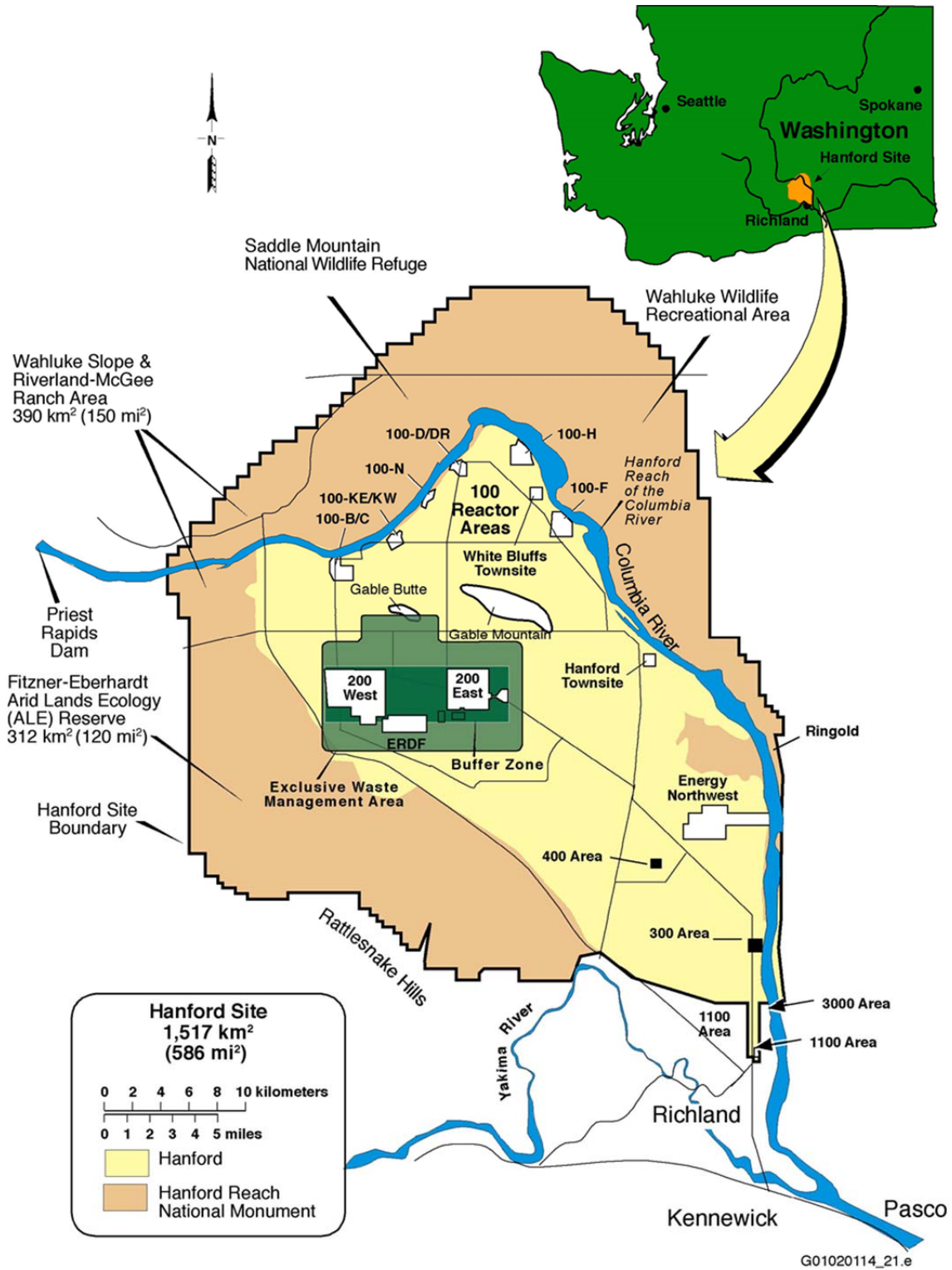
Figure 1.1. The Hanford Site and its Location Within Washington State
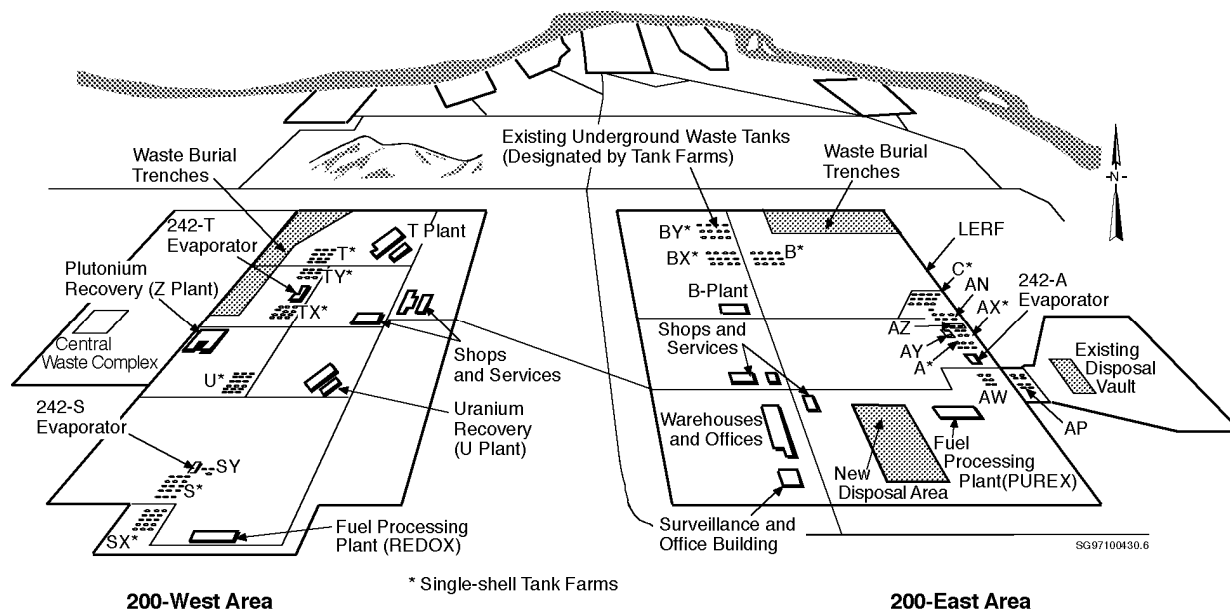
Figure 1.2. Hanford 200 Areas. The IDF is located in the south-central part of the 200 East Area and is labeled "New Disposal Area" (from Meyer et al. 2004)

1.2 IDF Performance Assessment

Radiological performance objectives and dangerous material (hazardous chemical) performance goals proposed for use in the (unpublished) 2005 IDF performance assessment (PA) are described in Mann (2002). The radiological performance objectives include dose limits for an all-pathways scenario and an inadvertent intruder scenario as well as concentration and dose limits in groundwater, surface water, and air. Performance objectives are evaluated for 1,000 years (except for the inadvertent intruder scenario), but are calculated to the time of peak or 10,000 years, whichever is longer. In addition to a base case simulation, sensitivity calculations will be performed to demonstrate that the design for the IDF disposal achieves impacts that are as low as reasonably achievable (ALARA).

The current PA for the IDF is the *Hanford Immobilized Low-Activity Waste Performance Assessment: 2001 Version* (Mann et al. 2001). The ILAW PA was updated annually for a number of years, most recently as Mann (2003). The 2001 ILAW PA was prepared assuming that only ILAW would be disposed at the IDF location. The most recent annual summary acknowledged anticipated changes in the waste types to be disposed at the facility. A risk assessment for the IDF was prepared previously that considers a single facility containing the WTP melters that is used for the combined disposal of ILAW, LAW, and MLLW (Mann et al. 2003a). This risk assessment uses information from the ILAW PA (Mann et al. 2001) and the PAs completed for the Hanford Solid Waste Burial Grounds (Wood et al. 1995; Wood et al. 1996).

Previous long-term environmental assessments at the Hanford Site have consistently shown that the groundwater pathway is the most important (Mann et al. 2003a). This pathway involves water movement into and through the disposal facility, dissolution of the waste, transport of contaminants out of the facility and through the vadose zone to the unconfined aquifer, transport in the aquifer to an extraction well, and human exposure via domestic use of the pumped water. To support the IDF PA, a variety of

data have been collected and analyses performed to document the geologic, geochemical, and hydraulic conditions at the IDF site, the expected groundwater recharge rates during the life of the facility, the hydraulic and transport conditions within the facility, and the waste form release (for ILAW). These data and analyses were documented in a set of data packages published prior to the 2001 ILAW PA (Mann and Puigh 2001) and included in the PA as appendices.

In preparation for a revision of the 2001 ILAW PA (the 2005 IDF PA), data packages were updated with additional data and analyses conducted in the intervening years. The most recent data packages (prior to the current report) included information on geology (Reidel 2005), groundwater recharge (Fayer and Szecsody 2004), flow and transport in near-field materials (Meyer et al. 2004), flow and transport in the natural sediments (also known as far-field materials) (Khaleel 2004), geochemistry (Krupka et al. 2004), and waste form release (Pierce et al. 2004). The relatively long period (10 years) since the issuing of those data packages, and renewed research and development efforts associated with revised glass formulations under the current ILAW project, has led to the review and revision of some of the earlier data packages. This report provides parameter estimates and related information for both the near- and far-field materials, updating the data packages of Meyer et al. (2004) and Khaleel (2004).

This report is organized as follows. Section 2 describes the IDF design and the near- and far-field materials. Section 3 defines the physical, hydraulic, and transport parameters for which values are provided in this report. Section 4 provides the "best-estimate" physical and hydraulic parameters for near-field materials. Section 5 provides best-estimate transport parameters for near-field materials. Section 6 provides best-estimate physical and hydraulic parameters for far-field materials. Section 7 provides best-estimate transport parameters for far-field materials. Section 8 discusses several factors affecting the parameter estimates, and Section 9 contains concluding remarks.

1.3 Quality Assurance

This work was conducted with funding from Washington River Protection Solutions under contract 36437-161, ILAW Glass Testing for Disposal at IDF. The work was conducted as part of Pacific Northwest National Laboratory (PNNL) Project 66309, ILAW Glass Testing for Disposal at IDF.

All research and development (R&D) work at PNNL is performed in accordance with PNNL's Laboratory-level Quality Management Program, which is based on a graded application of NQA-1-2000, *Quality Assurance Requirements for Nuclear Facility Applications*, to R&D activities. To ensure that all client quality assurance (QA) expectations were addressed, the QA controls of the WRPS Waste Form Testing Program (WWFTP) QA program were also implemented for this work. The WWFTP QA program consists of the WWFTP Quality Assurance Plan (QA-WWFTP-001) and associated QA-NSLW-numbered procedures that provide detailed instructions for implementing NQA-1 requirements for R&D work.

The work described in this report was assigned the technology level "Applied Research" and was planned, performed, documented, and reported in accordance with Procedure QA-NSLW-1102, *Scientific Investigation for Applied Research*. All staff members contributing to the work have technical expertise in the subject matter and received quality assurance training prior to performing quality-affecting work.

2.0   Facility Design and Description of
Near- and Far-Field Materials

This section briefly summarizes the hydrologic and geologic setting and the natural sediments (a.k.a. far-field materials) underlying the IDF. This is followed by a discussion of the current design of the IDF and near-field materials to be used in its construction.

2.1   Hydrologic and Geologic Setting

The Hanford Site is located in the semiarid Pasco Basin of the Columbia Plateau in southeastern Washington State, within the rain shadow of the Cascade Mountain Range. The Hanford Meteorological Station, located between the 200 East and 200 West Areas on the Hanford Site, has been collecting climatological data representative of the IDF disposal site since 1945 (Hoitink et al. 2003). The following summary is from Hoitink et al. (2003). Precipitation at the Hanford Meteorological Station has averaged 17.2 cm/yr since 1946, with 52% of the annual precipitation occurring from November through February. Days with more than 1.3 cm of precipitation occur on average less than once each year. Rainfall intensities of 1.3 cm/hr with a 1-hour duration are expected to occur once every 10 years. Rainfall intensities of 2.5 cm/hr with a 1-hour duration are expected to occur once every 500 years. Monthly average snowfall ranges from 0.8 cm in March to 13.7 cm in December. The maximum recorded monthly snowfall is 60 cm; the maximum recorded seasonal snowfall is 142 cm. On average, snowfall accounts for about 38% of precipitation from December through February. Average daily maximum temperature varies from 2°C in late December and early January to 35°C in late July. On average, there are 52 days during the summer months with a maximum temperature greater than or equal to 32°C and 12 days with a maximum temperature greater than 38°C. From mid-November through early March, minimum temperatures average less than or equal to 0°C. The recorded maximum temperature is 45°C; the recorded minimum is -31°C.

The Hanford Site is characterized as a shrub-steppe ecosystem that is adapted to the region's mid-latitude, semiarid climate (Neitzel 1998). Such ecosystems are typically dominated by a shrub overstory with a grass understory. Livestock grazing and agricultural production prior to government control of the Hanford Site contributed to colonization by non-native vegetation species that currently dominate portions of the landscape. In addition, summer range fires have tended to eliminate fire-intolerant species and have allowed more opportunistic and fire-resistant species to become established. The dominant non-native species on the site is cheatgrass.

Three soil types occur near the IDF disposal site: 1) Burbank Loamy Sand, a coarse-textured soil usually about 40 cm thick, underlain by a subsoil with a gravel content ranging from 20 to 80 volume percent; 2) Ephrata Sandy Loam, a medium-textured soil underlain by gravelly material; and 3) Rupert Sand, generally characterized as a coarse sand developed under grass, sagebrush, and hopsage in coarse sandy alluvial deposits (Hajek 1966).

The semiarid climate results in fairly low rates of groundwater recharge. Natural recharge rates across the Hanford Site are estimated to range from 0 to more than 10 cm/yr depending on surface soils, vegetation, and topography (Fayer and Walters 1995). Minimal recharge rates occur in fine-textured soils where deep-rooted plants prevail. Larger recharge rates are likely to occur in areas with coarse, gravelly

surface sediments and little or no vegetation. Estimates of the recharge rates expected to occur on the IDF disposal site are provided in Fayer and Szecsody (2004).

The IDF disposal site is located on the Cold Creek bar (commonly referred to as the 200 Areas Plateau), a geomorphic remnant of the Ice Age floods of the Pleistocene epoch. The stratigraphy in the area consists of basalt flows overlain by the Ringold Formation sediments, Hanford Formation sediments, and surficial deposits. The Ringold Formation consists of clay, silt, compacted mud, fine- to coarse-grained sand, and granular to cobble gravel. The Hanford Formation, deposited by the Ice Age floods, consists of pebble-to-boulder sized gravel, fine- to coarse-grained sand, and silt. The fine-grained sediments were deposited under slack-water and back-flooded conditions. The surficial sediments consist of alluvial and eolian silt, sand, and gravel deposits that are generally less than 5 m thick. The southernmost 200 m of the IDF disposal site is covered with a stabilized sand dune that is as high as 8 m.

2.2 Far-Field Materials

The vadose zone, which is approximately 100 m thick beneath the IDF site, and underlying aquifer sediments are the far-field materials of concern for IDF PA model calculations. Partitioning of these vadose zone sediments and aquifer materials into distinct lithofacies, hydrostratigraphic layers, or other meaningful subdivisions for use in subsurface flow and transport modeling is subject to interpretation, depending on available data and analyst experience. For this report, far-field materials are grouped into three primary categories: the Hanford formation, clastic dikes, and (water-saturated) aquifer sediments.

Reidel (2005) provides detailed descriptions of available geologic information for the IDF disposal site based on data from a number of boreholes and wells near the IDF. Figure 2.1 shows the interpreted generalized stratigraphy for the IDF site based on Reidel's (2005) review of selected available data. Figure 2.2 shows a fence diagram depicting the spatial distributions of major sediment types. Figure 2.3 shows the locations of wells near the IDF, and lines of cross-section that are depicted in subsequent figures. Figure 2.4 and Figure 2.5 show two representative cross-sections.

2.2.1 Hanford Formation

Reidel (2005) describes the upper portion of the Hanford formation as a sand-dominated facies, consisting of fine- to coarse-grained sand with minor amounts of silt and clay and some gravelly sands. The lower portion of the Hanford formation is described as a gravel-dominated facies. Reidel (2005) also states, however, that the texture of the sand-dominated facies changes across the IDF site, with increasing sand content and decreasing silt/clay content toward the east. Northeast of the site (borehole 299-E24-4), gravel content increases at the expense of the sand content. These (non-stationarity) effects occur mainly at a depth greater than 15 m (50 ft). The upper 15 m consists primarily of sand sediments with a significant gravel content observed over a small fraction of the depth in each borehole. Reidel (2005) also notes the presence of at least three paleosols (buried soil horizons), which could be used to subdivide the sediment profile for the Hanford formation into at least three major layers (Figure 2.1). These paleosols are potentially important owing to their contrast in properties relative to overlying and underlying sediments, and spatial continuity, which could enhance lateral flow. However, the longer-range spatial continuity of these paleosols across the wider area of interest is currently unclear (see Figure 2.4 and Figure 2.5).
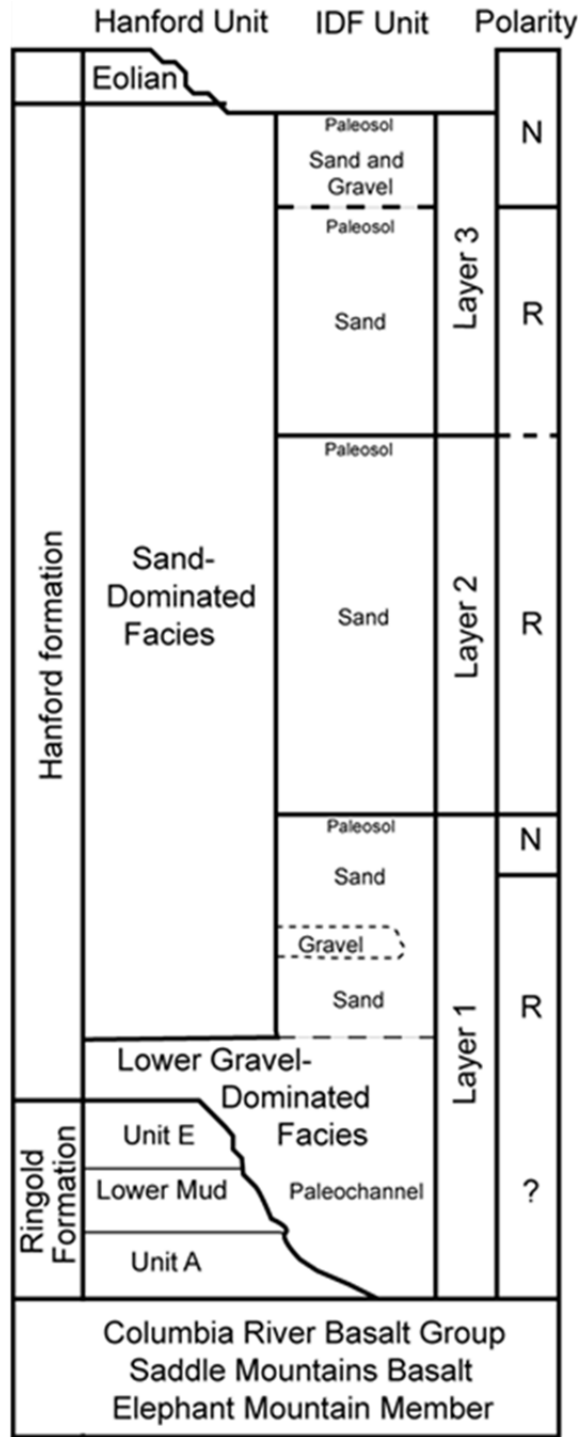
Figure 2.1. Interpreted Generalized Stratigraphy for IDF Site (from Reidel 2005). N and R refer to normal and reversed polarity (see Reidel, 2005 for details).
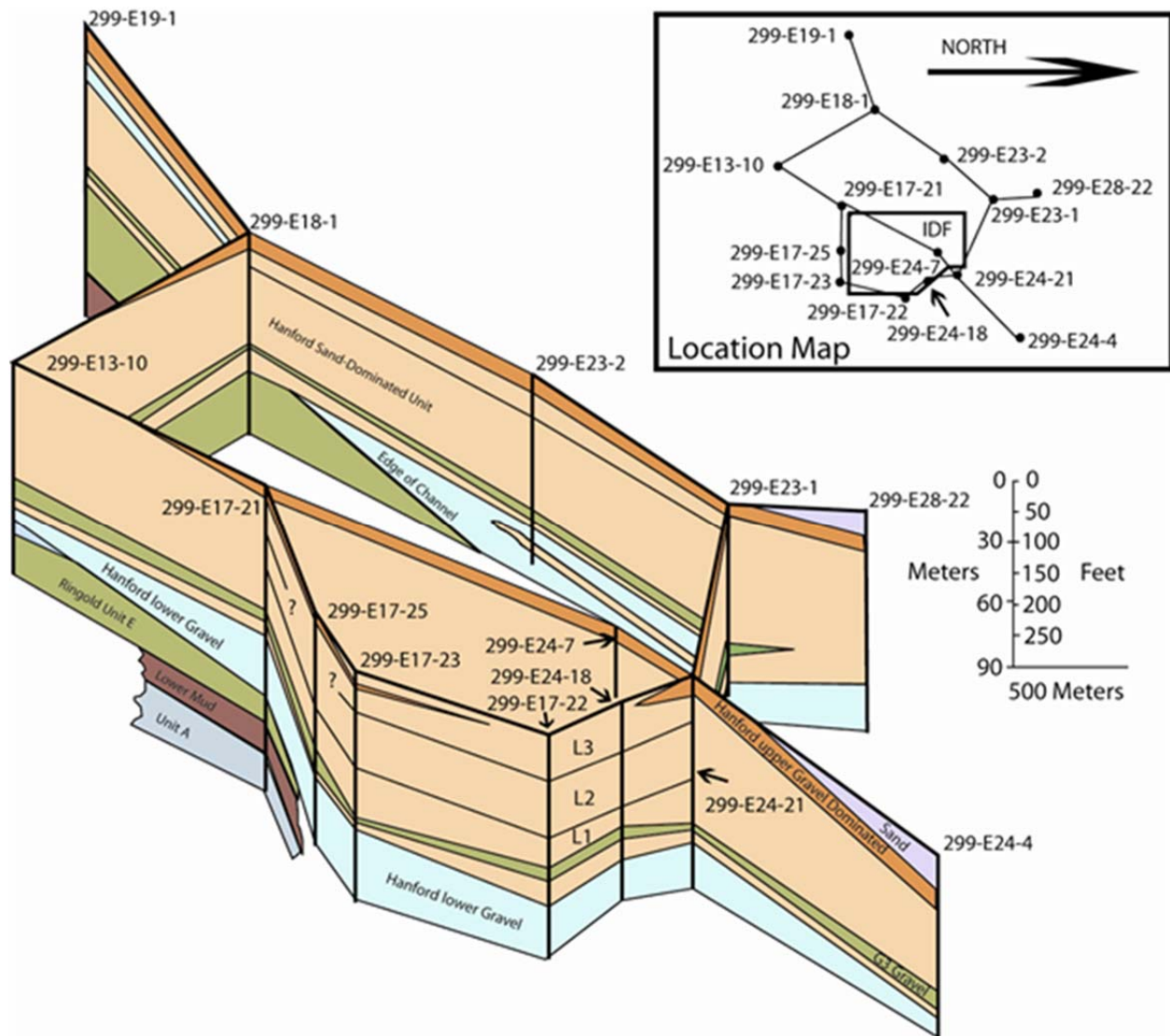
Figure 2.2. Fence Diagram of the IDF Site and Vicinity (from Reidel 2005)

An earlier data package for far-field materials (Khaleel 2004) considered only two major material types within the vadose zone underlying the IDF site, which were referred to simply as "sandy" and "gravelly" sediments. Khaleel (2004) notes that base case simulations for earlier IDF PAs considered "layer-cake" stratigraphy (i.e., two perfectly horizontal layers with "sandy" sediment overlying "gravelly" sediment). Smaller-scale heterogeneities within these larger layers were not represented explicitly, but effective properties intended to capture the effects of small-scale heterogeneities were estimated using equations developed from stochastic theories (Polmann 1990; Gelhar 1993). Further details on the application of these stochastic theories are provided later in this report. According to Khaleel (2004), sloped layering was also to be considered in earlier IDF PAs for a simulation case intended to address the sensitivity of model predictions to uncertainties in geologic structure or layering.
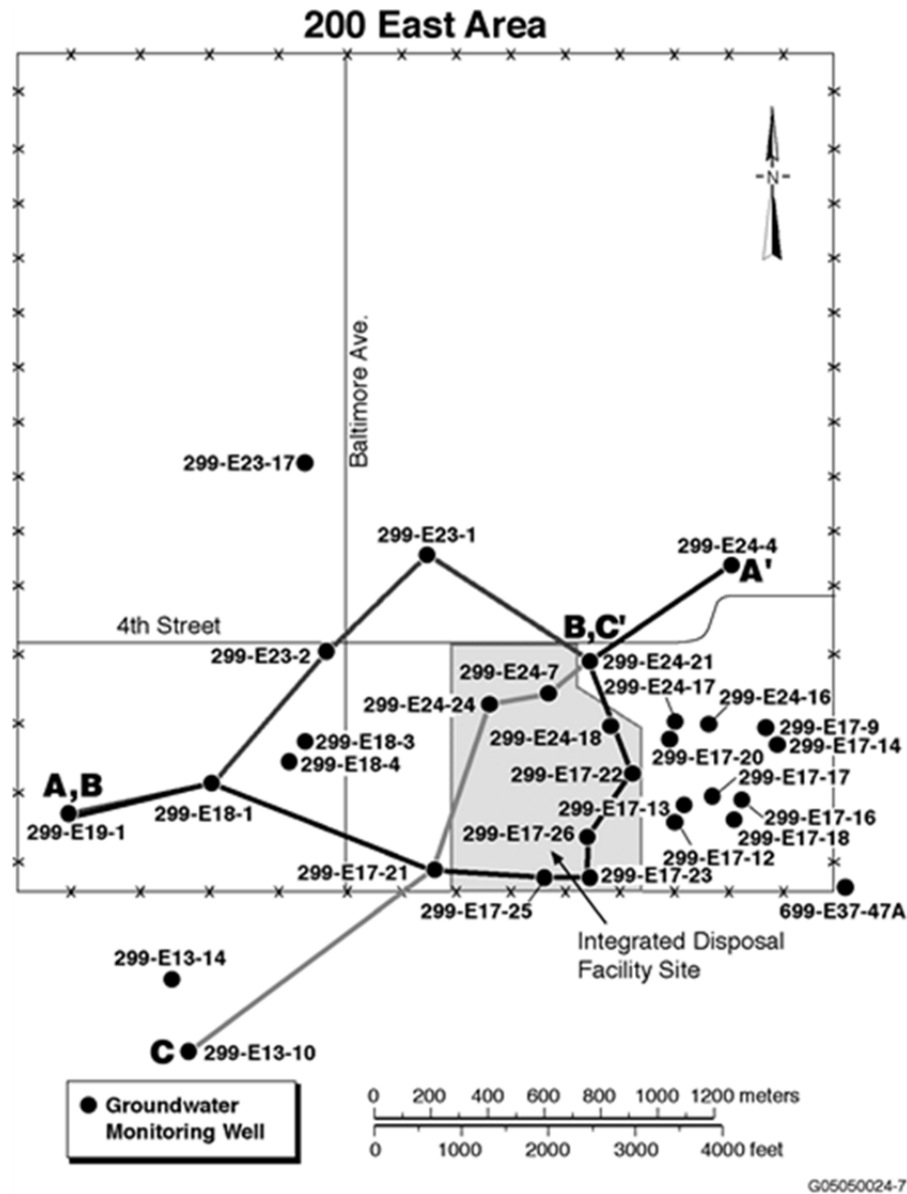
Figure 2.3. Location of Wells and Cross-sections Used in Reidel (2005) to Interpret the IDF Site Geology

Note that Figure 2.4 and Figure 2.5 show up to 10 different sediment textural classes within the geologic domain of interest. Although Reidel (2005) did not attempt to do so, more-detailed interpretations of lithofacies and/or smaller-scale heterogeneities are possible using available core and high-resolution geophysical wire-line log data from IDF boreholes/wells, using methods such as those described by Last et al. (2007) and Oostrom et al. (2006). A facies-based modeling approach, similar to that described by Freedman et al. (2014) and Last et al. (2007), is currently being used for modeling subsurface flow and transport for the WMA-C (C Tank Farms). A similar approach could be considered for future IDF PA modeling to evaluate alternative conceptual models of the vadose zone.
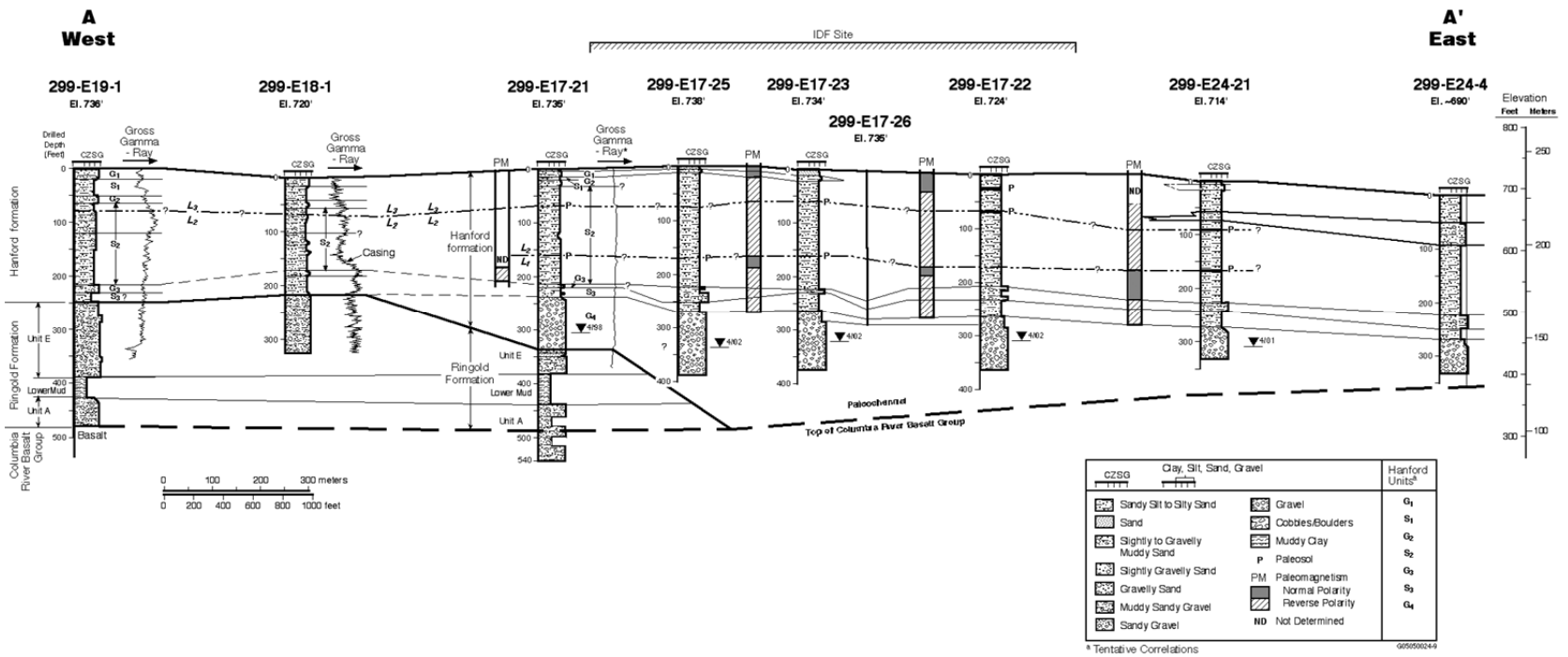
Figure 2.4. Cross-section A-A' Across the IDF Site (from Reidel 2005). See Figure 2.3 for location of cross-section.
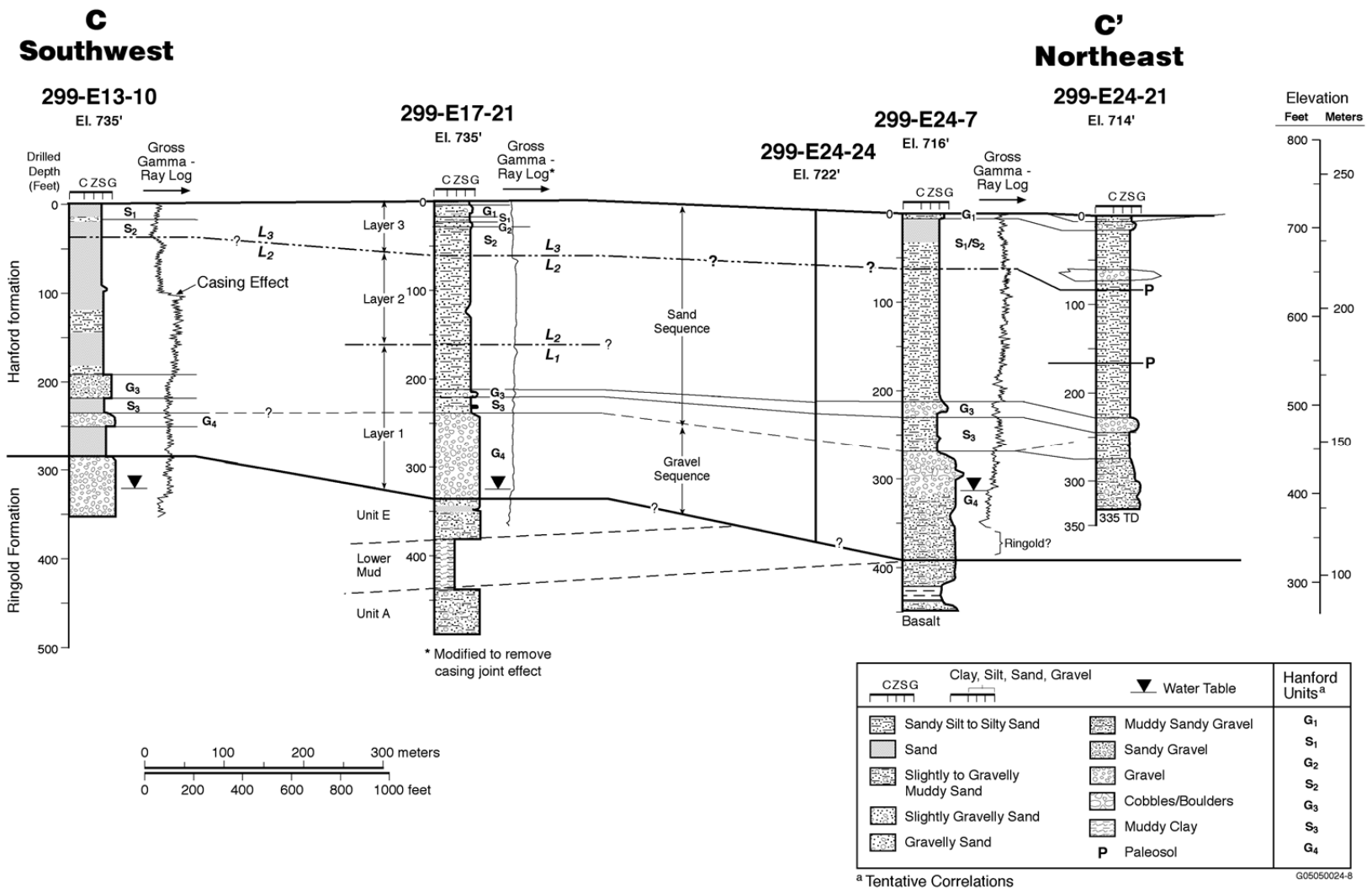
Figure 2.5. Cross-section C-C' Across the IDF Site (from Reidel 2005). See Figure 2.3 for location of cross-section.

2.2.2   Clastic Dikes

In addition to the "sandy" and "gravelly" sediments of the Hanford formation, physical and hydraulic parameter estimates were provided by Khaleel (2004) for clastic dike samples (after Fayer and Ritter 1999).[1] Clastic dikes (Figure 2.6) are vertical to sub-vertical sedimentary structures that cross-cut sedimentary layering (Fecht et al. 1998; Johnson et al. 1999).

Figure 2.6. Photograph of a Clastic Dike Cutting Horizontal Layers of the Hanford Formation (after Murray et al. 2007)

---

[1] Fayer MJ and JS Ritter. 1999. *Physical and hydraulic measurements of FY 1998 clastic dike samples.* Letter Report to Fluor Daniel Northwest, Inc. March 1999. Pacific Northwest National Laboratory, Richland, WA.

Although the locations of clastic dikes at depth under the IDF are largely unknown, a clastic dike was encountered during excavation of the IDF pit (Reidel and Fecht, 2005). An extensive network of clastic dikes has also been mapped along the Army Loop Road about 5 km south of the IDF site (Figure 2.7). Clastic dikes have also been mapped at other Hanford locations, as well as in the greater area surrounding the Hanford Site, as shown in Figure 2.8.

According to Murray et al. (2007), clastic dikes appear to be common across the entire Hanford Site, but are usually covered by surface sediment deposits or cultural features. The hydraulic properties for clastic dike materials were reported by Khaleel (2004) for potential use in addressing the sensitivity of model predictions to uncertainties associated with the possible presence of these geologic features. The clastic dike samples analyzed by Fayer and Ritter (1999) (and reported by Khaleel 2004) were collected from multiple locations both on and off the Hanford Site. For completeness, these data are provided in Section 6.0 of this report.
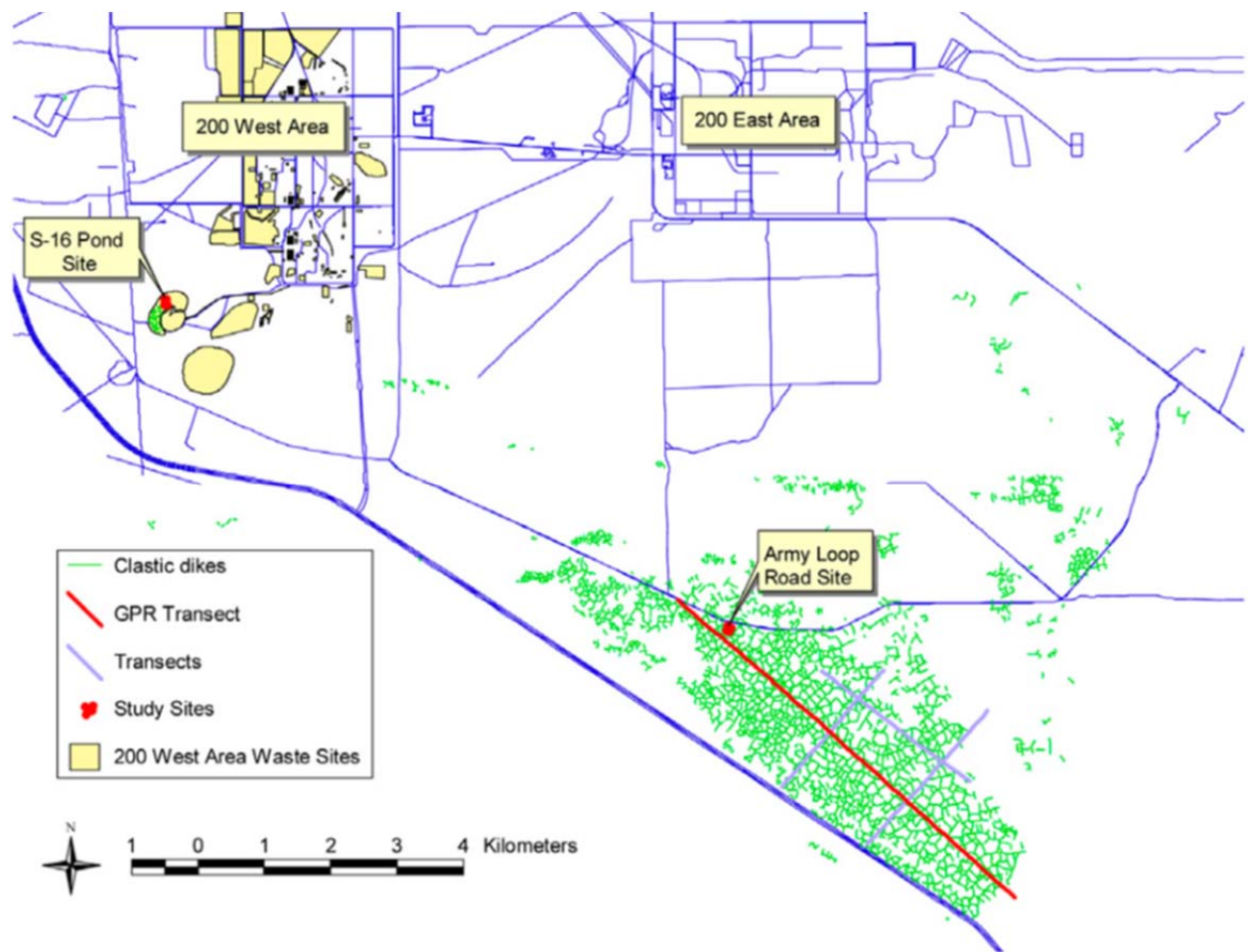
Figure 2.7. Map Showing Exposed Clastic Dike Network Around the Army Loop Road at the Hanford Site (from Murray et al. 2007)
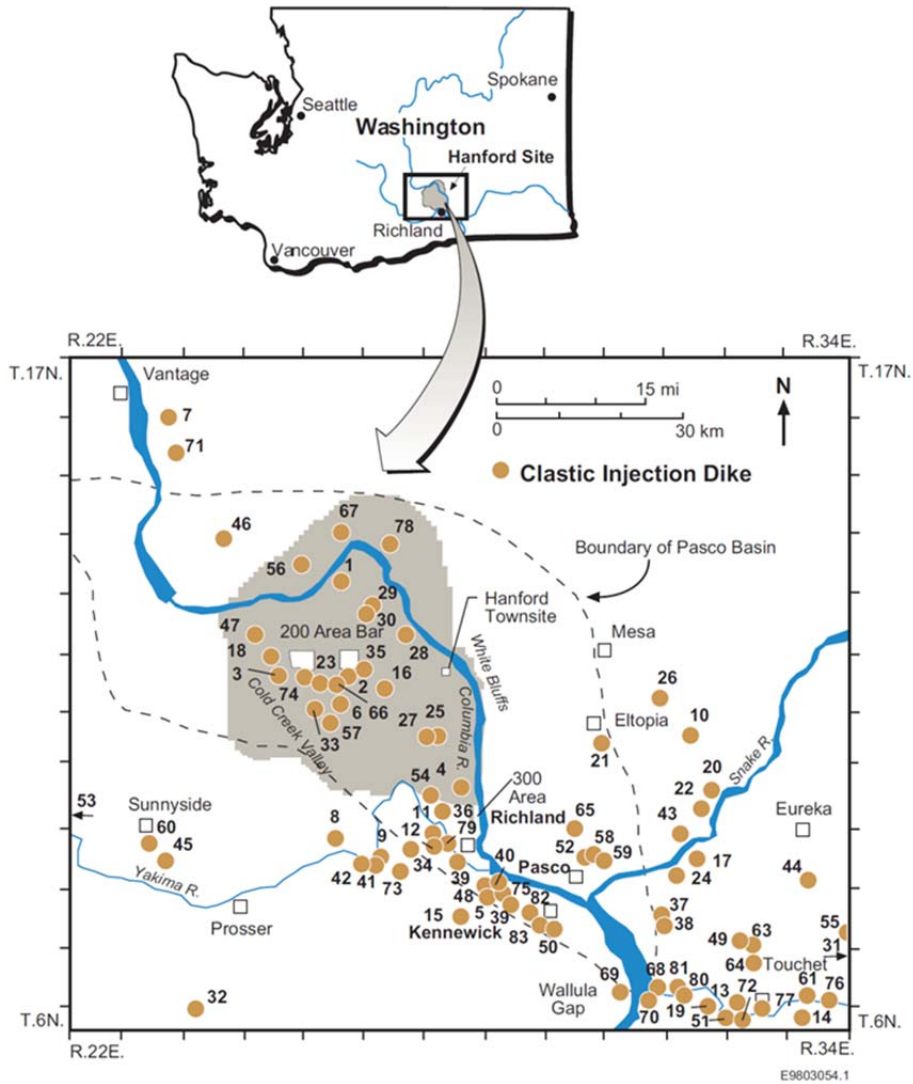
Figure 2.8. Map Showing Locations of Mapped Clastic Injection Dikes In and Around the Hanford Site (from Fecht et al. 1998)

Clastic dike widths and lengths range from 1 mm to >2 m and from 0.3 to >100 m, respectively (Johnson et al. 1999). These geologic features, which tend to form polygonal networks at the ground surface (e.g., like mud cracks), are of interest because of concerns that they may provide preferential flow paths for vertical migration of contaminants through the vadose zone to groundwater. In one field test, vertical flow rates were found to be more than 10 times faster in the clastic dike than in the surrounding horizontally layered sediments (Fecht et al. 1998). The presence of clastic dike networks may also provide some compartmentalization of the vadose zone, which could restrict lateral flow and transport.

The influence of clastic dikes on the vertical migration of contaminants at Hanford was studied relatively recently in the field and with numerical simulations by Murray et al. (2007). They note that, in general, clastic dikes are composed of an outer skin of clay with coarser infilling material. Clay linings are commonly 0.03 to 1.0 mm thick, but linings up to ~10 mm have also been found (Murray et al. 2007). The width of infilling layers ranges from 0.01 mm to >30 cm, and their length can vary from ~0.2 to >20 m. Infilling sediments are typically poorly to well-sorted sand but may contain clay, silt, and gravel (Murray et al. 2003; Fecht et al. 1998).

Murray et al. (2007) determined that clastic dikes may indeed provide preferential flow paths for transport of some contaminants (e.g., tritium and technetium-99), but only under certain flux conditions. Figure 2.9 shows spatial variation of sediment texture for an excavation at the Army Loop Road site.
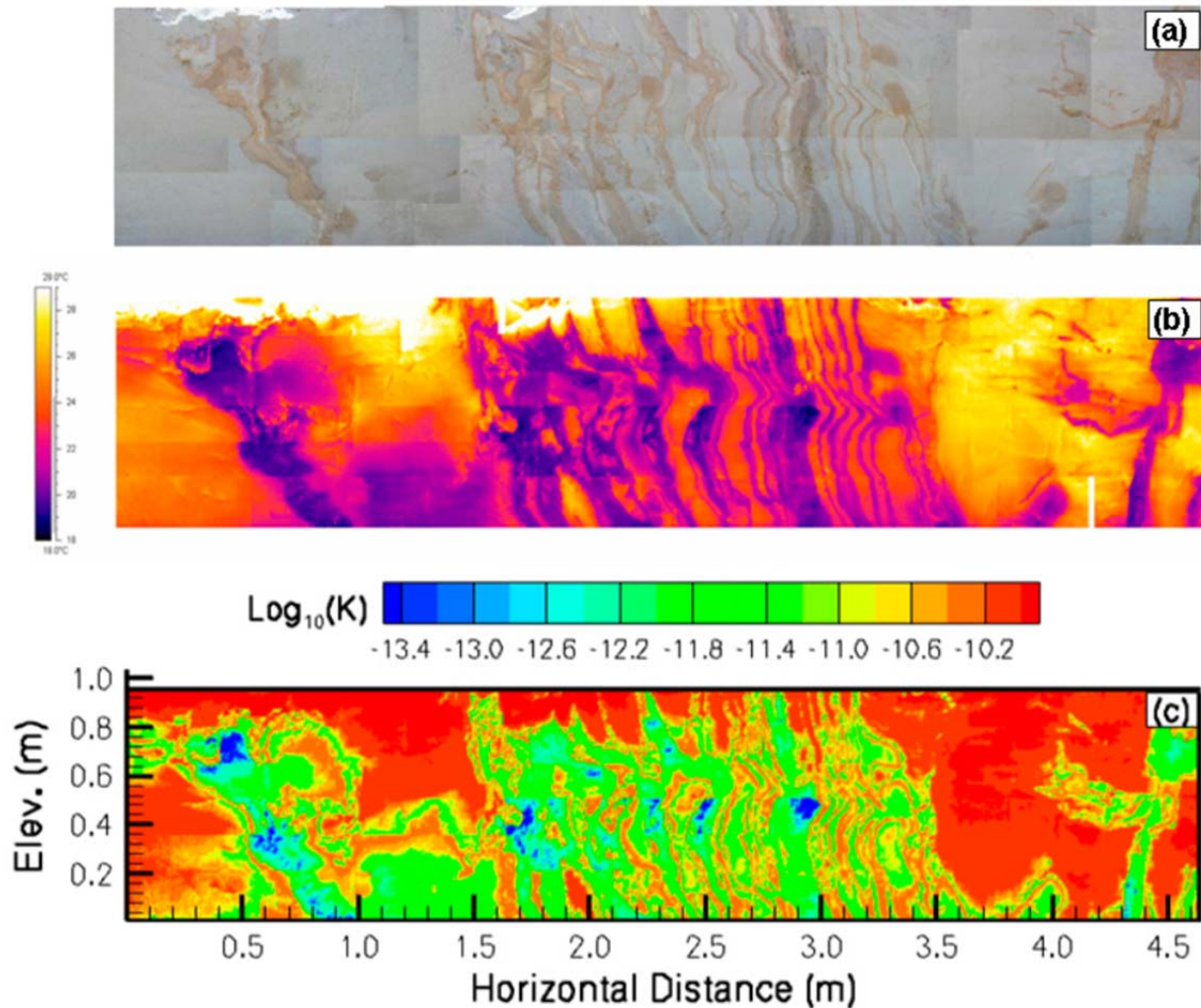
Figure 2.9. Spatial Variability of Sediments Along Tier 2 of the Excavation at the Army Loop Road Clastic Dike Study Site (after Murray et al. 2007) shown by (a) photograph of soil textures; (b) measured infrared temperatures; (c) vertical saturated hydraulic conductivity (cm/s) inferred from the relationship between geometric mean grain size and intrinsic permeability.

These data were used by Murray et al. (2007) for estimating hydraulic properties, which were then used in numerical simulations with the Subsurface Transport Over Multiple Phases (STOMP) simulator (White and Oostrom 2006). Figure 2.10 shows simulation results for the spatial domain depicted in Figure 2.9 for different dimensionless water fluxes.
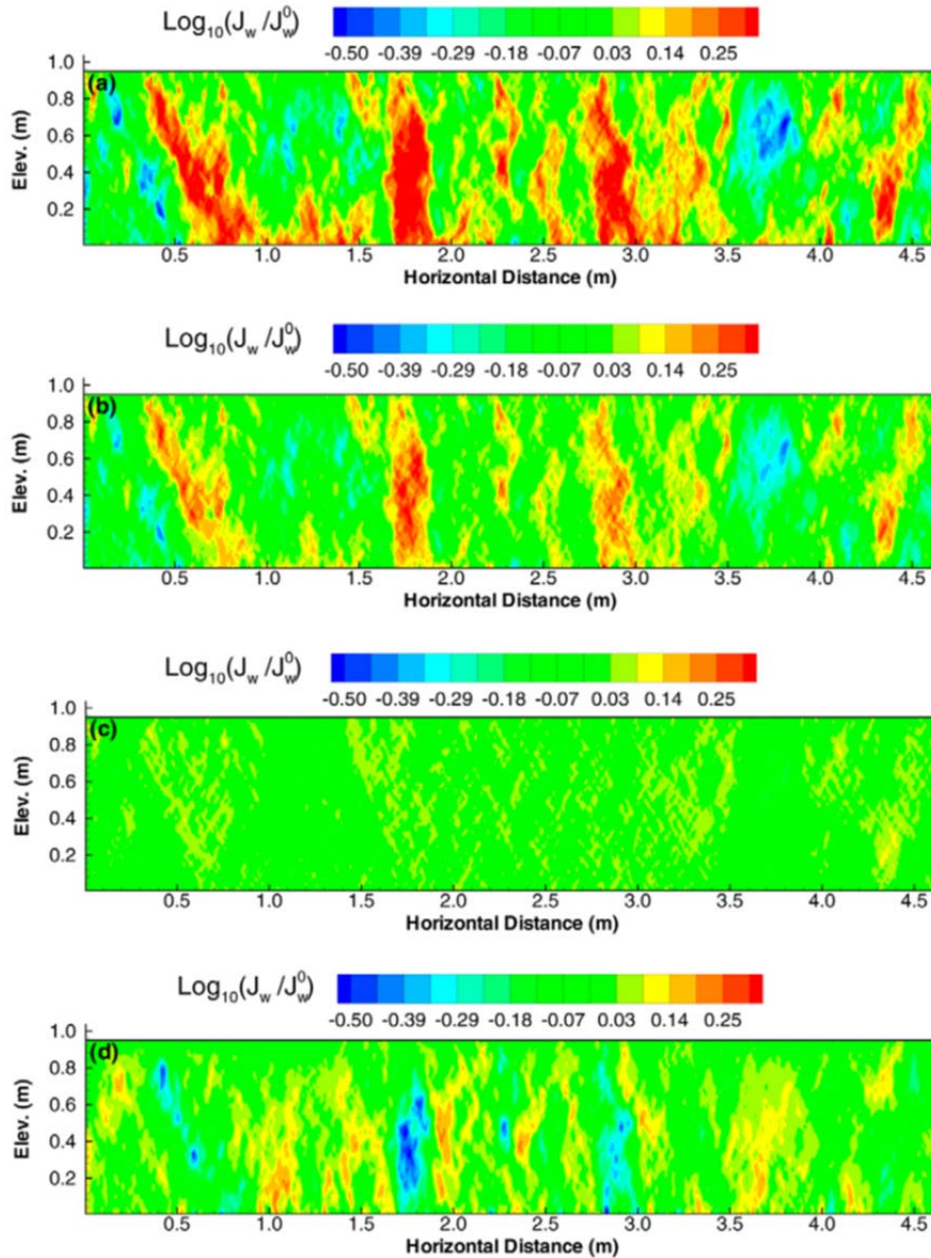
Figure 2.10. Simulated Distributions of Dimensionless Water Flux $|J_w|/J_w^0$ During Steady Infiltration Under a Constant Surface Flux, J_w^0, of (a) 1 mm yr^{-1}, (b) 10 mm yr^{-1}, (c) 10^2 mm yr^{-1}, and (d) 10^3 mm yr^{-1} (after Murray et al. 2007). Regions shown in red are the preferential flow paths under different flux conditions.

Comparing Figure 2.9 and Figure 2.10, it can be seen that for the lower fluxes shown in the top two images of Figure 2.10, flow is predominantly through the dike materials (shown as regions in red). It should also be emphasized that these low applied fluxes (<10 mm yr^{-1}) are comparable to the natural groundwater recharge rates that have been estimated for undisturbed areas of the Hanford Site (Fayer and Szecsody 2004; Rockhold et al. 2009a). At higher fluxes (bottom two images in Figure 2.10), flow transitions into the coarser, higher-permeability matrix materials surrounding the dike materials. Although these results suggest that the dike materials may provide preferential vertical flow paths, particularly under low water flux conditions, the finer-grained nature of clastic dikes (with up to 19% clay-sized materials in the finer portion of the Army Loop Road site clastic dike) also suggests that more-reactive contaminants would be unlikely to travel far in clastic dikes, owing to increased sorption on the clay-sized materials that have larger specific surface areas (Murray et al. 2007). Therefore, the real importance or significance of preferential flow through clastic dikes is still largely unknown.

The results of Murray et al. (2007) were not available to inform modeling decisions for earlier IDF PAs. Although detailed three-dimensional information is still lacking, aerial mapping of the clastic dike networks around the Army Loop Road site (Figure 2.7) has provided information that could be used for stochastic modeling of clastic dike networks (Murray et al. 2003). Methods are also available for upscaling physical and hydraulic properties generated at arbitrarily fine geostatistical grid resolution to the size of grid blocks required for numerical flow and transport modeling (Oostrom et al. 2006). Therefore, it would now be possible to more realistically assess the sensitivity and uncertainty of subsurface flow and transport behavior to the presence of clastic dike networks. It may be of interest to note that Johnson et al. (1999) also considered the presence of clastic dikes in their characterization of the subsurface for the S-SX waste management area (Figure 2.11).

2.2.3   Aquifer Sediments

Figure 2.4 and Figure 2.5 indicate that the top of the water table lies within the Hanford formation for most of the area around the IDF site, owing to a deep paleo-channel that runs through the central and eastern portions of the site (Reidel 2005). However, the water table appears to lie within the Ringold Formation to the west and southwest of the site. Therefore, physical and hydraulic properties for the Ringold Formation in this area may also be of interest, depending on the spatial extent of the groundwater model to be used for IDF PA calculations. Khaleel (2004) did not provide parameter estimates specifically for aquifer materials or for Ringold Formation sediments underlying the IDF site. However, Appendix A of Reidel (2005) provides slug test analysis results [by Frank Spane, Pacific Northwest National Laboratory (PNNL)] for five wells (299-E17-21, 299-E17-22, 299-E17-23, 299-E17-25, and 299-E24-21) that bound the IDF site. These results should be applicable for a local model of groundwater flow and transport representing the IDF site.
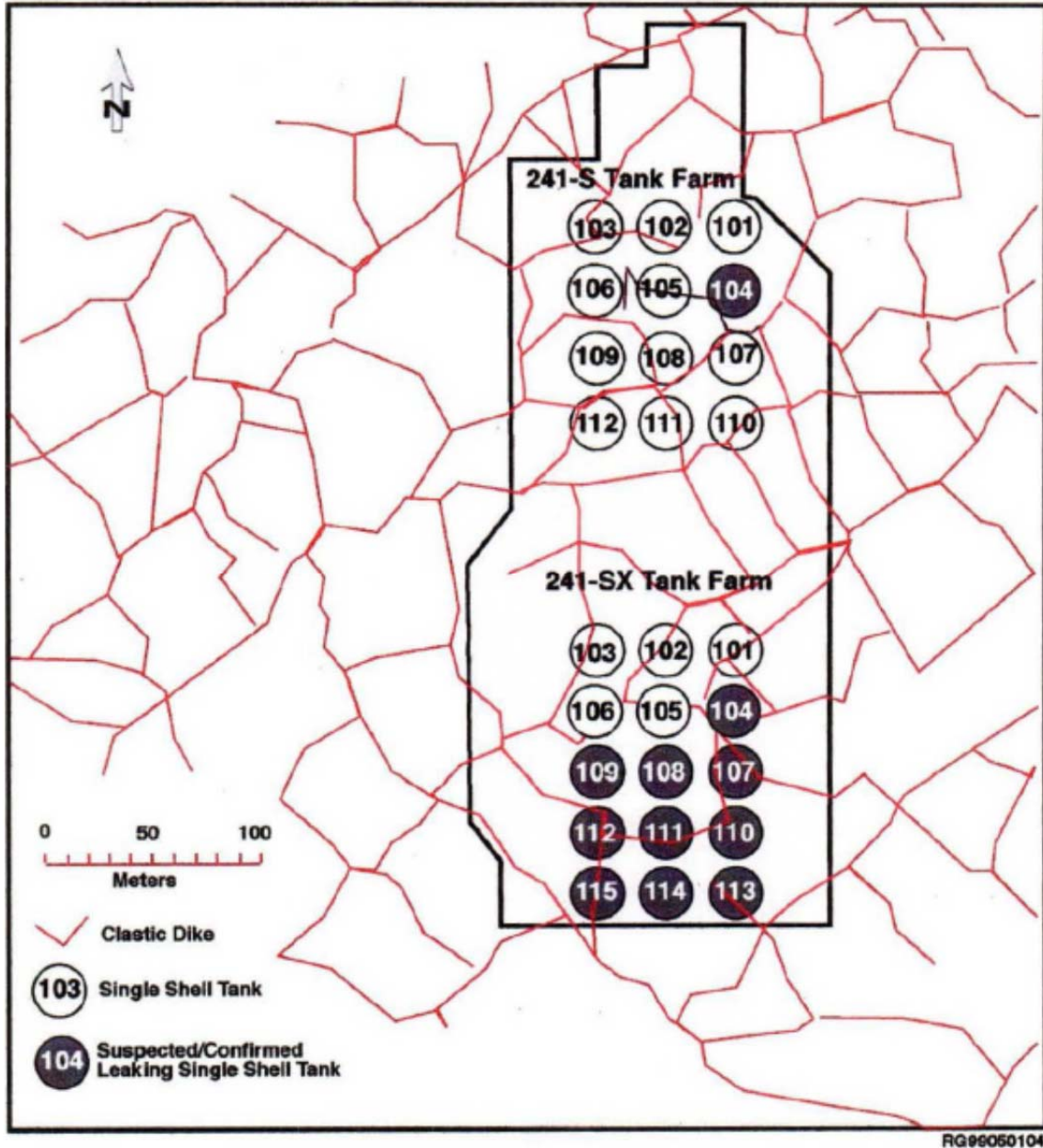
Figure 2.11. Projection of Clastic Dikes Onto the S-SX Waste Management Area (after Johnson et al. 1999)

2.3 Facility Design and Near-Field Materials

The IDF will be constructed in excavations within the surficial and upper Hanford formation sediments. Excavations will likely be no more than 15 m deep. The IDF is to be constructed as a double-lined trench with two initial disposal cells and room for expansion of the cells, as shown in Figure 2.12 (CHG 2003b, 2003c). Figure 2.13 and Figure 2.14 are cross-sections through the trench illustrating the trench geometry. Figure 2.15 provides details of the trench liner system, which relies on

two geomembrane liners for control of moisture. Prior to closure, a protective surface cover will be constructed over the trench to provide a barrier to vertical water flow (Burbank 2002). Components of the cover will also serve as an inadvertent intruder barrier. It is anticipated that the surface cover will consist of a Modified RCRA Subtitle C Barrier Design as described in DOE (1993a). The components of this cover and their minimum thicknesses are shown in Figure 2.16. The combined minimum thickness of the cover is 1.7 m. Puigh (2004) discusses the IDF facility design as it relates to the PA.

The materials currently specified or that may potentially be used in the IDF are described below. The following discussion is from Meyer et al. (2004).

2.3.1   Surface Cover

A description of each component of the surface cover is given below, taken primarily from DOE 1993a. This section is nearly identical to that presented in Meyer and Serne (1999), but is included here for completeness. See Figure 2.16 for the locations and order of materials in the surface cover.

2.3.1.1   Layer 1: Silt Loam Soil with Gravel

This layer consists of 50 cm of sandy silt to silt loam soil (matching the characteristics of such soil from the McGee Ranch area on the Hanford Site) with 15% pea gravel by weight. The design bulk density of this layer is about 1.46 g/cm^3. The surface slope is limited to a maximum of 2% (after allowances for settlement and subsidence). The purpose of Layer 1 is to support vegetation and provide maximum storage capacity for precipitation and snowmelt. A large storage capacity in conjunction with evapotranspiration from vegetation will tend to minimize percolation from the cover (recharge). The pea gravel provides resistance to erosion of the silt loam.

2.3.1.1   Layer 2: Compacted Silt Loam Soil

This layer consists of an additional 50 cm of silt loam soil, but without the addition of pea gravel. This layer will be compacted during construction to a design bulk density of about 1.76 g/cm^3. The purpose of Layer 2 is to provide water storage capacity for precipitation and snowmelt and support for vegetation. The purpose of the compaction is to reduce the hydraulic conductivity of the layer.
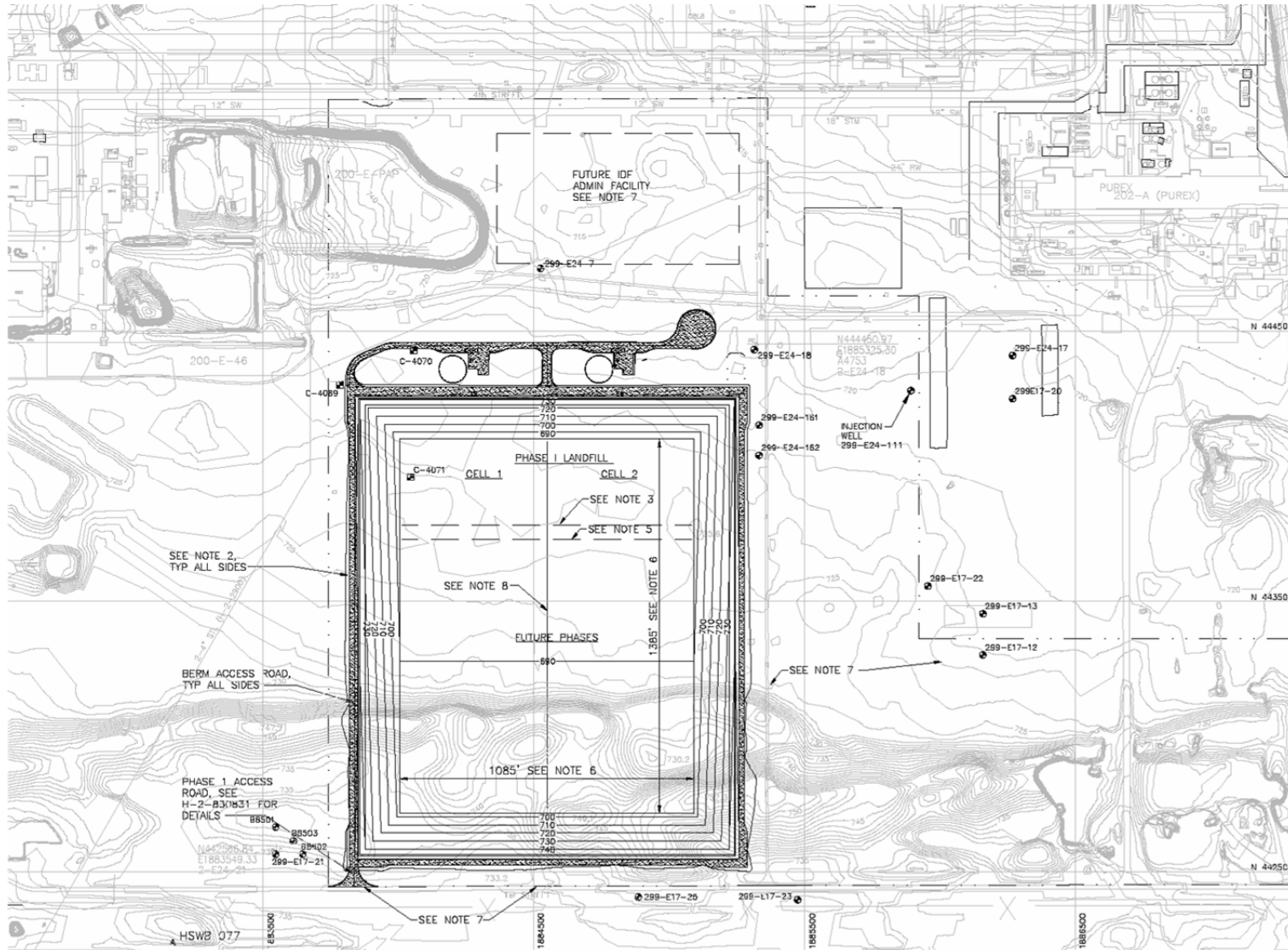
Figure 2.12. Layout of the IDF Within the Site
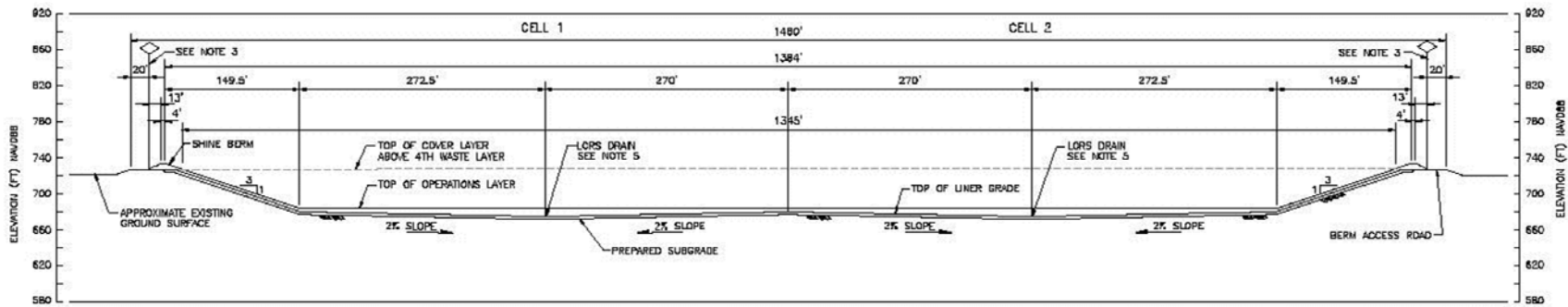
Figure 2.13. East-west Cross-section Through the IDF Trench (from CHG 2003c)
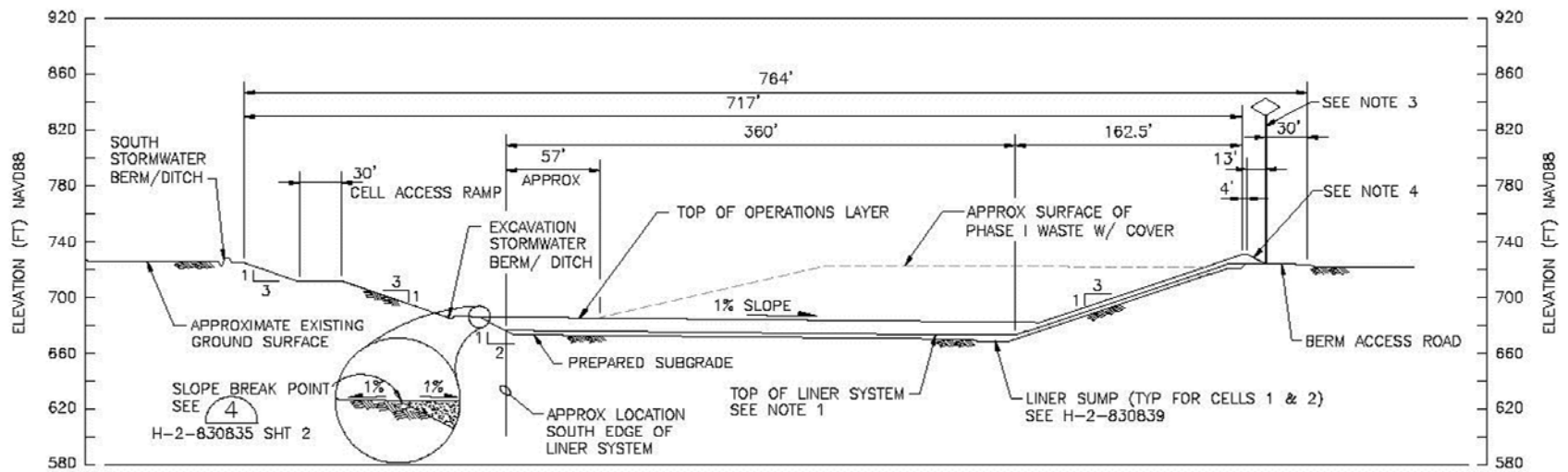
Figure 2.14. North-south Cross-section Through the IDF Trench (from CHG 2003c)

2.17

BOTTOM LINER DETAIL

OPERATIONS LAYER

DRAIN GRAVEL

ADMIX LINER

PREPARED SUBGRADE

7.0'
3.0' MIN. (SEE NOTE 1)
1.0' (SEE NOTE 1)
3.0' (SEE NOTE 2)

- SEPARATION GEOTEXTILE
- CUSHION GEOTEXTILE
- PRIMARY GEOMEMBRANE
- PRIMARY GCL
- LDS CDN
- SECONDARY GEOMEMBRANE
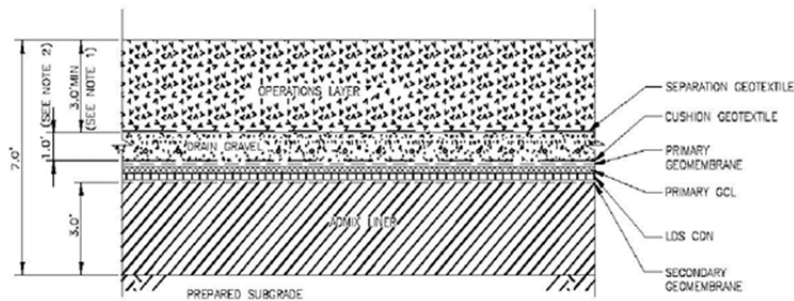
NOTES:
1. OPERATIONS LAYER THICKNESS VARIES ACROSS CELL BOTTOM WITH A 3-FOOT MIN. THICKNESS.
2. INCREASE DRAIN GRAVEL THICKNESS IN VICINITY OF LEACHATE COLLECTION AND RISER PIPES IN LCRS SUMP AS SHOWN ON B AND D H-2-830848 H-2-830845

BOTTOM LINER DETAIL 1
NTS
H-2-830836, H-2-830839
H-2-830840

SIDE SLOPE LINER DETAIL

OPERATIONS LAYER (SEE NOTE 1)
LCRS CDN
PRIMARY GEOMEMBRANE
LDS CDN
SECONDARY GEOMEMBRANE
ADMIX LINER

3.0'
3.0'
3 / 1
1 / 3
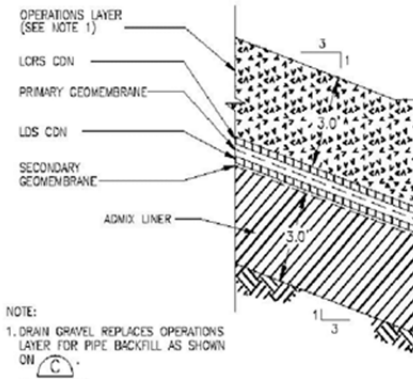
GENERAL NOTE (H2-830838 THROUGH 830840)
SPACING BETWEEN GEOSYNTHETIC LAYERS IS EXAGGERATED FOR CLARITY.

NOTE:
1. DRAIN GRAVEL REPLACES OPERATIONS LAYER FOR PIPE BACKFILL AS SHOWN ON C. H-2-830848

SIDE SLOPE LINER DETAIL 2
NTS
H-2-830836, H-2-830839,
H-2-830840, H-2-830848

LINER ANCHOR TRENCH DETAIL

EDGE OF LINER SHOWN ON PLAN (SEE NOTE 1)
3.0' / 2.0' MIN.
3 / 1
OPERATIONS LAYER
SIDE SLOPE LINER SEE DETAIL 2
ADMIX LINER
PREPARED SUBGRADE
1 / 3

SEE C AND D H-2-830834 H-2-830834 FOR SHINE BERM DETAIL AT ANCHOR TRENCH

CONTROL LINE SHOWN ON CIVIL GRADING PLANS (SEE H-2-830830)

2.0' / 3.0'
1
2.0' MIN. / 2.7' / 17.3'
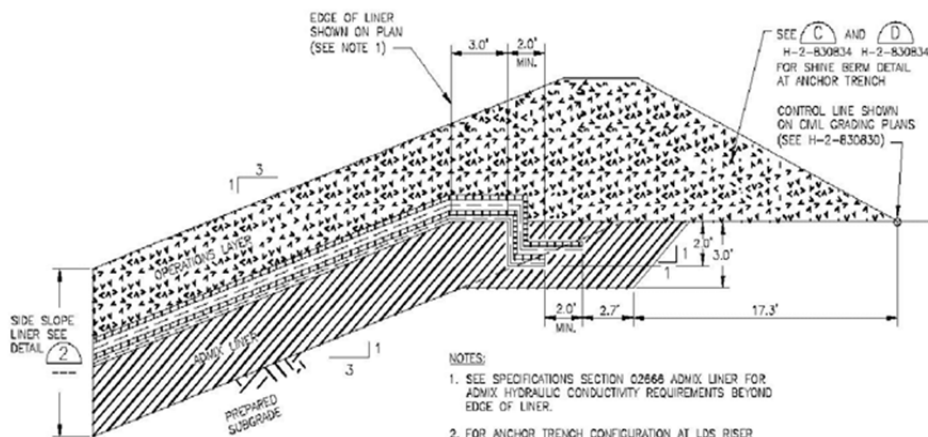
NOTES:
1. SEE SPECIFICATIONS SECTION 02668 ADMIX LINER FOR ADMIX HYDRAULIC CONDUCTIVITY REQUIREMENTS BEYOND EDGE OF LINER.
2. FOR ANCHOR TRENCH CONFIGURATION AT LDS RISER PIPE TRENCH SEE SECTION C ON DWG. H-2-830847.

LINER ANCHOR TRENCH DETAIL 3
NTS
H-2-830834, H-2-830836

TOE OF SLOPE LINER DETAIL

TOE OF SLOPE PRIMARY LINER
3.0' GCL EXTENSION (SEE NOTE 2)
10.0' MIN. CDN EXTENSION
GEOTEXTILE CUSHION (SEE NOTE 1)
OPERATIONS LAYER
DRAIN GRAVEL
BOTTOM LINER DETAIL 1
ADMIX LINER
PREPARED SUBGRADE
1 / 3
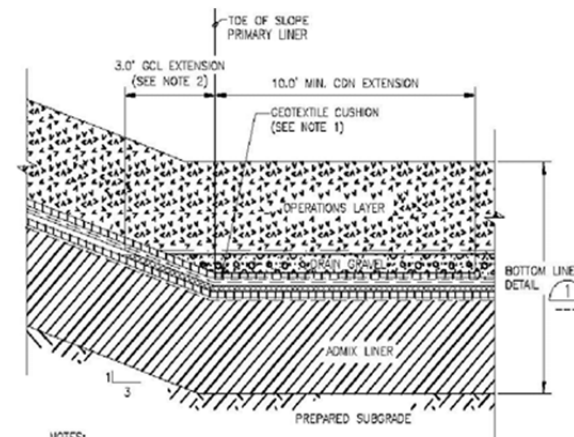
NOTES:
1. GEOTEXTILE CUSHION ENDS AT TOE OF SLOPE
2. EXTEND GCL 3.0' UP SLOPE (HORIZONTAL LENGTH) TO TOP OF DRAIN GRAVEL.

TOE OF SLOPE LINER DETAIL 4
NTS
H-2-830836, H-2-830839

Figure 2.15. Details of IDF Trench Liner (from CHG 2003c)

2.18

Modified RCRA Subtitle C Barrier

Cover Vegetation: Mixed perennial grasses

Layer 1: (50 cm; 20 in.) Silt loam topsoil with pea gravel admixture

Layer 2: (50 cm; 20 in.) Compacted silt loam topsoil

Layer 3: (15 cm; 6 in.) Sand filter layer

Layer 4: (15 cm; 6 in.) Gravel filter layer

Layer 5: (15 cm; 6 in.) Lateral drainage layer (drainage gravel)

Layer 6: (15 cm; 6 in.) Low-permeability asphalt layer

Layer 7: (10 cm; 4 in.) Asphalt base course

Layer 8: (variable thickness) Grading fill

H9408029.2

Figure 2.16. Schematic Profile of the Modified RCRA Subtitle C Barrier

2.3.1.2   Layer 3: Sand Filter

This layer consists of 15 cm of graded sand that is intended to serve, in conjunction with Layer 4, as a filter, preventing the fine particles of Layer 2 from moving into the lateral drainage layer (Layer 5). Particle size requirements for the sand filter were taken from Cedergren (1989) (also cited in Ecology 1987 and EPA 1989) and are given below. The D values refer to the particle diameters on a particle size distribution (PSD) curve (e.g., D_{15} is the particle diameter at which 15% of the particles are smaller).

Retention Criteria: D_{15} (Sand)/ D_{85} (Silt Loam) < 4 to 5
                                     D_{50} (Sand)/ D_{50} (Silt Loam) < 25

Permeability Criterion: D_{15} (Sand)/ D_{15} (Silt Loam) > 4 to 5

These filtration criteria were developed for applications in earth dams under saturated conditions. They are expected to be conservative for the unsaturated conditions of the ILAW surface cover.

The presence of the relatively coarse textured sand layer immediately beneath the fine textured silt loam will produce a capillary barrier effect at the interface. This effect arises because the unsaturated hydraulic conductivity of the sand will be significantly less than that of the silt loam for a large range of matric potential. Significant flow into the sand layer will not occur until the matric potential at the silt loam-sand interface becomes sufficiently large (close to zero) that water can move into the relatively large pores of the sand (Hillel 1980). The capillary barrier formed by the silt loam (Layer 2) overlying the sand (Layer 3) will, in effect, increase the water storage capacity of the silt loam layers. The capillary barrier's ability to do so will depend on the hydraulic properties of the silt loam and sand materials.

2.3.1.3   Layer 4: Gravel Filter

This layer consists of 15 cm of a graded gravel that functions, with Layer 3, as a filter, preventing the fine particles of Layer 2 from moving into the lateral drainage layer (Layer 5). Particle size requirements for this layer are identical to those of the sand filter (Layer 3), except that the filter material in this case is the gravel and the filtrate material is the sand. No slope is specified for the sand and gravel filter layers. It is assumed that they will be constructed at a 2% slope to minimize required thickness of the surface cover.

2.3.1.4   Layer 5: Gravel Lateral Drainage Layer

This layer consists of 15 cm of screened gravel with a required saturated hydraulic conductivity of no less than 1.0 cm/s. This layer will be constructed at a 2% slope. Its purpose is to divert (to the edge of the cover) water that passes through the filter layers and reaches the asphalt layer (Layer 6).

2.3.1.5   Layer 6: Asphaltic Concrete

This layer consists of 15 cm of a durable asphaltic concrete mixture consisting of double-tar asphalt with added sand as binder material, conforming to WSDOT M41-10, Section 9-02.1(4), Grade AR-4000W (WDOT 1991). The asphaltic concrete will potentially be coated with a spray-applied asphaltic material. This layer will be constructed at a 2% slope. The asphalt layer is intended to function as a low permeability layer and as an inadvertent intruder barrier. As a low permeability layer, analogous to the compacted soil component of a standard RCRA Subtitle C Barrier, the asphalt layer should be expected to have a maximum saturated hydraulic conductivity of 10^{-7} cm/s.

2.3.1.6   Layer 7: Asphalt Base Course

This layer serves as a stable base for placement of the asphalt and consists of 10 cm of screened, crushed surfacing material, with 100% passing the 32 mm sieve. The material must conform to WSDOT M 41-10, Section 9-03.9(3) (WDOT 1991).

2.3.1.7   Layer 8: Grading Fill

This material consists of a well-graded, granular soil mixture, which may include as much as 20% by volume of cobbles measuring no more than 75 mm in the greatest dimension. This material will be used as needed to establish the base for construction of the other cover layers. Backfill material from excavation of the trench may serve as the grading fill.

2.3.1.8   Other Potential Surface Cover Components

A water conditioning layer consisting of quartz sand or crushed glass has been considered as a component of the surface cover. This layer is intended to increase the silica content of water that contacts the waste, reducing the dissolution of silica in the ILAW glass and decreasing the contaminant flux from the facility. No specifications have been given for this material.

A diversion layer consisting of a sand and gravel capillary barrier may potentially be used in the final design of the facility cover. The diversion layer would be used as an alternative to, or in addition to, the asphalt low permeability layer and would consist of well-graded sand overlying well-graded gravel. The diversion layer would likely be constructed at a 2% slope, corresponding to the other surface cover components. Specifications for the diversion layer component have not been given.

2.3.2   Trench Liner

Liner details are shown in Figure 2.15. Complete specifications for the liner components are given in CHG (2003c). A summary of the liner components and specifications is given here, listed in order from bottom to top as shown in Figure 2.15.

2.3.2.1   Liner Subgrade

The liner will be placed on a prepared subgrade consisting of native soils compacted to 95% relative compaction.

2.3.2.2   Admix Liner

The admix liner is intended to provide a low permeability barrier against the infiltration of liquids or contaminants. The admix liner consists of a moisture-conditioned admixture of natural base soil obtained from the IDF site and bentonite, compacted to achieve a hydraulic conductivity of no more than 10^{-7} cm/s. The base soil will be less than 1% by weight rocks greater than 2.54 cm diameter and will be at least 20% by weight finer than 0.075 mm (No. 200 U.S. Sieve). The admixture will consist of 12% by dry weight commercially prepared bentonite. Minimum required thickness of the admix liner is 3 feet.

2.3.2.3   Geomembrane Liners

The primary and secondary geomembranes are 60 mil textured high density polyethylene (HDPE). Specific requirements for physical, mechanical, and seam properties are given in CHG (2003c).

2.3.2.4   Geosynthetic Clay Liner

The bottom liner includes a geosynthetic clay liner (GCL) between the HDPE geomembranes. The low permeability component of the GCL is bentonite; the permeability to water of the GCL is required to be no greater than 5×10^{-9} cm/s.

2.3.2.5   Other Geosynthetic Materials

Various other geosynthetic materials are specified as components of the liner. These include geotextiles for separating soil layers (such as the operations layer and the drain gravel layer) and for cushioning the geomembrane liner (from the drain gravel layer). A geosynthetic composite drainage network (CDN) is specified above one or both of the geomembrane liners to facilitate drainage to the sumps. The geotextiles should have a minimum impact on the movement of water. The required transmissivity of the CDN is 5×10^{-4} m^2/s.

2.3.2.6   Drain Gravel

A 1-foot-thick layer of subrounded to rounded gravel is specified for the bottom liner of the trench above the primary geomembrane liner. This layer is intended to provide drainage to the sumps. The drain gravel must have a hydraulic conductivity greater than 0.1 cm/s.

2.3.3   Operations Layer

The waste packages will be placed on an operations layer consisting of excavation spoils and borrow materials with a maximum particle size of 2 inches and no more than 25% by weight finer than 0.075 mm diameter.

2.3.4   Waste Package Materials

These materials include the waste forms themselves as well as the materials of the waste packages and the filler material used to fill the void space within the waste packages. As stated above, the IDF is designed to accept several categories of waste. The characteristics of the disposed WTP melter packages are currently unspecified. The IDF risk assessment (Mann et al. 2003a) assumed that the melters contained some volume of waste glass and that the melters were grouted into steel overpacks $4.38 \times 5.29 \times 5.29$ m (for high-level waste melters) or $4.86 \times 6.79 \times 9.28$ m (for low-activity waste melters). The space between waste containers will be filled with a porous backfill material such as sand obtained from the trench excavation.

2.3.4.1   ILAW Glass and Container

The current design calls for the molten ILAW glass to be poured into steel cylindrical containers (1.22 m diameter by 2.29 m tall), with 85% of the container volume filled by the ILAW glass. The void space within ILAW containers is expected to be filled with an inert material, such as sand from a local source. Significant fracturing of the glass is anticipated, particularly where the glass forms an edge. In previous PA simulations, fracturing has been assumed to increase the surface area of the glass by about

ten times. The steel container is expected to corrode and have little impact on waste form release or flow and transport (Mann et al. 2001).

2.3.4.2   LLW/MLLW and Container

It is anticipated that the LLW/MLLW will be packaged in containers composed of steel, wood, or concrete (Wood et al. 1996). For such packages disposed in the Hanford Solid Waste Burial Grounds, void fractions are required to be no greater than 10%, although there are no requirements addressing compressibility (Puigh 2004). According to Mann et al. (2003a), there are no performance requirements for the waste form or the waste package for most LLW. For MLLW, waste package and waste form performance is generally provided by concrete containers or by grouting the waste. In past PAs (Wood et al. 1995, Wood et al. 1996), relatively simple, conservative models of waste form release have been used. These simple models do not require the unsaturated hydraulic properties of the LLW/MLLW waste forms.

2.3.4.3   WTP Melters and Overpack

The waste package designs for the WTP melters have not been specified. Puigh (2004) describes the current assumptions regarding the content and dimensions of these waste packages. The overpacks are assumed to consist of carbon steel boxes with the steel 8 inches thick for the HLW melters and 1 inch thick for the LAW melters. Overall dimensions of the waste packages, including overpacks, are assumed to be 5.29 m square by 4.38 m in height for the HLW melters and 6.79 by 9.38 by 4.86 m high for the LAW melters. It is assumed that the melter will contain a residual glass waste with a maximum glass volume of 5.75 m^3 for the HLW melters and 14.52 m^3 for the LAW melters (density of the cold glass is assumed to be 2.6 g/cm^3). It is also assumed that the melters will be grouted into their overpacks.

2.3.4.4   Supplemental ILAW Waste Forms

Alternative technologies, supplemental to the baseline vitrification process, are being considered for producing ILAW. A preliminary risk assessment for the disposal of supplemental ILAW waste forms at the IDF was completed in 2003 (Mann et al. 2003b). This risk assessment considered three supplemental technologies: bulk vitrification, Cast Stone (a cementitious waste form), and steam reformer. In earlier IDF PA analyses, it was assumed that all WTP supplemental technology waste would be processed by bulk vitrification (Puigh 2004), a process that involves mixing LLW, soil, and glass-forming chemicals and melting them in a large container (which becomes the waste package) by electrical resistance heating. However, Cast Stone is the current preferred alternative.

2.3.5   Backfill

Backfill within the trench will consist of excavation spoils and borrow materials. CHG (2003c) specifies such backfill (referred to as Earthfill) to have a maximum particle size of 10.1 cm (4 in.). For the fill around and between waste packages, the maximum particle size may be less to limit the potential formation of void spaces. As a result of the excavation, re-emplacement, and compaction, the backfill hydraulic properties are expected to differ from the properties of the naturally occurring sediments. The backfill is likely to be more homogeneous and isotropic.

3.0   Required Properties and Parameters

This section briefly describes the properties and parameters required for modeling unsaturated flow and contaminant transport in both the near- and far-field environments associated with the IDF. Additional parameters required for reactive transport modeling of the near-field environment are discussed in Krupka et al. (2004) and Pierce et al. (2004). This section is largely taken from Meyer et al. (2004).

3.1   Particle Size Distribution

The PSD is typically presented as the cumulative fraction by weight of particles whose mean diameter is less than a specific value. This physical property is useful for classifying soils and sediments (e.g., muddy sand, sandy gravel), but is not typically used directly in modeling. Those particles greater than 2 mm in diameter are often removed from the sample before measuring the PSD using standard methods (Gee and Or 2002). For ILAW PA purposes, however, the fraction greater than 2 mm should be included in the PSD or recorded as a gravel percentage. Classification of sediments that may include a large gravel fraction typically follows the Folk-Wentworth classification scheme (Folk 1980).

In the absence of a direct measurement of water retention (see Section 3.5), the PSD can be used to estimate water retention by assuming the PSD reflects the pore size distribution (Arya and Paris 1981; Arya et al. 1999a). PSD has also been related to the unsaturated hydraulic conductivity function (Arya et al. 1999b), other hydraulic and sorption parameters (Ward et al. 2006; Oostrom et al. 2006), and dispersivity. The PSD thus represents a fundamental property from which both sediment classification and flow- and transport-related properties and parameters can be estimated.

3.2   Particle Density

Particle density (ρ_p) is the mass of solids in a sample divided by the volume of the solids. It is typically used to calculate porosity. The sample fraction with a nominal diameter less than 2 mm may be used in the measurement of particle density. Flint and Flint (2002a) discuss methods to estimate particle density.

3.3   Bulk Density

The dry bulk density (ρ_b) is the mass of solids in a sample divided by the total (bulk) volume of the sample. The total volume includes the volume occupied by the solids, water (or other liquid), and air. Due to the potential for compaction during sampling, bulk density measured in the laboratory may vary from that measured in situ. Bulk density is often used to calculate porosity and retardation coefficients. Some techniques for estimating water retention and hydraulic conductivity may also use the bulk density.

3.4   Porosity

Porosity (ϕ) is the volume of voids in a sample (the air- and liquid-filled volume) divided by the total volume of the sample. It is typically calculated using measured values of particle and dry bulk densities.

$$\phi = 1 - \rho_b/\rho_p \tag{3.1}$$

The porosity can also be measured directly (Flint and Flint 2002b). For some materials, a fraction of the void space is disconnected and cannot take part in flow. For these materials, a distinction may be made between the total porosity and the effective porosity (also referred to as the connected or apparent porosity). The effective porosity is always less than or equal to the total porosity.

3.5 Water Retention Characteristics

Water retention [$\theta = f(\psi)$] in a porous medium refers to the relationship between water content and matric potential. Volumetric water content (θ) is the volume of water in a sample divided by the total volume of the sample. The matric potential (ψ) represents the capillary and adsorptive forces that attract and bind water to the soil matrix. (Matric potential is also referred to as soil water pressure or negative soil water tension.) A variety of methods are available to obtain water retention data (Dane and Topp 2002). In some cases, laboratory measurements of water retention have been conducted on samples for which the gravel fraction (particle diameter >2 mm) has been removed. The water contents obtained on such samples should be corrected for the gravel content (Bouwer and Rice 1983) before estimating the parameters of a water retention model.

Water retention is typically represented in simulation codes using one of a number of water retention models that have been presented in the literature. In this report, the model proposed by van Genuchten (1980) is used:

$$S_e(\psi) = [1 + (\alpha\psi)^n]^{-m} \tag{3.2}$$

where:
  ψ = matric potential
  S_e = effective saturation = $\dfrac{\theta - \theta_r}{\theta_s - \theta_r}$, $0 \le S_e \le 1$
  α = curve fitting parameter related to air entry pressure
  n, m = curve fitting parameters related to pore size distribution; the relationship, m=1-1/n, is often
        assumed
  θ_r = residual (or irreducible) water content
  θ_s = saturated water content.

The saturated water content is often assumed to be equal to porosity. It has been observed in laboratory and field measurements, however, that soils often cannot be saturated to the full porosity. This effect is more pronounced in the field, presumably because of the greater variation in soil structure and the inability to carefully control wetting. For this reason, θ_s is sometimes a fitted parameter, in which case it represents a field-saturated water content. Klute (1986) states that field-saturated water content is typically 80% to 90% of the porosity.

The residual water content is interpreted here as an empirical parameter and thus is generally a fitted parameter. This interpretation is a subject of debate (Nimmo 1991; Luckner et al. 1991). At very low matric potentials (large negative values), the van Genuchten (1980) model may provide a poor

representation of water retention. Alternative models have been proposed that improve the fit at low water contents (Rossi and Nimmo 1994; Fayer and Simmons 1995). Because water contents in the ILAW disposal facilities and the surrounding soils are expected to be low, accurate representation by the water retention model may be important. This is especially true if diffusion dominates the transport of contaminants and a water-content-dependent diffusion coefficient is used.

The remainder of the parameters in the van Genuchten water retention model are fitting parameters, estimated using measured or inferred water retention data.

There are many water retention models that could be used. Although the parameters in the van Genuchten model are related to the parameters used in other models (e.g., Lenhard et al. 1989), the transformation from one to the other is not always straightforward. Caution should be exercised in using the results presented in this report with water retention models other than the van Genuchten model.

Water retention in soils and sediment exhibits hysteresis: the observed water content at a given matric potential depends on whether the soil is being wetted or is drying. Models have been developed for describing this hysteresis (e.g., Parker and Lenhard 1987; Lenhard and Parker 1987), but the data on which the parameters of hysteresis can be estimated are often not available. Hysteresis is likely to be most important near the ground surface, where water content changes with time will be the largest. In the deeper materials (below the cover), water content changes will be less significant and hysteresis effects are not anticipated to be significant.

3.6 Saturated Hydraulic Conductivity

Darcy's law is used in models of subsurface flow to relate water flux to the potential gradient. Under saturated conditions, the proportionality constant in this relationship is the saturated hydraulic conductivity (K_s). Measurements can be made using a variety of methods (Dane and Topp 2002). Saturated hydraulic conductivity may exhibit anisotropy: a value that depends on the direction in which it is measured. Data on anisotropy are typically not available. Hydraulic conductivity anisotropy is not expected to be significant in any single near-field material because they will be relatively homogeneous, but may be very significant in the far-field materials. At a scale that encompasses multiple near-field materials that have contrasting properties, anisotropy should be considered.

Saturated hydraulic conductivity measurements are often made on small-scale laboratory samples. Because of the variability in natural materials, these small-scale measurements should not be interpreted as field-measured hydraulic conductivity values, which are typically larger. Values used in numerical models should represent the scale of the numerical grid size. The appropriate scaling methods for deriving model values of saturated hydraulic conductivity from laboratory measurements is currently a matter of scientific debate. Because the near-field materials will be relatively homogeneous, the scaling issue is expected to be less important for near-field materials than it is for the naturally occurring (far-field) sediments that may have significant geologic structure.

3.7 Unsaturated Hydraulic Conductivity

Under unsaturated conditions, the water flux occurring through a porous material in response to a specified potential gradient is strongly dependent on the water content of the material. The unsaturated

hydraulic conductivity [$K = f(\theta, \psi)$] describes this dependence. Direct measurement of the unsaturated hydraulic conductivity as a function of water content is possible using a variety of methods (Dane and Topp 2002). The expense of acquiring such data, however, means that it is often not available. More typically, the unsaturated hydraulic conductivity relationship is estimated using water retention and saturated hydraulic conductivity measurements and adopting a particular model (e.g., Mualem 1976). Hopmans et al. (2002) discuss indirect estimation of unsaturated hydraulic conductivity using inverse methods; these methods also require adopting a specific model.

The unsaturated hydraulic conductivity model used in this report is the model derived by van Genuchten (1980) using the relationship of Mualem (1976). This model can be written in terms of either the water content or the matric potential.

$$K(S_e) = K_s \sqrt{S_e} [1 - (1 - S_e^{1/m})^m]^2 \tag{3.3}$$

$$K(\psi) = K_s \frac{\{1 - (\alpha\psi)^{n-1}[1 + (\alpha\psi)^n]^{-m}\}^2}{[1 + (\alpha\psi)^n]^{Lm}} \tag{3.4}$$

Parameters in these equations are as defined for the water retention model and can be estimated using both water retention and unsaturated hydraulic conductivity data when available. The parameter L in the exponent of the denominator of Eq. (3.4) accounts for the lumped effects of pore connectivity and tortuosity and is treated as a fitting parameter. A value of $L = 0.5$ is typically assumed, although fitted data often yield values significantly different (e.g., Schaap and Leij 2000).

Khaleel et al. (1995) found that the van Genuchten-Mualem model did not accurately estimate unsaturated hydraulic conductivity for Hanford sediments at low water contents when these estimates were based solely on water retention data and a saturated hydraulic conductivity measurement, K_s. This condition may be explained by observing that the saturated hydraulic conductivity for these relatively coarse materials is dominated by large pores, whereas the unsaturated hydraulic conductivity appears to be dominated by small pores. Khaleel et al. (1995) recommended the use of at least one direct measurement of hydraulic conductivity at low water content as a match point, and that K_s values be fit instead of using their measured values. One concern with this approach, however, is that the fitted K_s values for disparate material types (e.g., Hanford sand and Plio-Pleistocene caliche) may end up being very similar, when in fact they should differ by orders of magnitude (Rockhold et al. 2009b).

Anisotropy in the unsaturated hydraulic conductivity is known to be dependent on saturation (Zaslavsky and Sinai 1981), with the anisotropy factor increasing as saturation is reduced (Stephens and Heermann 1988). In an earlier data package for far-field materials, Khaleel (2004) advocated the use of the Polmann (1990) model of anisotropy for representing sediments underlying the IDF site. Zhang et al. (2003b) provide an alternative model for representing the saturation-dependent anisotropy by assigning a directional dependence to L, which is referred to as the tensorial pore-connectivity-tortuosity (TCT) model. A detailed discussion of both the Polmann (1990) and TCT models of anisotropy for variably saturated porous media is provided in Section 7.0 of this report. We recommend the use of the TCT model for future IDF PA model calculations.

3.8   Dispersivity

Dispersivity (λ), when multiplied by the pore water velocity, yields the mechanical dispersion coefficient, which relates the dispersive solute flux to the solute concentration gradient. Dispersivity is generally larger in the direction of flow than in transverse directions and it is also scale dependent. Khaleel et al. (2002) and Khaleel (2004) discuss the issues related to scale-dependent dispersion with particular application to modeling flow and transport in the far-field IDF environment. Because of the smaller scale and the relative homogeneity within a given material, this issue is likely to be less important for the near-field materials.

Field measurements of dispersivity are rare and small-scale laboratory measurements may have marginal utility in estimating field-scale values, depending on the details of the porous media and column or flow cell setup. Therefore, in the absence of data, dispersivity values are often based on simple guidelines related to the size of the computational elements used in numerical simulation codes. For far-field modeling, Khaleel (2004) advocated the use of formulas from stochastic transport theory developed for saturated aquifer systems for application to unsaturated systems. An alternative method for estimating dispersivity values of variably saturated porous media is discussed in Section 7.0 of this report.

3.9   Diffusion Coefficient

The diffusion coefficient is the proportionality factor in Fick's law that relates the diffusive transport flux to the gradient in solute concentration. Diffusion results in mass transport from regions of high solute concentration to regions of lower concentration and occurs as a result of the random thermal motion (Brownian motion) of molecules and atoms. Diffusive transport in a dilute water solution is quantified by the free-water diffusion coefficient, D_f. For most simple aqueous species, D_f is about 10^{-5} cm^2/s (10^{-9} m^2/s). Kemper (1986) provides a table of diffusion coefficients of common ions in water; values range from approximately 4.8×10^{-6} to 1.6×10^{-5} cm^2/s at 15°C (see also Flury and Gimmi 2002).

In the constrained geometry of a porous medium, the diffusion coefficient is reduced compared to the diffusion coefficient in free aqueous solution. The intrinsic diffusion coefficient for a species within a saturated porous medium, D_i, can be expressed as

$$D_i = D_f \, \phi \, \delta / \tau \qquad\qquad (3.5)$$

where δ = a constrictivity factor

$1/\tau$ = a tortuosity factor.

The intrinsic diffusion coefficient has also been referred to as the effective diffusion coefficient.

The constrictivity factor in Eq.(3.5) represents a reduction in diffusion due to the constricted flow path caused by small pores and pore throats in the porous medium. The tortuosity factor represents a reduction in diffusion due to the increased path length taken by solute molecules in traveling through the porous medium. The tortuosity factor is given by $1/\tau = (L_s/L_e)^2$, where L_e is the length of the tortuous path and L_s is the straight-line path length (Porter et al. 1960).

In a saturated porous medium, the porosity, ϕ, in Eq. (3.5) will be the total porosity if all porosity in the porous medium is interconnected and can thus contribute to contaminant diffusion. If there are pores that do not contribute to diffusion (such as unconnected pores), the porosity appearing in Eq.(3.5) will be less than the total porosity. In unsaturated porous media, Eq.(3.5) must be modified to account for the additional reduction in pore-volume available for diffusion as a result of the reduced volumetric water content.

In practice, it is difficult to directly measure or reliably estimate the constrictivity and tortuosity factors. As a result, the intrinsic diffusion coefficient is frequently modeled empirically as a function of the porosity and/or water content (e.g., Millington 1959; Papendick and Campbell 1980; Kemper and van Schaik 1966). The value of the diffusion coefficient can vary significantly depending on which of the empirical relationships is used, particularly at low water contents. Under the appropriate conditions, these differences may significantly impact predicted contaminant concentrations. Differences are potentially greatest for diffusion-dominated transport, such as occurs within the IDF near-field environment. A generalization of the power function model proposed by Campbell (1985) is recommended for use in the IDF PA. This model has the form

$$D_i(\theta) = a\, D_f\, \theta^{\,b}$$
(3.6)

where a and b are empirical coefficients. Appropriate values of these coefficients for use in the IDF PA are discussed in Section 4.0.

The chemical contributions to diffusion can potentially be quite varied and significant. If we assume a very simple chemical process, i.e., reversible surface adsorption having fast kinetics and a linear isotherm (adsorption proportional to the concentration in solution via a fixed constant, K_d), then diffusion of a reactive contaminant can be characterized by an apparent diffusion coefficient, D_a,

$$D_a = D_i \,/\, (\theta + \rho_b K_d)$$
(3.7)

Estimated values of K_d for a given constituent and sediment can be obtained from an earlier geochemistry data package (Krupka et al. 2004).

4.0 Best Estimates of Physical and Hydraulic Properties and Parameters for Near-Field Materials

This section contains best-estimate values for the hydraulic parameters of near- and far-field materials to be used in PA analyses of the IDF. The best-estimate values for near-field materials are taken from Meyer et al. (2004). The technical basis for some of the near-field material parameter values is provided by Meyer and Serne (1999). For the sake of completeness, however, all parameter values are included in the summary table.

In determining the best-estimate parameter values, it has been assumed in most cases that the saturated volumetric water content is equal to the porosity. This assumption was made to avoid the application of an arbitrary factor to account for field saturation in such disparate materials as gravel, fractured glass, and concrete. In those cases where a model was fit to water retention data, the saturated water content was a fitted parameter and may be less than the porosity. Best-estimate values for transport parameters of near-field materials are discussed in Section 5.0.

4.1 Surface Cover Materials

In the most recent PA analysis conducted for the disposal of ILAW (Mann et al. 2001), the surface cover was not explicitly simulated. (This was also the case for previous versions of the ILAW PA.) Instead, a piece-wise steady-state water flux through the surface cover was assigned based on data and analyses described in Fayer et al. (1999). Meyer and Serne (1999) nonetheless presented best-estimate parameter values for the components of the surface cover. The only component of the surface cover for which the best-estimate parameters are updated here is the compacted silt loam.

4.1.1 Compacted Silt Loam

The water retention parameter values for this material were previously estimated using water retention data measured on silt loam samples compacted to a bulk density of 1.37 g/cm^3. These water retention data were adjusted for the effect of increasing the bulk density to 1.76 g/cm^3 (the value for this material specified in DOE 1993a using the particle size-water retention relationship given in Arya and Paris (1981).

Estimates of the water retention parameters for the compacted silt loam component of the surface cover were improved by making laboratory measurements on compacted samples of silt loam soil obtained on the Hanford Site. The surface cover design calls for the 0.5 m layer of silt loam to be compacted to 90% of optimum dry density with the estimated in-place bulk density given as 1.76 g/cm^3. Fayer et al. (1999) reported that a Warden silt loam soil could not be compacted to an in-place bulk density greater than 1.6 g/cm^3 in a lysimeter study. In addition, DOE (1993b) reported a maximum dry bulk density of 1.75 g/cm^3 for the McGee Ranch silt loam soil. A bulk density of 1.58 g/cm^3 is 90% of this maximum for the McGee Ranch silt loam. For the surface cover, an in-place bulk density of about 1.6 g/cm^3 thus appears to be a practical target for silt loam soils from the Hanford Site.

Water retention measurements were made on three samples of silt loam soil packed to a bulk density of 1.58 g/cm^3 using the method of Lenhard and Parker (1988) for capillary pressures between 0 and

200 cm and using a pressure chamber apparatus for pressures of 1000 and 3000 cm.[1] Both nonhysteretic and hysteretic water retention measurements were conducted. Hysteresis was significant and should be considered when modeling the compacted silt loam (and silt loam – gravel admix) component of the surface cover. Unsaturated hydraulic conductivity was also measured on two samples packed to a bulk density of 1.63 g/cm^3 using a steady-state centrifugation method (ASTM D6527-00).

Parameters of the van Genuchten model [Eq. (3.2) and Eqs. (3.3)/(3.4)] were fit to the compacted silt loam data using nonlinear least squares regression. The hysteretic data were fit to the model of Parker and Lenhard (1987) and Lenhard and Parker (1987). This model uses similar expressions to Eq. (3.2), except for two differences. The model accounts for entrapped air using a parameter, θ_{at}, which is the maximum amount of air entrapment when the initial condition is air-dry. In addition, instead of a single α parameter, two α parameters are used: one for describing the water drainage relation ($^d\alpha$) and one for describing water imbibition ($^i\alpha$). Based on the analysis of the experimental data, the following best-estimate parameter values (for the hysteretic model) are proposed for the compacted silt loam. The best-estimate value for the air entrapment parameter is $\theta_{at} = 0.03$.

Table 4.1. Best-Estimate Parameter Values for Compacted Silt Loam (from Meyer et al. 2004)

ρ_p (g/cm^3)	ρ_b (g/cm^3)	θ_s	θ_r	$^d\alpha$ (cm^{-1})	$^i\alpha$ (cm^{-1})	n	K_s (cm/s)
2.72	1.58	0.39	0.09	0.006	0.014	1.92	5.2×10^{-5}

4.2 Trench Liner Materials

The proposed design of the ILAW disposal facility at the time Meyer and Serne (1999) was written involved the placement of the ILAW waste packages within a concrete vault constructed within a trench. Meyer and Serne (1999) did not include any liner components in their analysis. In the 2001 ILAW PA (Mann et al. 2001), the concrete vault was not considered in the PA simulations. That is, the performance of the facility was evaluated assuming that the disposal facility consisted solely of the ILAW waste form surrounded by backfill. The contaminated water at the lower extent of the backfill traveled directly into the upper vadose zone. In effect, these analyses assumed that the life of the trench liner will be insignificant with respect to the time-frame for corrosion of the waste form, and that a degraded liner will not impact flow and transport.

The current design of the trench liner includes a number of low permeability components: the admix liner, two geomembrane liners, and a geosynthetic clay liner. It is conservative to assume that these components do not impact the long-term performance of the IDF, as long as the so-called bathtub effect does not occur. This effect would occur if water infiltrates into the facility faster than it is transmitted through the liner (or removed from the liner via the sumps). The upper bound recharge rate through the Modified RCRA C cover is estimated to be 1.3×10^{-9} cm/s (Fayer and Szecsody 2004). This is less than the design hydraulic conductivity of the admix liner and is comparable to the geosynthetic clay liner permeability. Because the design permeability of the geomembrane is lower than 1.3×10^{-9} cm/s, a

---

[1] Lenhard RJ and PD Meyer. 2000. *Hydraulic and Diffusion Property Measurements of ILAW Near-Field Materials: FY00 Status Report.* Letter Report to CH2MHill Hanford Group, Inc., November 3, 2000, Pacific Northwest National Laboratory, Richland, Washington.

potential for the bathtub effect exists. The actual occurrence of this effect and the resulting accumulation of water above the liner will depend on the quality and longevity of the geomembrane liners.

Best-estimate unsaturated hydraulic parameters are not provided for the trench liner components since the assumption that the liner has no impact on flow and transport is likely to be conservative. A sensitivity case can be run to determine the potential impact of the bathtub effect on waste form release and facility performance.

4.3   Operations Layer

It is recommended that this material be assumed to have the same hydraulic properties as the high-density backfill (see Section 4.5).

4.4   Waste Package Materials

4.4.1   ILAW Glass

It is anticipated that the glass waste will be poured into steel packages and allowed to cool, whereupon significant fracturing is anticipated, particularly on the exterior of the glass and along edges. The 2001 ILAW PA (Mann et al. 2001) assumed that the fracturing will be sufficient to allow the glass waste to be treated as an effective porous medium, instead of a fractured medium, and thus the parameters are the same as for the other materials. All porosity in the glass will reside in the fractures (i.e., the glass matrix has no porosity). Total porosity is anticipated to be small—on the order of a few percent.

Meyer and Serne (1999) based the ILAW glass hydraulic properties on expected physical features of the glass. To provide direct measurements of glass hydraulic properties, samples of simulated ILAW glass (the glass known as HAN-28) were produced and fractured by rapid cooling. A photograph of the top of one of these samples is shown in Figure 4.1. Indirect methods must be used to characterize small fractures in materials. A common approach is to use mercury porosimetry, which involves injecting mercury into a porous medium under controlled pressures. Based on the volume of mercury injected over a change in pressure, the volume of fractures with known effective radii can be determined. In the petroleum industry, the pore-size distribution of consolidated rock cores is typically determined by mercury porosimetry. The diameter of the rock cores used in mercury porosimetry is generally less than 1 inch (i.e., 2.54 cm). Because of the 1-inch size limitation associated with commercially available mercury porosimetry, another measurement procedure needed to be developed that was suitable for larger-sized glass cylinders such as the glass samples used here.

The approach adapted relies on methods used in soil science to characterize the relations between fluid pressures and saturations. Theoretically, wetting fluid will remain in pores/fractures until the difference between the non-wetting and wetting fluid pressures (i.e., the capillary pressure) exceeds a critical value. The relationship between capillary pressure and size of pores/fractures is based on Laplace's equation of capillarity:

$$P_c = \sigma\left(\frac{1}{R_1} + \frac{1}{R_2}\right) \tag{4.1}$$

where P_c is the capillary pressure, σ is the interfacial tension between the non-wetting and wetting fluids, and R_1 and R_2 are radii of curvature of the fluid interfaces in orthogonal directions. The radii of pores or fractures can be determined from the radii of curvature of the fluid interfaces in the pores/fractures and knowledge of the angle that the wetting fluid makes with the solid surfaces (i.e., contact angle). For simplicity, it is common to assume that the contact angle the wetting fluid makes with the pore/fracture walls is zero, which makes the radii of curvature of the fluid interface equal to the pore/fracture radii. This assumption is common because it is difficult to characterize contact angles in the complex pore/fracture geometry that occurs in porous media.

Assuming that the contact angle is zero and the length of the fracture (R_1) is much larger than the diameter (i.e., opening) of the fracture ($2R_2$), then Eq. (4.1) reduces to

$$P_c = \frac{2\sigma}{D_f}$$
(4.2)

where D_f is the diameter of the fracture. Using this theory, measurements of air-water saturation-pressure relations can be used to characterize the effective size distribution of fractures in the glass cylinders.

Two different apparatuses were used to measure saturation-pressure relations on three glass cylinders.[1] For capillary pressures greater than 100 cm of water height, a pressure chamber was used (Dane and Hopmans 2002). Measurements were conducted at capillary pressures of 200, 400, 600, 800, and 1,000 cm of water height. For capillary pressures less than 100 cm of water height, a tension table was used (Romano et al. 2002). Water saturations were measured at capillary pressures of 2, 10, 20, 30, 40, 50, and 60 cm of water height. A tension table allows for greater sensitivity in conducting measurements, but can only be employed for lower capillary pressures.

From Eq. (4.2), it can be seen that a unique effective fracture diameter corresponds to a capillary pressure, provided hysteresis is neglected. The difference in water mass between two saturation-pressure measurements is therefore related to the volume of fractures with sizes corresponding to the capillary pressures. In differential form, the effective fracture diameter distribution can be determined from

$$\frac{dS_e}{dD_f} = \frac{dS_e}{d\left(\dfrac{1}{P_c}\right)}$$
(4.3)

To solve Eq. (4.3), one needs to express S_e in terms of P_c, which was accomplished here using the van Genuchten water retention function. The effective fracture diameter distribution for the three glass samples was estimated.

Because of potential errors associated with boundary effects (between the glass and the steel cylinder), the difference between the water mass at a capillary pressure of 2 cm of water height and dry conditions was used to represent the total fracture volume in the glass. A water mass density of 0.998 g/cm^3 was used to convert the water mass measurements into volumes. Using the 2 cm capillary

---

[1] Lenhard RJ and PD Meyer. 2000. *Hydraulic and Diffusion Property Measurements of ILAW Near-Field Materials: FY00 Status Report.* Letter Report to CH2MHill Hanford Group, Inc., November 3, 2000, Pacific Northwest National Laboratory, Richland, Washington.

pressure measurements to calculate the total volume of fractures and using the average total volume of the glass cores (core diameter ~5 cm; core height ~6 cm), the total porosity of the glass fractures was estimated to be 2% or 3% of the total glass volume for each of the samples. This porosity is consistent with the expected porosity of the ILAW glass.

By calculating the difference in water mass between the capillary pressure measurements and employing Eq. (4.2) to relate capillary pressure to a fracture diameter, the volume of fractures between fracture sizes was determined. An air-water interfacial tension of $0.07\ \mathrm{N\ m^{-1}}$ was used in these calculations. The fracture volumes for the three samples are given in Table 4.2. This information may be useful in the event that the actual fracture characteristics of the ILAW glass are measured. A model could then be used to estimate bulk effective hydraulic properties from knowledge of the fracture characteristics. Such a model has been developed for potential use in the IDF PA.[1]

The van Genuchten model was fit to the pressure-saturation data for the fractured glass samples. Geometric mean values are given below as the best-estimate parameter values. The saturated hydraulic conductivity of these samples was not measured because of the void space between the boundary of the glass and the steel cylinder.

Table 4.2. Volume of Fractures as a Function of Fracture Diameter Measured on Samples of Simulated ILAW (HAN-28) Glass (from Meyer et al. 2004)

Fracture Diameters (m)	Volume of Fractures ($\mathrm{cm^3}$)		
	Glass Sample 1	Glass Sample 2	Glass Sample 3
7.16×10^{-4} to 1.43×10^{-4}	0.07	0.06	0.17
1.43×10^{-4} to 7.16×10^{-5}	0.68	0.50	1.36
7.16×10^{-5} to 4.77×10^{-5}	0.21	0.24	0.37
4.77×10^{-5} to 3.58×10^{-5}	0.12	0.10	0.08
3.58×10^{-5} to 2.86×10^{-5}	0.22	0.19	0.20
2.86×10^{-5} to 2.39×10^{-5}	0.06	0.05	0.07
2.39×10^{-5} to 7.16×10^{-6}	1.16	0.93	0.98
7.16×10^{-6} to 3.58×10^{-6}	0.03	0.07	0.08
3.58×10^{-6} to 2.39×10^{-6}	-	0.01	0.04
2.39×10^{-6} to 1.79×10^{-6}	-	0	0.01
1.79×10^{-6} to 1.43×10^{-6}	-	0	-
$< 1.43 \times 10^{-6}$	-	0.20	-

Saturated hydraulic conductivity measurements were made on a $7.5 \times 7.5 \times 5$ cm block of simulated ILAW glass.[2] The glass block was subjected to mechanical stress on all sides simultaneously to cause

---

[1] Freedman VL, EJ Freeman, and PD Meyer. 2002. *Status Report for ILAW Near-Field Hydrology Efforts Performed in FY02, Modeling Methodology for Determining the Unsaturated Hydraulic Properties of ILAW Glass.* Letter Report to CH2MHill Hanford Group, Inc., September 30, 2002, Pacific Northwest National Laboratory, Richland, Washington.

[2] Saripalli KP, MJ Lindberg, and PD Meyer. 2003. *Effect of Chemical Reactions on the Hydraulic Properties of ILAW Near-field Materials: Experimental Investigation.* Letter Report to CH2MHill Hanford Group, Inc., September 30, 2003, Pacific Northwest National Laboratory, Richland, Washington.

internal fracturing; approximately one to two fractures that progressed into the block were formed on each face. Care was taken to form at least some of the fractures to be connective, but none of the fractures to be connecting two opposite faces continuously. Overall, the fractures were conductive and assumed to be randomly connected. The fractured blocks were secured together using a platinum wire wrap. The measured porosity of this block was 0.03, similar to the small cylinders discussed above and consistent with the expected ILAW glass porosity. Saturated hydraulic conductivity of the fractured glass block was measured using a static head permeameter method. Three replicates yielded an average value of 3.1×10^{-5} cm/s (standard deviation was 2.0×10^{-7} cm/s). This is significantly lower than the assumed value of Meyer and Serne (1999), but since this is a direct measurement on a fractured glass sample, it is given in Table 4.3 as the best-estimate value. However, since current glass formulations differ from those considered in earlier IDF PA calculations, we recommend that these types of measurements also be performed on samples of the current glass formulations.

Table 4.3. Best-Estimate Parameter Values for ILAW Glass (from Meyer et al. 2004)

ρ_p (g/cm^3)	ρ_b (g/cm^3)	θ_s	θ_r	α (cm^{-1})	n	K_s (cm/s)
2.68	2.63	0.02	0.0006	0.044	1.88	3.1×10^{-5}

Figure 4.1. Photograph of Fractured Glass Cylinder 2 inches in Diameter and 2.75 inches High (from Meyer et al. 2004)

4.4.2   LAW/MLLW

As stated previously, there are generally no performance requirements for the waste form or the waste package for most LAW (Mann et al. 2003a). For MLLW, waste package and waste form performance is generally provided by concrete containers or by grouting the waste. In past PAs (Wood et al. 1995; Wood et al. 1996), relatively simple, conservative models of waste form release have been used. These simple models do not require the unsaturated hydraulic properties of the LAW/MLLW waste forms. Should flow

and transport through the LAW/MLLW packages be explicitly modeled, however, the concrete properties from Meyer and Serne (1999) can be used to represent the grout/concrete components of the waste packages. These parameters were obtained using centrifuge measurements on 50-year-old concrete cores taken from a bunker on the Hanford Site and are presented below.

Table 4.4. Best-Estimate Parameter Values for Concrete (from Meyer et al. 2004)

ρ_p (g/cm^3)	ρ_b (g/cm^3)	θ_s	θ_r	α (cm^{-1})	n	K_s (cm/s)
2.63	2.46	0.067	0.00	3.87×10^{-5}	1.29	1.33×10^{-9}

4.4.3 WTP Melters and Overpack

Should flow and transport through the WTP melter waste packages be explicitly modeled, the residual waste material remaining in the WTP melters can be modeled as ILAW glass using the hydraulic parameters given in Table 4.3. Assuming the melters are grouted into their overpacks, the hydraulic parameters for concrete given in Table 4.4 can be used for the grouted portion of the waste package. The steel components of the melters and overpack will be impermeable as long as they are intact. Meyer and Serne (1999) presented representative hydraulic parameters for fully corroded steel based on measurements made on crushed rock samples of hematite, goethite, and lepidocrocite, the expected dominant steel corrosion products. Those parameters are reproduced here for potential use in modeling the steel components of the WTP melter waste packages.

Table 4.5. Best-Estimate Parameter Values for Fully Corroded Steel (from Meyer et al. 2004)

ρ_p (g/cm^3)	ρ_b (g/cm^3)	θ_s	θ_r	α (cm^{-1})	n	K_s (cm/s)
4.16	2.30	0.39	0.04	0.0008	1.77	2.2×10^{-6}

4.4.4   Supplemental ILAW Waste Forms

Cast Stone is the current preferred alternative for supplemental ILAW waste forms. Properties for Cast Stone materials are being measured and will be reported in a separate data package. For completeness, however, information regarding properties of the previously considered bulk vitrification waste package is still included here.

Based on tests of the bulk vitrification process (see Section 2.3.4.4), the materials of the waste package could include the steel container, insulating foam board, sand, an insulating cast (brick-like) material, and the glass waste vitrification product. Parameters for fully corroded steel are given in Section 4.4.3. No properties are provided here for the foam board. Properties of backfill (Section 4.5) can be used for the sand. (If the sand used has a more uniform PSD than the backfill, these parameters should be modified.) Unless or until more-specific data are available, a vitrified waste product could be assigned the parameters of the ILAW glass given in Table 4.3.

Physical properties were measured on a sample cast material used in bulk vitrification tests.[1] The particle and bulk densities are reported in Table 4.6. Total porosity calculated from these values is 0.27. Effective porosity measured on the sample cast material was reported to be 0.17,[2] only 63% of the total porosity. For comparison, Hall and Hoff (2002) report a particle density range of 2.6 to 2.8 g/cm^3 for typical brick ceramic compositions and a porosity range of 0.1 to 0.45 depending on the type of brick material. Assuming an average particle density of 2.68 g/cm^3, the corresponding bulk density range is about 2.4 to 1.5 g/cm^3.

Unsaturated hydraulic property measurements of cast materials are rare. Hall and Hoff (2002) discuss water flow in building materials, including brick materials, but do not report any water retention data. They provide a figure of water retention measurements on "common clay brick ceramic"[3] illustrating a van Genuchten model fit. The data of Hall and Hoff (2002) exhibited significant hysteresis. Due to the heat associated with the vitrification process, the cast material is likely to be dry when moved to the IDF. Use of the wetting curve was therefore felt to be appropriate. Figure 2.3 of Hall and Hoff (2002) was scanned, the data were digitized, and Eq. (3.2) was fit to the data. The resulting water retention parameters are given in Table 4.6. Note that this procedure resulted in a saturated water content (0.15) less than the effective porosity measured on the sample bulk vitrification material (0.17).

Hall and Hoff (2002) reference two measurements of the hydraulic conductivity in clay brick ceramic. The values reported are 3.2×10^{-6} cm/s for a brick with porosity of 0.40 and 3.8×10^{-7} cm/s for a brick with porosity of 0.31. The geometric mean of these values is included in Table 4.6.

Table 4.6. Best-Estimate Parameter Values for the Cast Material of the Bulk Vitrification Waste Package (from Meyer et al. 2004)

ρ_p (g/cm^3)	ρ_b (g/cm^3)	θ_s	θ_r	α (cm^{-1})	n	K_s (cm/s)
3.1	2.26	0.15	0.00	0.00064	1.90	1.1×10^{-6}

Once again, Cast Stone is the current preferred alternative supplemental ILAW waste form and properties of Cast Stone materials will be reported in a separate data package.

4.5 Backfill

The best-estimate parameters for the backfill presented in Meyer and Serne (1999) were based on analysis of a single sample composited from 85 individual samples obtained at depths of 3 to 17 m from 200 East Area boreholes. Additional data were collected and used to update the backfill hydraulic parameter estimates in Meyer et al. (2004).

Two samples were collected from a borehole (B8501, discussed in Reidel et al. 1998) adjacent to borehole 299-E17-21 near the southwest corner of the IDF site. The samples were collected at depths of

---

[1] EM Pierce, May 2004, personal communication with PD Meyer.
[2] EM Pierce, May 2004, personal communication with PD Meyer.
[3] Hall and Hoff (2002), Figure 2.3, page 50.

6.7 and 8.2 m and texturally were classified as sands. Water retention measurements were made on these samples using the method of Lenhard and Parker (1988). Bulk density for these measurements was 1.65 g/cm^3. Unsaturated hydraulic conductivity measurements were conducted on the same samples using the steady-state centrifugation method (ASTM D6527-00). Bulk densities for the samples analyzed in the centrifuge were higher at approximately 1.86 g/cm^3. In addition to these two samples, 60 samples were collected at depths of 4 to 16 m from an experimental site adjacent to the IDF site (the Vadose Zone Transport Field Study Site). These samples were collected in a (mostly) undisturbed condition and analyzed for PSD, bulk density, water retention, and hydraulic conductivity (Schaap et al. 2003). For these 60 samples, sand percentage was always greater than 72.5%, clay percentage was always less than 7.5%, and silt percentage ranged from 6% to 22%. Bulk densities ranged from 1.39 to 1.71 g/cm^3, with an average value of 1.57 g/cm^3.

Excavation spoils and borrow material from the IDF site are likely to be used in two conditions: a relatively high-bulk-density application in which the soil can be well compacted, and a relatively low-bulk-density application in which compaction will be more difficult (such as when the soil is used to fill between the waste packages). The data from the samples described above were divided into two groups based on the sample bulk densities, with a density of 1.60 g/cm^3 being the cutoff between the groups. Estimated parameter values were then examined to determine best-estimate values for the IDF backfill materials for each of the two groups. The direct water retention and saturated hydraulic conductivity measurements were used for the data from Schaap et al. (2003). A particle density of 2.71 g/cm^3 was assumed. Values for α, n, and K_s are based on the geometric means of the measurements.

Table 4.7. Best-Estimate Parameter Values for Low- and High-Density Backfill (from Meyer et al. 2004)

ρ_p (g/cm^3)	ρ_b (g/cm^3)	θ_s	θ_r	α (cm^{-1})	n	K_s (cm/s)
2.71	1.51	0.37	0.03	0.057	2.8	1.86×10^{-2}
2.71	1.66	0.35	0.03	0.065	1.7	4.91×10^{-3}

4.6 Summary Tables

Values of best-estimate parameters for near-field materials of the IDF are summarized here in two tables: one for the materials of the surface cover and one for the remainder of the materials. For those materials not appearing in tables earlier in this chapter, values were taken from Meyer and Serne (1999) and are presented here solely for reader convenience. Similarly, parameter symbols are defined in a footnote to Table 4.9 to assist the reader.

Table 4.8. Summary of Best-Estimate Parameter Values for Components of the Surface Cover (from Meyer et al. 2004)

Material	ρ_p (g/cm^3)	ρ_b (g/cm^3)	θ_s	θ_r	α (cm^{-1})	n	K_s (cm/s)
Silt Loam-Gravel Admix	2.72	1.48	0.456	0.0045	0.0163	1.37	8.4×10^{-5}
Compacted Silt Loam	2.72	1.58	0.39	0.09	$0.006^{\dagger}$	1.92	5.2×10^{-5}
Sand Filter	2.76	1.88	0.318	0.030	0.538	1.68	8.58×10^{-5}
Gravel Filter	2.72	1.94	0.290	0.026	8.10	1.78	1.39×10^{-2}
Gravel Drainage	2.72	1.94	0.290	0.006	17.8	4.84	2.0
Asphaltic Concrete	2.63	2.52	0.04	0.000	1.0×10^{-7}	2.0	1.0×10^{-11}

Table 4.9. Summary Table of Best-Estimate Parameter* Values for IDF Near-Field Materials (from Meyer et al. 2004)

Material	ρ_p (g/cm^3)	ρ_b (g/cm^3)	θ_s	θ_r	α (cm^{-1})	n	K_s (cm/s)
ILAW Glass	2.68	2.63	0.02	0.0006	0.044	1.88	3.1×10^{-5}
Concrete	2.63	2.46	0.067	0.00	3.87×10^{-5}	1.29	1.33×10^{-9}
Fully Corroded Steel	4.16	2.30	0.39	0.04	0.0008	1.77	2.2×10^{-6}
Bulk Vit. Cast Material	3.1	2.26	0.15	0.00	0.00064	1.90	1.1×10^{-6}
Low-Density Backfill	2.71	1.51	0.37	0.03	0.057	2.8	1.86×10^{-2}
High-Density Backfill	2.71	1.66	0.35	0.03	0.065	1.7	4.91×10^{-3}

$*\rho_p$ – particle density
ρ_b – bulk density
θ_s – saturated water content
θ_r – residual water content
α - water retention parameter
n – water retention parameter
K_s – saturated hydraulic conductivity

---

† Drainage curve α. Imbibition curve α is 0.014 cm^{-1}.

5.0 Best-Estimate Values for Transport Parameters of Near-Field Materials

Meyer and Serne (1999) discussed the best-estimate transport parameter values for near-field materials of the ILAW disposal facility. Consideration of transport parameters was limited to dispersivity and diffusion coefficients. Diffusion is expected to be the dominant transport mechanism from the IDF. Parameters governing the chemistry of the near-field materials (e.g., adsorption distribution coefficients and solid phase solubility controls) can be found in other data packages (Pierce et al. 2004; Krupka et al. 2004).

5.1 Dispersivity

Meyer and Serne (1999) recommended a dispersivity value of 10 cm based on a field experiment conducted at the IDF site,[1] and the expected conditions of the IDF near field (limited scale, relative homogeneity, low pore-water velocities). No modification of this value is recommended here. Separate estimates of dispersivities for far-field materials are provided in a later section.

5.2 Diffusion Coefficient

5.2.1 Concrete

Diffusion in concrete was reviewed in detail by Meyer and Serne (1999), with best-estimate apparent diffusion coefficient values for a variety of constituents provided. That discussion is not repeated here and no modification of the best-estimate diffusion coefficient values is recommended.

5.2.2 Backfill (and Other Granular Materials)

Measurements of intrinsic diffusion coefficients were reported in Conca and Wright (1990, 1991) for a variety of materials, including sediments from the Hanford Site. Conca and Wright (1991) observed that the measured $D_i(\theta)$ relationship (for a chemically nonreactive solute) was remarkably similar for a variety of materials, which included porous and nonporous tuff gravels, bentonite clays, Hanford sandy soils and gravels, and whole rock cores of non-welded tuff. Conca and Wright (1990) also observed, however, that the diffusion coefficient at a given water content tended to be lower for samples with larger particle sizes and more-hydrophobic mineral surfaces.

The data of Conca and Wright (1991) were fit to the power function model given earlier as Eq. (3.6) $[D_i(\theta) = a\, D_f\, \theta^b]$. Using a value of $D_f = 1.84 \times 10^{-5}$ cm^2/s resulted in best-fit values for the coefficients of a = 1.65 and b = 1.96. The data of Conca and Wright (1991) are shown in Figure 5.1 as the circles, with the fitted relationship represented by the dashed curve.

---

[1] Ward AL, RE Clayton, and JS Ritter. 1998. *Hanford Low-Activity Tank Waste Performance Assessment Activity: Determination of In Situ Hydraulic Parameters of the Upper Hanford Formation.* Letter Report to Fluor Daniel Hanford, Inc., December 31, 1998, Pacific Northwest National Laboratory, Richland, Washington.

The intrinsic diffusion coefficient was estimated for two sand samples obtained from a borehole near the southwest corner of the IDF site and for two coarse sand samples obtained northeast of the IDF site at the former grout site using electrical conductivity measurements made at a series of water content values following the procedure described in Conca and Wright (1990). The estimated diffusion coefficients for the grout site sand and IDF borehole sands are shown on Figure 5.1 (as the solid symbols). The borehole sand data lie very close to the data of Conca and Wright (1991), although the minimum water contents were 8% to 10%, much larger than the minimum values measured by Conca and Wright (1991). (Measurements using the centrifuge equipment were limited to hydraulic conductivities greater than about 5×10^{-10} cm/s.) The grout site samples had diffusion coefficients that were somewhat smaller than the range of values measured by Conca and Wright (1991), particularly at the lowest water content value measured for each sample. The smaller diffusion coefficients for this relatively coarse material are consistent with the observations of Conca and Wright (1990).

A linear fit to the logarithm of the combined diffusion data for the grout site and borehole sand samples resulted in best-fit values for the parameters of the power function of a = 3.95, b = 2.64. The estimated variance of these parameter values was much larger than for the fit to Conca and Wright's data. The best-fit parameter values for the complete set of data were a = 1.49, b = 1.96. A value of $D_f = 1.84 \times 10^{-5}$ cm^2/s was assumed in determining the empirical parameters. These best-fit power function relationships are included in Figure 5.1.
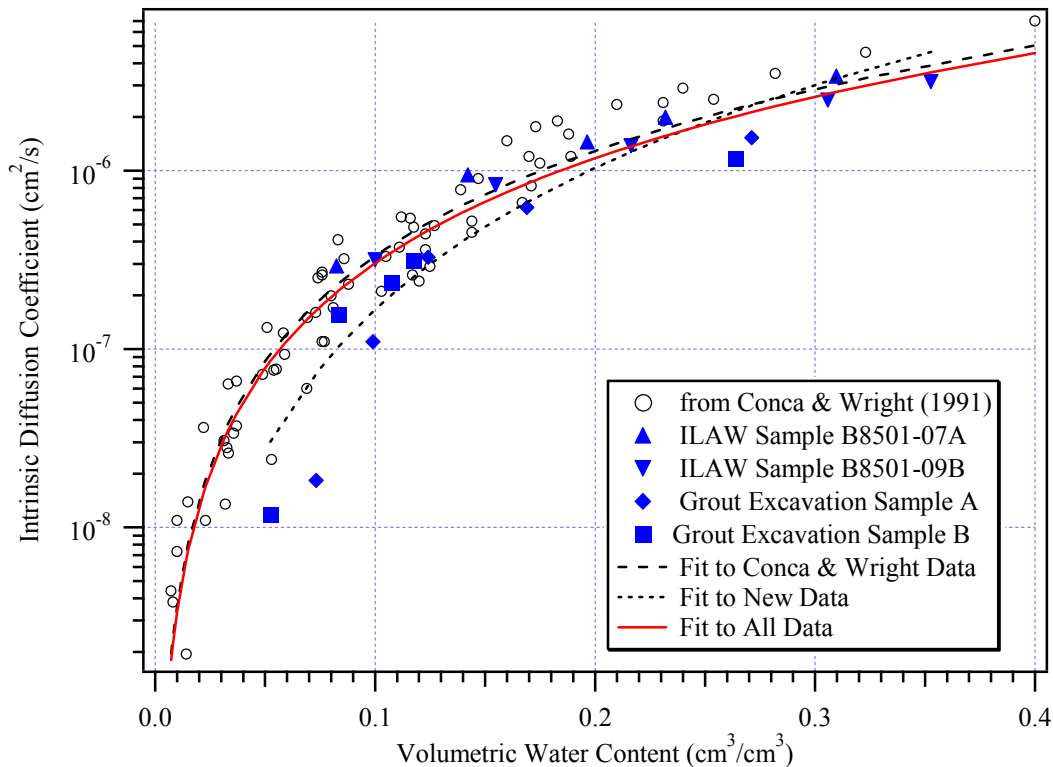
Figure 5.1. Diffusion Coefficient Estimates from Conca and Wright (1991) and for Samples Obtained Near the IDF Site. Best-fit power function relationships [Eq. (3.6)] are shown as well (from Meyer et al. 2004).

It is recommended that Eq. (3.6) be used in the ILAW PA simulations to model diffusion in backfill and other granular materials of the near field. The results presented here suggest that a = 1.49, b = 1.96 are appropriate parameters for this diffusion model. The recommended equation for the diffusion coefficient in backfill and other granular materials of the near field is thus

$$D_i(\theta) = 1.49\, D_f\, \theta^{1.96} \tag{5.1}$$

The free-water diffusion coefficients, D_f, for individual contaminants can be selected from Table 5.3 of Meyer and Serne 1999 or calculated using one of the available equations (see Grathwohl 1998).

5.2.3   ILAW Glass

Measurements of diffusion of three solutes (Cs, Sr, and pentafluorobenzoate (PFBA)) through a saturated fractured glass block were made on a $7.5 \times 7.5 \times 5$ cm block of simulated ILAW glass (LAWBP1).[1] The glass block was subjected to mechanical stress on all sides simultaneously to cause internal fracturing; approximately one to two fractures that progressed into the block were formed on each face. Care was taken to form at least some of the fractures to be connective, but none of the fractures to be connecting two opposite faces continuously. Overall, the fractures were conductive and randomly connected. The fractured blocks were secured together using a platinum wire wrap. Diffusion experiments were conducted using an experimental method, similar in design to that reported by Grathwohl (1998), called the time-lag method. In this method, a constant concentration boundary condition is maintained at the inlet face of the porous medium over a long period (typically several weeks depending on the D_i of the particular solute and medium combination). The mass of solute at the outlet face is monitored as a function of time to yield a solute mass-time relationship that can be used to obtain the diffusion coefficient. Under saturated conditions, the diffusion coefficients obtained from the Cs, Sr, and PFBA tracers were 1.42×10^{-5}, 1.66×10^{-5}, and 1.54×10^{-5} cm^2/s, respectively, in a fractured glass block with a porosity of 0.016. These results suggest that the assumption of diffusion coefficients on the order of 10^{-5} cm^2/s for saturated ILAW fractured glass media appears to be reasonable. Additional measurements of this type are underway for new glass formulations.

The diffusion coefficient recommended for backfill and other granular materials (Eq. 5.1) is inappropriate for low-porosity, fractured glass waste. Since the ILAW glass is expected to have a porosity of just a few percent (best-estimate saturated water content is 2%), application of Eq. (5.1) will result in very small diffusion coefficient values within the glass waste even under saturated conditions. This contradicts the laboratory measurements discussed above. If we assume that the intrinsic diffusion coefficient in the glass waste is a very low value (e.g., 10^{-7} cm^2/s) at the residual water content (0.0006 cm^3/cm^3) and that the free-water diffusion coefficients are on the order of 1.5×10^{-5} cm^2/s at saturation, then diffusion within the glass waste will be extremely sensitive to water content within the glass. Since the actual water content within the glass is uncertain, we recommend choosing a constant, conservative value for the intrinsic diffusion coefficient in the ILAW glass. For example, the use of Eq. (3.6) with parameters a = 1, b = 0 will maximize diffusion within the glass waste. That is,

---

[1] Saripalli KP, MJ Lindberg, and PD Meyer. 2003. *Effect of Chemical Reactions on the Hydraulic Properties of ILAW Near-field Materials: Experimental Investigation.* Letter Report to CH2MHill Hanford Group, Inc., September 30, 2003, Pacific Northwest National Laboratory, Richland, Washington.

$$D_i(\theta) = D_f \qquad (5.2)$$

The effect of this assumption can be examined in the sensitivity analyses conducted for the IDF PA.

5.2.4   Supplemental ILAW Waste Forms

Effective diffusion coefficients are being measured for a Cast Stone supplemental waste form. Those measurements will be reported in a separate data package. Diffusion in supplemental waste form materials can be modeled using the power function [Eq. (3.6)] as discussed in Section 5.2.2. For example, Buchwald (2000) measured diffusion in a brick sample as a function of water content using methods similar to those of Conca and Wright (1990). They fit a power function model [Eq. (3.6)] to their results, finding best-fit empirical parameters of a = 1.9, b = 1.6 (i.e., $D_i(\theta) = 1.9\, D_f\, \theta^{1.6}$). Their brick material had a bulk density of 1.81 g/cm^3, particle density of 2.81 g/cm^3, total porosity of 0.36, and an effective porosity of 0.34.

6.0 Best-Estimates of Physical and Hydraulic Properties and Parameters for Far-Field Materials

Because of the existence of stratification, natural porous media tend to be anisotropic. For unsaturated sediments, the anisotropy in hydraulic conductivity is also dependent on saturation (McCord et al. 1991; Stephens and Heermann 1988; Ursino and Gimmi 2004; Ursino et al. 2001). Given the very large spatial extent of the vadose zone underlying the IDF site, the primary focus of this section is on anisotropy of unsaturated hydraulic conductivity. Best-estimate values of physical and hydraulic properties and parameters for far-field materials are provided at the end of this section.

6.1 The Stochastic (Polmann 1990) Model

In the 1980s and early 1990s, a series of papers were published to address the effective unsaturated hydraulic conductivity for anisotropic porous media using a stochastic-perturbation method in conjunction with the Gardner (1958) exponential hydraulic conductivity function. Yeh et al. (1985a, b, c) applied this approach to steady unsaturated flow. Mantoglou and Gelhar (1987a, b, c) extended the model to transient unsaturated flow with no correlation between parameters. Polmann (1990) extended the approach further by considering the input correlation scale aspect ratios and the influences of cross-correlation among the various input hydraulic properties. Because the stochastic models were based on the log-linear K(h) function, they may be applicable only to a relatively narrow pressure head range over which the parameters were derived.

Simplified forms of the Polmann (1990) model anisotropy equations were adopted for use at Hanford by Khaleel et al. (2000). Khaleel and Relyea (2001) also examined the applicability of the Gardner model for describing the unsaturated hydraulic conductivity of coarse-textured Hanford sediments, and stated that the majority of their samples could be adequately described by the single-slope Gardner exponential K(h) model. Although not discussed in any previous Hanford reports on this subject, the assumptions used in the development of the particular equations that have been adopted for use at Hanford are (see Polmann, 1990; p. 155):

- Steady state flow

- Uniform mean tension

- Perfect stratification

- Statistically homogeneous, stationary properties

In addition, the Polmann (1990) model was further modified when it was incorporated into the STOMP numerical flow simulator (White and Oostrom 2006; White et al. 2001) by enforcing a minimum and maximum anisotropy coefficients to truncate unrealistic values.

The Polmann (1990) equations for strongly stratified porous media for deriving the effective parameters are as follows.

$$K_h^{eq} = \exp[<LnK> + (\sigma_{LnK}^2 / 2)]$$

(6.1)

$$K_v^{eq} = \exp[< LnK > -(\sigma_{LnK}^2 / 2)] \tag{6.2}$$

where

K_h^{eq} = equivalent unsaturated hydraulic conductivity in the horizontal direction,

K_v^{eq} = equivalent unsaturated hydraulic conductivity in the vertical direction,

$< LnK >$ = mean of log unsaturated conductivity (which depends on mean tension but not on flow direction),

σ_{LnK}^2 = variance of $< LnK >$.

The values of $< LnK >$ and σ_{LnK}^2 are estimated by

$$< LnK >=< LnK_0 > -A < \psi > -\sigma_{LnKs}^2 \lambda [p - p^2 < \psi > -\zeta^2 < \psi >]/(1 + A\lambda) \tag{6.3}$$

$$\sigma_{LnK}^2 = \sigma_{LnK0}^2 [(1 - p < \psi >)^2 + \zeta^2 < \psi >^2]/(1 + A\lambda) \tag{6.4}$$

where

$<\psi>$ = mean tension

$< LnK_0 >$ = mean LnK_0 of the samples considered, where LnK_0 is the intercept between the LnK vs. ψ regression at $\psi = 0$

p = slope of LnK_0 versus α_g regression line for the samples considered (i.e., $LnK_0 = p_0 + p\alpha_g$, where p_0 is the intercept of regression but not needed by the model; α_g is the slope between LnK and pressure head ψ)

$\zeta = \sigma_\delta/\sigma_{LnK0}$, where σ_δ is the standard deviation of the residuals in the LnK_0 vs. α_g regression for all the samples considered and σ_{LnK0} is the standard deviation of LnK_0

A = mean slope of α_g for LnK vs. ψ regressions

λ = vertical correlation lengths for LnK_0 and α_g (assume that λ for α_g is the same as that for lnK_0).

Eqs. (6.1) and (6.2) are essentially the arithmetic and harmonic means of K (Ababou 1996), which can be considered the effective K values of a layered soil in the directions parallel and perpendicular to the stratification, respectively. When λ decreases, a porous medium becomes more heterogeneous per Eq. (6.4) and more anisotropic [K_h is larger per Eq. (6.1), and K_v is smaller per Eq. (6.2)].

Eqs. (6.1) through (6.4) were given as Eqs. 3-161, 3-157, 3-164, and 3-167, respectively, in Polmann (1990). Note that there is an error in Eq. 3-164 of Polmann (1990), in which the $\overline{\alpha}$ in the second term on the right side should be $\overline{\alpha}H$ after comparing Eq. 3-164 with their Eqs. 3-49 and 3-56. Eqs. (6.3) and (6.4) are simplified versions of the third and last equations in the Table 3-2 (page 155) of Polmann (1990) for perfectly stratified soils after assuming that the normalizing functions β_{F0} and β_α are unity, namely, $\beta_{F0} = 1$ and $\beta_\alpha = 1$. This assumption was used in Section 2.3.4.3 of Polmann (1990). According to

Section 2.3.3 of Polmann (1990), these normalizing functions may be any form in order to keep the stochastic variables stationary.

Because the Polmann (1990) model is based on the log-linear K(h) function, it may be applicable only to a relatively narrow pressure head range over which the parameters are derived. The full K(h) curve is approximated using multiple log-linear segments and the Polmann (1990) model is applied to each of the segments. In this case, multiple sets of input parameters [see Eqs. (6.1) to (6.4)] must be determined. A modified version of the Polmann (1990) model was implemented in STOMP, per instructions from CH2M Hill Hanford Group, Inc. (White et al. 2001). In this implementation, user-determined anisotropy parameters are specified for a single-segment Gardner (1958) Ln[K(h)] function, which would typically be evaluated for a small range of soil moisture tension. In addition, user-specified upper and lower anisotropy coefficient truncation limits can be specified. Khaleel (2004) provided input parameters for the modified Polmann (1990) model in an earlier data package for the IDF site. Note, however, that Khaleel (2004) did not specify the truncation limits that were to be used for application of the modified Polmann model to the IDF site.

Anisotropy coefficients estimated by the modified Polmann (1990) model are very sensitive to the range of soil moisture tension or pressure head used for estimating model parameters (Figure 6.1).
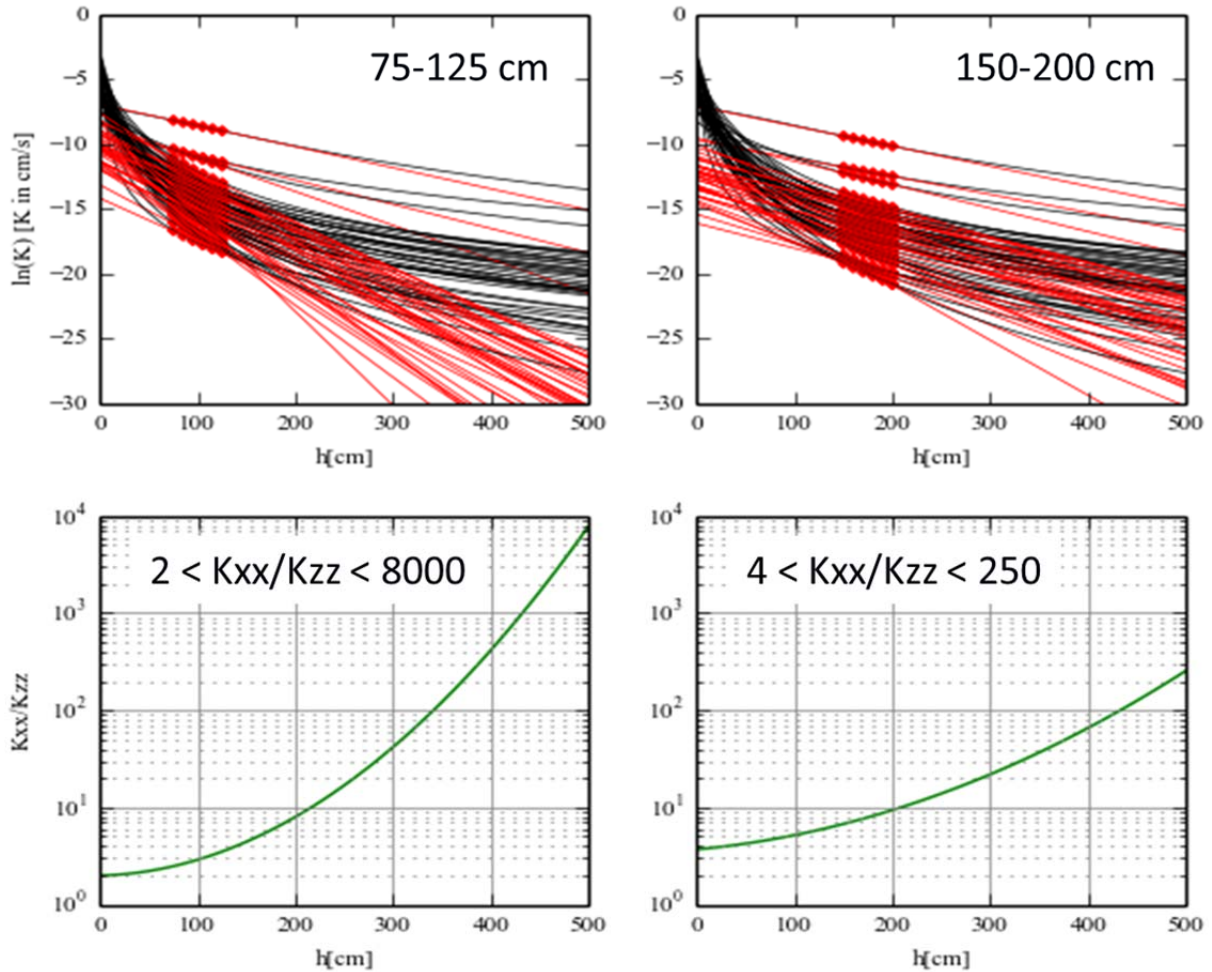
Figure 6.1. K(h) Functions (black lines in upper plots) for Samples of the Sand-dominated Facies at IDF
Site. The points (red dots) were the selected K(h) data to which Gardner (1958) exponential
functions (red lines) were fit to estimate Polmann (1990) model parameters. The green lines
(lower plots) show the predicted anisotropy coefficients. Note that the plots on the left and
right sides represent results for fitted soil moisture tension ranges of 75-125 cm and
150-200 cm, respectively.

Figure 6.1 (top plots) shows curves (black lines) representing K(h) relationships for the Mualem
(1976) model for samples of the sand-dominated facies at the IDF site. The discrete points (red dots)
were the selected data to which the Gardner (1958) exponential K(h) model was fit (red lines) to estimate
parameters for the modified Polmann (1990) model for the listed ranges of soil moisture tension. The
deviation of the red lines from the black lines away from the fitted range of soil moisture tension values
illustrates how poorly the single-slope Gardner LnK(h) function represents data outside the range of data
used for fitting. The green lines in the lower plots show the estimated anisotropy coefficients. The plots
of the left side of the Figure 6.1 represent results for a fitted tension range of 75-125 cm, while the plots
on the right side of the figure represent results for a tension range of 150-200 cm. For a soil-moisture
tension of 400 cm, which is well within the range of values measured in the field at Hanford (Zhang et al.
2011; Rockhold et al. 2009a), the predicted anisotropy coefficients for the results on the left and right
sides of Figure 6.1 are ~450 and 70, respectively. Also note how the ranges for the predicted anisotropy
coefficients differ for the two ranges of soil moisture tension. This sensitivity of predicted anisotropy

coefficients to the range of tensions used for parameter estimation, and the extremely high and unrealistic anisotropy coefficients that can be generated using this method, led to the addition of user-specified upper and lower anisotropy coefficient truncation limits for the implementation of the modified Polmann (1990) model in STOMP (White et al. 2001).

In summary, the modified Polmann model has several potential limitations:

- The modified Polmann model is based on the following assumptions: 1) steady state flow, 2) uniform mean tension, 3) strong stratification, 4) statistically homogeneous, stationary properties. Any or all of these assumptions may be invalid.

- The model assumes that the log-linear unsaturated hydraulic conductivity function of Gardner (1958) is applicable, which is often only acceptable for a narrow range of pressure head conditions.

- The full Polmann (1990) model of anisotropy requires that the hydraulic conductivity-pressure head function be approximated using multiple log-linear segments, each represented by its own set of input parameters. However, the current implementation of the modified Polmann model in STOMP accepts only a single log-linear K-ψ relationship which may limit its range of applicability.

- In deriving Eqs. (6.3) and (6.4) by simplifying the equations from Table 3-2 of Polmann (1990), terms in the normalizing functions used to ensure stationary are implicitly assumed to be equal to unity, which simplifies the final forms of the equations. This assumption may not be appropriate.

- Application of the modified Polmann (1990) model requires knowledge of a series of six additional parameters (plus two more parameters representing truncation limits in the STOMP implementation) for each material type over that which is usually required for unsaturated flow modeling, compared to just one additional parameter that is required for an alternative model of anisotropy described in the next section.

- Given the limited range of tensions over which the single-segment Gardner function is typically evaluated to estimate parameters for the modified Polmann model, the STOMP models that use this parameterization should (strictly speaking) only be applied to scenarios in which the simulated soil moisture tensions are within that same range.

6.2   The Tensorial Connectivity-Tortuosity Model

Zhang et al. (2003b) proposed a TCT model to describe the directional unsaturated hydraulic conductivity of anisotropic porous media. The model implies saturation-dependent anisotropy and was further formulated in Raats et al. (2004) with the tensor of the saturated hydraulic conductivity and the tensor of the tortuosity. Details of the model will be given in a following section.

Ward and Zhang (2007) inversely estimated the directional connectivity-tortuosity of a Hanford soil at the Army Loop site based on infiltration from a 60-meter-long line source. They found that there was evidence of saturation-dependent anisotropy and the anisotropy could be adequately described using the TCT model.

Zhang and Khaleel (2010) developed a practical approach to estimate the 3D effective unsaturated hydraulic conductivity via a combined power-averaging and tensorial connectivity-tortuosity (PA-TCT) model. An application of the PA-TCT model to data collected at the Sisson and Lu site in the Hanford

200 East Area suggests that the model provides a reasonable framework for upscaling core-scale measurements as well as an accurate simulation of moisture flow in a heterogeneous vadose zone.

6.2.1   Comparison of the Parameter Requirements for Stochastic and TCT Models

A comparison between the parameter requirements for the TCT and Polmann models is given in Table 6.1. The TCT model has distinct advantages over the Polmann model in terms of the parsimony of input parameters, the applicable range of soil water pressure, and the flexibility to describe different degrees of anisotropy.

Zhang and Khaleel (2007) evaluated the modified the Polmann (1990) model, the TCT model, and the pancake anisotropy model by simulating an injection experiment conducted in 2000 at the Hanford's Sisson and Lu site by treating the soil as an equivalent homogeneous medium (EHM). An additional simulation was conducted using the TCT model and treating the medium as one with five layers. Overall, the TCT model with the layering structure predicted the flow the best and the TCT model without the layering the second best (Zhang and Khaleel 2007).

Table 6.1. Comparison Between the TCT and Polmann Models

	TCT	Polmann
Number of input parameters	1	6[a] times the number K(h) segments
Range of soil water pressure	Full range	Range the log-linear model applies
Degree of stratification of porous media	From no to strong	Strong
(a) 8 for the modified Polmann model in STOMP (the additional two are the upper and lower limits of soil anisotropy).		

In the following, first the findings on the connectivity-tortuosity coefficient, L, for isotropic porous media are reviewed to understand that L varies over a large range instead of being a constant value of 0.5, which is typically assumed. Next the TCT model for describing the directional unsaturated hydraulic conductivity for anisotropic soils is presented. The findings on soil anisotropy at Hanford are then reviewed. Finally, a method to upscale hydraulic properties is presented and the parameters for the TCT model are estimated for the IDF site.

6.3   Unsaturated Hydraulic Conductivity of Isotropic Soils

Soil water retention characteristics for an isotropic soil can be described by the Brooks and Corey (1966) relationship:

$$S_e = \left(\frac{h_e}{h}\right)^{\lambda}, \; |h| > |h_e| \tag{6.5}$$

or the van Genuchten (1980) model

$$S_e = \left[1 + (\alpha \, | h \, |)^n\right]^{-m}, \; |h| > 0 \tag{6.6}$$

where S_e denotes the effective saturation of the soil

$$S_e = \frac{\theta - \theta_r}{\theta_s - \theta_r} \tag{6.7}$$

and where θ_s and θ_r are the saturated and residual water content, respectively; θ is water content; h is pressure head and is often negative; h_e is the pressure head at air-entry; λ and n are fitting parameters that characterize the width of pore-size distribution; α is a fitting parameter that is inversely proportional to the pressure head at air-entry; and m is a constant that is commonly approximated by m = 1-1/n (van Genuchten 1980). Eqs. (6.5) or (6.6) may also be used to describe the retention curve of a heterogeneous soil with all the parameters being replaced by their corresponding effective values.

With the assumption of pore continuity and connectivity, Burdine (1953) and Mualem (1976) proposed relationships for unsaturated hydraulic conductivity in terms of water content or pressure head. A general expression of the two can be written as (Hoffmann-Riem et al. 1999):

$$K(S_e, K_s, L, \beta, \gamma) = K_s S_e^L A(S_e, \beta, \gamma) \tag{6.8}$$

$$A(S_e, \beta, \gamma) = \left[\frac{\int_0^{S_e} \left(\frac{dS_e}{|h|^\beta} \right)}{\int_0^1 \left(\frac{dS_e}{|h|^\beta} \right)} \right]^\gamma \tag{6.9}$$

where L is a lumped parameter that accounts for pore connectivity and tortuosity and hence is called the connectivity-tortuosity coefficient, and β and γ are constants. Eq. (6.9) reduces to the Burdine (1953) relationship when $\beta = 2$ and $\gamma = 1$ and to the Mualem (1976) relationship when $\beta = 1$ and $\gamma = 2$. The term A can be simplified for the combination of the van Genuchten (1980) and Mualem (1976) (VGM) models and the Brooks and Corey (1964) and Burdine (1953) (BCB) models:

VGM:
$$A = \left[1 - \left(1 - S_e^{1/m} \right)^m \right]^2 \tag{6.10}$$

BCB:
$$A = S_e^{1+2/\lambda} \tag{6.11}$$

When the retention parameters are known, parameter L can be determined according to Eq. (6.8). As noted by Mualem (1976), L might be positive or negative. Values of the L parameter estimated in various studies are summarized in Table 6.2. Although L varies over a very large range, the most common approach in modeling K(h) is to assume a constant value of 0.5, which was an optimal value determined by Mualem (1976) for a data set of 45 disturbed and undisturbed samples. This value of L=0.5 has become firmly entrenched as a default value for this parameter in most unsaturated flow modeling applications. More-accurate descriptions of soil unsaturated hydraulic conductivity can often be obtained if L is treated as a fitting parameter, as suggested in Schaap and Leij (2000).

Table 6.2. Values of the Connectivity-Tortuosity Coefficient Reported in the Literature

Reference	Number of Samples	L	Texture	Notes
Mualem (1976)	45	Mean: 0.5		Optimal value
Wosten and van Genuchten (1988), Table 1	105 43 49	Range: -0.432 to 0.826 Range: -4.59 to -0.534 range: -9.38 to -5.50	Coarse-textured Medium-textured Fine-textured	
Schuh and Cline (1990), Table 3	75	Median: 1.06 95% CI: (-0.88, 2.44) Range: -8.73 to 14.80	Sand to loam	
Yates et al. (1992), Table 1	36	Average 0.63 95% CI: (-0.88, 2.44) Range: -3.31 to >100	Sand to clay	
Hendrayanto et al. (1999), page 111, lower right panel for l-VG	30	Mean: -0.009 SD: 2.72 Range: -6.18 to 5.82	Forest soils	
Schaap and Leij (2000), Table 1	235	Average: -3.09 SD: 8.75 Range: -6.97 to -1.22	Sand to clay (UNSODA soils)	Average of texture groups
Shinomiya et al. (2001), Page 224, left panel	87	Mean: -0.94 SD: 1.73 Range: -5.23 to 3.20	Sandy loam to heavy clay	
Schaap et al. (2003), Table 1 for Inv VG	51	Average: 0.535 SD: 1.112; Range: -3.144 to 4.353	Sand to Silt	Inversely estimated; van Genuchten-Mualem model; for 51 of 60 samples from Hanford's Sisson and Lu site
Ward and Zhang (2007), Table 1	59	Mean: -0.155 95% CI: 1.60	Sand	Horizontal L at 59 field locations along a 60 m transection at Hanford's Army Loop site
Zhang and Khaleel (2010), Table 3		Range: -1.94 to 5.64	Sand to Silt	Upscaled value for five different geological units at the Hanford's Sisson and Lu site

6.4   Unsaturated Hydraulic Conductivity of Anisotropic Soils

The TCT model assumes that the anisotropy in K is determined not only by directional saturated hydraulic conductivity, but also by the directional connectivity-tortuosity coefficients, L_i, corresponding to the three principal directions. For an unsaturated anisotropic soil, directional hydraulic conductivity is defined for each of three principal directions, $i = 1, 2, 3$, by rewriting Eq. (6.8) (Zhang et al. 2003b):

$$K_i(S_e) = K_{si} S_e^{L_i} A(S_e)$$
(6.12)

Zhang et al. (2003b) pointed out that an optimized L is a lumped parameter that accounts not only for flow path tortuosity and pore connectivity, but for pore configuration as well. Physically meaningful results can be ensured by requiring $dK/dS_e > 0$ such that

$$L_i > L_{min} = -\frac{S_e}{A}\frac{dA}{dS_e}$$
(6.13)

For the Mualem-van Genuchten model, L_{min} is given as

$$L_{min} = -\frac{S_e^{1/m}\left(1-S_e^{1/m}\right)^{m-1}}{1-\left(1-S_e^{1/m}\right)^m}$$
(6.14)

The analysis of Durner et al. (1999) showed that $K(S)$ is always monotonic for $L > -2$ for the Mualem-van Genuchten model. When n increases from 1.25 to 5 (m varies from 0.2 to 0.8) as a soil becomes coarser, L_{min} increases from about -10 to about -2.5.

For the Burdine-Brooks and Corey model,

$$L_{min} = -(1+2/\lambda)$$
(6.15)

$K(S)$ is always monotonic for $L > -1$ for the Burdine-Brooks and Corey model. As λ increase from 0.2 for a very fine soil to 4 for a very coarse soil, L_{min} increases from -11 to -1.5. Hence, regardless of the model of selection, for soil with a wide pore-size distribution (small value of m or n or λ), L_{min} can be considered to be small and the constraint is often not an issue.

As pointed out in Raats et al. (2004), Eq. (6.12) assumes $\mathbf{K}(S_e)$ to be a symmetric second-order tensor, which in a coordinate system coinciding with the three principal directions can be represented as:

$$\mathbf{K}(S_e) = A(S_e,\beta,\gamma)\begin{pmatrix} K_{s1} & 0 & 0 \\ 0 & K_{s2} & 0 \\ 0 & 0 & K_{s3} \end{pmatrix}\begin{pmatrix} S_e^{L_1} & 0 & 0 \\ 0 & S_e^{L_2} & 0 \\ 0 & 0 & S_e^{L_3} \end{pmatrix}$$
(6.16)

Eq. (6.16) suggests that we can regard $T_i(S_e) = S_e^{L_i} = \left(S_e^{L_1}, S_e^{L_2}, S_e^{L_3}\right)$ as the principal components of the relative connectivity-tortuosity tensor $\mathbf{T}(S_e,L_i)$ corresponding to the three principal directions. According to Eq. (6.12), the anisotropy in the unsaturated hydraulic conductivity between the ith and j[th] directions is given as

$$C_{ij}(S_e) = \frac{K_{si}}{K_{sj}}S_e^{L_i-L_j}$$
(6.17)

6.9

If the hydraulic properties in the two horizontal directions are the same, the anisotropy coefficient, C, is defined as the ratio of K in the horizontal direction to that in the vertical direction. Eq. (6.17) is then written as

$$C(S_e) = \frac{K_{sh}}{K_{sv}} S_e^{L_h - L_v} \qquad (6.18)$$

An anisotropy coefficient of unity means isotropy and a value different from unity means anisotropy. A value larger than unity means the horizontal hydraulic conductivity is larger than the vertical counterpart and vice versa. The general magnitude of $L_h < L_v$ leads to the increasing anisotropy with decreasing effective saturation.

6.5 Soil Anisotropy at Hanford

Hydraulic properties have been measured for numerous soil or sediment samples from Hanford (Last et al. 2006; Rockhold et al. 2013; Rockhold et al. 2010; Rockhold et al. 1988; Schaap et al. 2003). However, almost all cores were taken vertically and the flow was perpendicular to bedding during measurement of these properties. Hence, measurements of unsaturated hydraulic conductivities during flow parallel to bedding are very sparse.

Mayes et al. (2003) measured the directional hydraulic conductivities for two sets of cores of upper and lower Ringold Formation at Hanford (Figure 6.2). For the upper Silt/Sand unit, their measured K_s value was 101 cm d^{-1} (4.17×10^{-3} cm s^{-1}) when flow was parallel to bedding (K_{sh}) and 36 cm d^{-1} (1.17×10^{-3} cm s^{-1}) when flow was perpendicular to bedding (K_{sv}), producing an anisotropy ratio of 2.8 for the saturated hydraulic conductivity. For the lower Silt/Sand unit, the measured K_{sh} and K_{sv} were 312 (3.61×10^{-5} m s^{-1}) and 108 cm d^{-1} (1.25×10^{-5} m s^{-1}), respectively, suggesting an anisotropy of 2.9 for saturated hydraulic conductivity. For these results the K_s was anisotropic, but the anisotropy was relatively low (much lower than 10, which is often assumed as a rule of thumb).

Ward and Zhang (2007) estimated the hydraulic properties of the surface soil (up to 0.80 cm depth) along a 60-meter-long transect at approximately 100 cm intervals based on a series of infiltration experiments and inverse modeling. The results show evidence of saturation-dependent anisotropy that was well-described with the connectivity tensor. For this site, variability of K_{sv} was larger than that of K_{sh}. The autocorrelation ranges in the horizontal direction for K_{sh}, K_{sv}, the inverse of the air entry value, α, and the horizontal connectivity coefficient, L_h, were between 2.4 and 4.6 m. The van Genuchten shape parameter, n, and saturated water content, θ_s, showed no autocorrelation. Their estimated mean values of the hydraulic parameters over the 60-m-long transect were $K_{sh} = 1.22 \times 10^{-3}$ cm s^{-1}, $K_{sv} = 2.06 \times 10^{-3}$ cm s^{-1}, $\alpha = 0.00428$ cm^{-1}, n = 1.883, $\theta_s = 0.317$ cm^3 cm^{-3}, and $L_h = -0.155$ (L_v was assumed to be a constant of 0.5). Based on these mean values, the anisotropy coefficient variation with the effective saturation is shown in Figure 6.3.
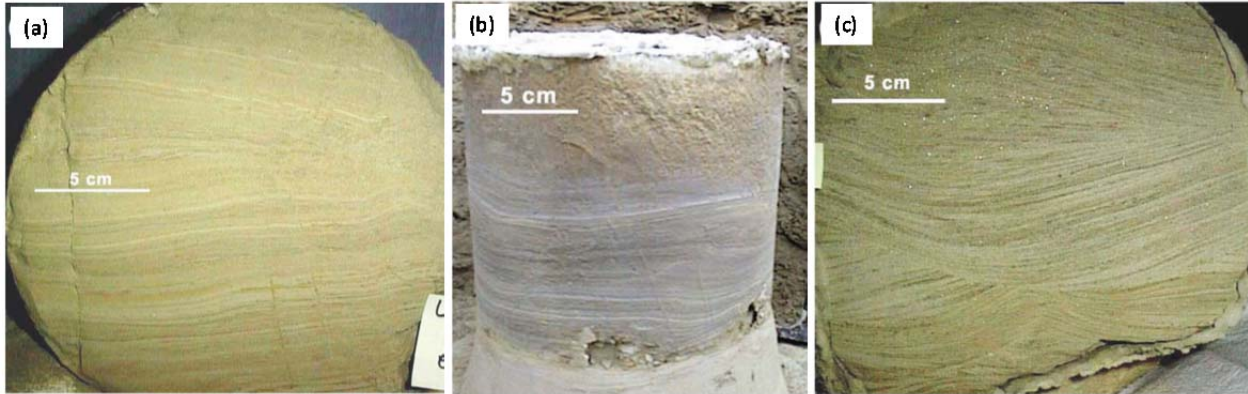
Figure 6.2. Soil Cores of the Typical Ringold Formation at Hanford: (a) upper silt/sand unit flow bedding parallel core, (b) upper silt/sand unit flow bedding perpendicular core, (c) lower sand/silt (LS/S) flow bedding parallel core (after Mayes et al. 2003).

The striking feature of Figure 6.3 is that the anisotropy coefficient $C < 1$ when $S_e > 0.45$. This means that unsaturated hydraulic conductivity in the horizontal direction K_h is less than that in the vertical direction K_v when $S_e > 0.45$ and $K_h > K_v$ when $S_e < 0.45$. The dominant direction of flow switches at S_e of 0.45. This phenomenon was also observed for several soils reported in Zhang (2014). The cause for the switch of flow dominance may be the existence of macro-pores such as worm burrows and channels of dead roots. For this site, the existence of a vertically-oriented clastic dyke may also have contributed to the observed behavior (Murray et al. 2007). The implication of this finding is that the use of the traditional concept of constant anisotropy over the full range of saturation in numerical simulations will cause errors but their significance may vary. Like other hydraulic properties, saturation-dependent anisotropy is also site-specific.
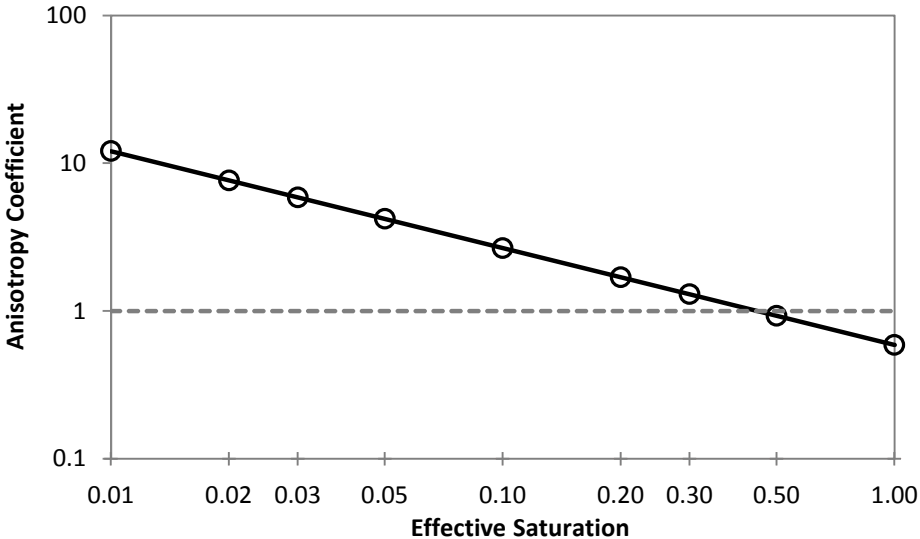
Figure 6.3. The Mean Behavior of the Anisotropy Coefficient With the Effective Saturation for the Hanford's Army Loop Road Site. The dashed line denotes an anisotropy coefficient of 1, i.e., $K_h = K_v$.

6.11

Zhang and Khaleel (2010) estimated the 3D effective unsaturated hydraulic conductivity of the Sisson and Lu site via a combined PA-TCT model. The heterogeneous media at the Sisson and Lu site were conceptualized as five geologic units (A through E), each of which was represented by an anisotropic EHM. The directional effective hydraulic conductivity for each anisotropic EHM was determined by upscaling the laboratory-measured hydraulic properties with the combined PA-TCT approach. Based on the degree of soil stratification, four matrix anisotropy levels, i.e., zero (isotropy), low, intermediate, and high anisotropy, were categorized. A high anisotropy of matrix corresponds to the perfect layered structure and a low anisotropy of matrix means weak stratification. Please note that, for a given soil, the soil stratification is independent of fluid condition and so is the level of matrix anisotropy. Even for an anisotropic soil, some properties (e.g., porosity) are isotropic, while others (e.g., hydraulic conductivity) is anisotropic. Because there were no data to determine the degree of soil stratification at Hanford, Zhang and Khaleel (2010) quantified the levels of anisotropy in K based on the use of typical power law values (p) to estimate the upscaled unsaturated K in the horizontal (K_h) and vertical (K_v) directions for the different matrix anisotropy categories. The definitions apply to the whole range of saturation and are:

- isotropic (ISO): $p = 0$, for both K_h and K_v

- low anisotropy (LA) of matrix: $p = 1$ for K_h and $p = {}^1\!/_3$ for K_v

- intermediate anisotropy (IA) of matrix: $p = 1$ for K_h and $p = 0$ for K_v

- high anisotropy (HA) of matrix: $p = 1$ for K_h and $p = -1$ for K_v

Note that the above calculation is equivalent to the arithmetic mean when $p = 1$, the geometric mean when $p = 0$, and the harmonic mean when $p = -1$. Larger differences between the p values in the horizontal and vertical directions mean higher degree of anisotropy in unsaturated hydraulic conductivity. Hence, the EHMs were isotropic (zero anisotropy) for the ISO case, and were equivalent to perfect layered media with the maximum anisotropy case HA. Figure 6.4 shows an example of the state-dependent anisotropy calculated for unit C at the Sisson and Lu Site (Zhang and Khaleel, 2010).
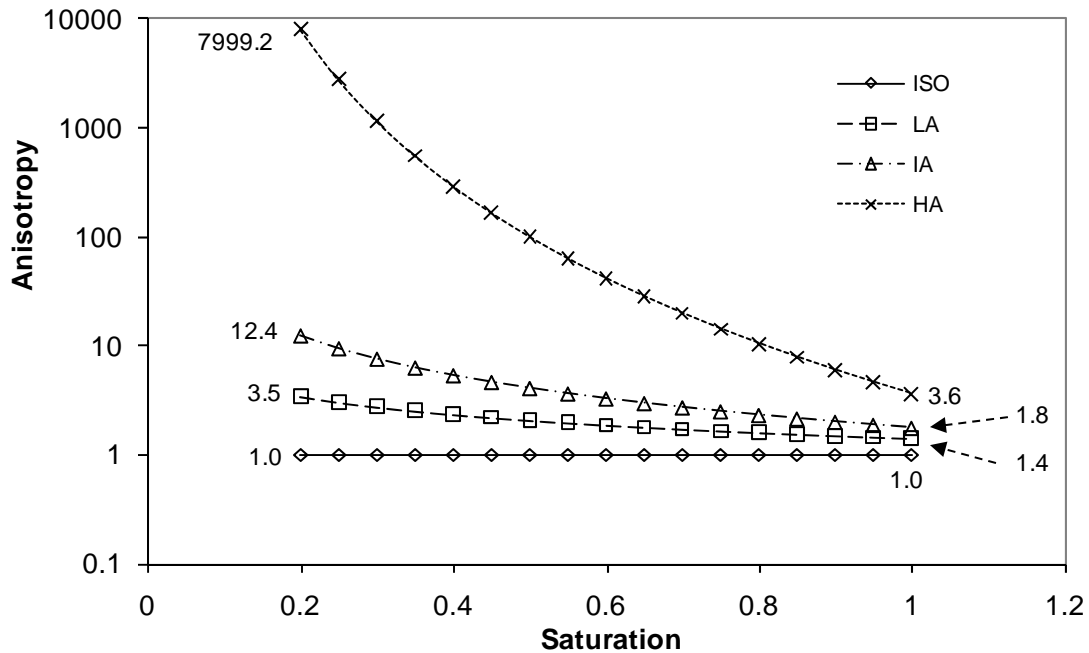
Figure 6.4. Macroscopic Anisotropy in Unsaturated Hydraulic Conductivity for Geologic Unit C at the Sisson and Lu Site for the Four Simulation Cases. The numbers in the figure represent the anisotropy at saturation of 0.2 and 1.0 (after Zhang and Khaleel, 2010).

Comparisons of numerical simulation results with field observations (Figure 6.5) showed that if the flow domain was treated as being ISO, the vertical migration was significantly overestimated while the lateral movement was underestimated. In contrast, if the media were treated as strongly stratified and highly anisotropic, the lateral moisture movement was considerably overestimated while the vertical movement was underestimated. However, when the flow domain was modeled as being mildly stratified with LA, the model could successfully predict the moisture flow and the simulated plume best matched the time-evolution of the center of mass and the spread of the injected water of the observed moisture plume.
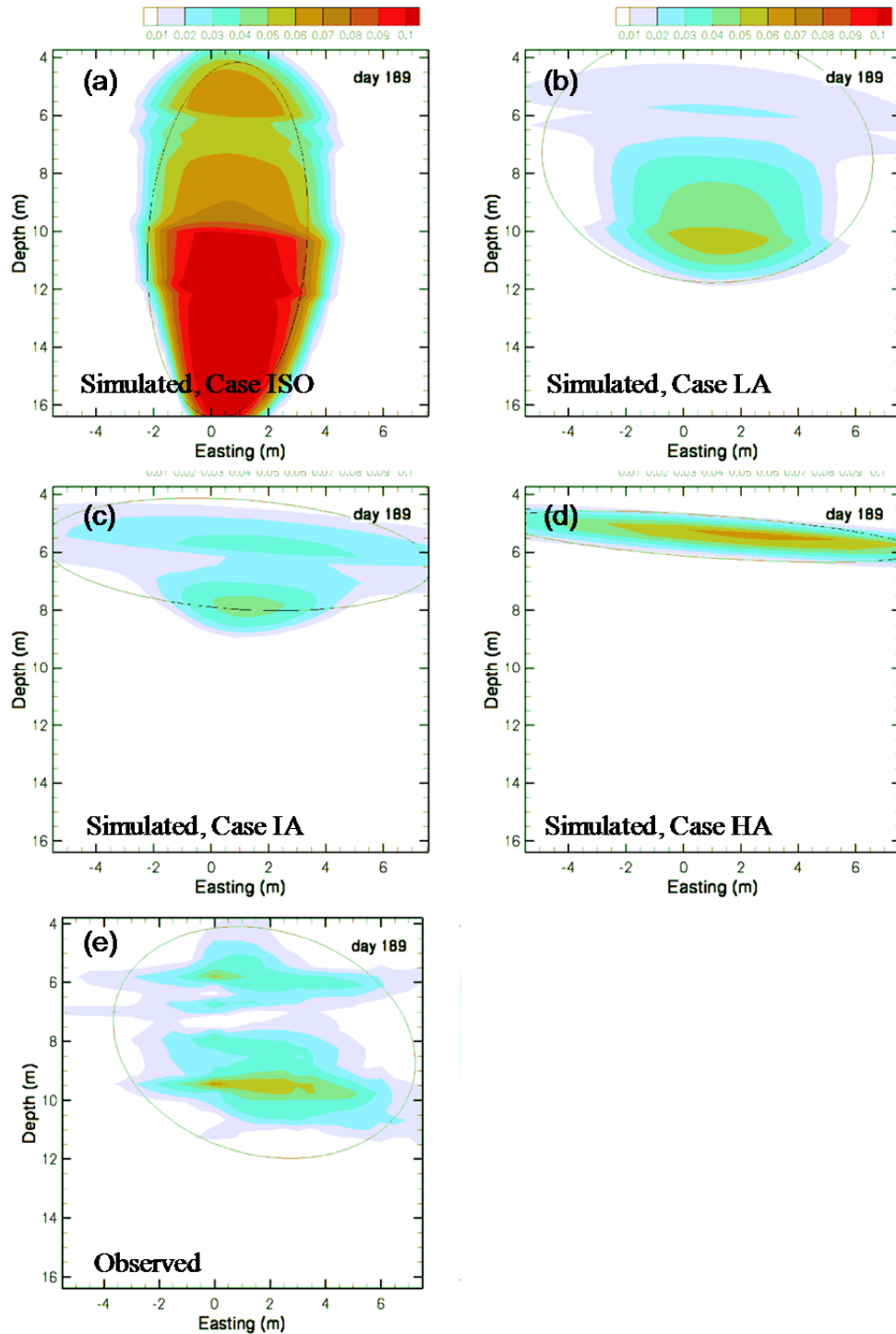
Figure 6.5. Moisture Content Difference on DOY 189, July 7 (9 days after the last injection). The ellipse in each plot shows the approximate plume size and shape based on the moment analysis (after Zhang and Khaleel 2010). The system was configured as five geological units.

6.6   Estimating the Directional Hydraulic Properties for the IDF Site

This section estimates the directional hydraulic properties for the IDF site sediments based on the available core samples and the assumed degree of anisotropy.

6.6.1   Input Data

The details of samples and methods of measurement were summarized in Khaleel (2004) and Rockhold et al. (2013). They are recaptured briefly below.

Sediment samples at the IDF site were obtained in fiscal years 1998, 2001, and 2002 in three boreholes. Details on sampling, laboratory procedures, and analysis of samples from these boreholes are included as Appendices A, B, and C of Khaleel (2004). According to Khaleel (2004), the Hanford formation sand sequence is about 200 ft thick and is the dominant facies at the site. The lower gravel sequence is about 70 ft thick. Multistep outflow and steady state flux control methods were used to obtain moisture retention and unsaturated conductivity data for the sand samples. Both methods were performed on the same core using the same sensor locations. These data were used in conjunction with a numerical inversion procedure to determine the optimal set of van Genuchten model (van Genuchten 1980) parameters. The hydraulic parameters for 44 samples of the sand sequence were from these boreholes and are summarized in Table 6.3.

There were no site-specific hydraulic data available for the gravel sequence. Instead, samples with high gravel contents from the 100 and 300 Areas were used. The 15 samples from the 100 Area (Khaleel 2004) contain a gravel fraction from 43% to 75% with an average of 62%. The moisture retention data for the fine fraction (<2 mm) were measured using the Tempe pressure cells or the pressure plate extraction method. The hydraulic conductivity was measured using a constant-head permeameter or a variation of the unit gradient method. All five unknown parameters, θ_r, θ_s, α, n, and K_s, with m = 1-1/n (van Genuchten 1980), were fitted to the data and the tortuosity-connectivity coefficient L was set as a constant 0.5. The hydraulic parameters for the 15 samples of the gravel sequence were summarized in Table 4 of Khaleel (2004) and are repeated in Table 6.4.

The 10 samples from the 300 Area (Rockhold et al. 2013) contain a gravel fraction from 45% to 89% with an average of 71%. The hydraulic properties of the intact cores were measured using the multistep methods (see appendices of Khaleel 2004). Measured pressure data from two locations in each core and measured cumulative outflow data were used to calculate average capillary pressures and water contents. These data were used to fit the retention parameters θ_r, α, and n. The parameters K_s and θ_s were measured independently. The tortuosity-connectivity coefficient L was set as a constant 0.5. These parameters were summarized in Table A.2 of Rockhold et al. (2013) and are repeated in Table 6.4. The two data sets noted above, reported by Khaleel (2004) and Rockhold et al. (2013), were combined to estimate properties for representing the gravel-dominated sequence at the IDF site.

Table 6.3. The van Genuchten Parameters (based on the multistep method) and Saturated Hydraulic Conductivity Data for 44 Borehole Samples from the Sand Sequence (after Khaleel 2004)

Sample	θ_s	θ_r	α (1/cm)	n	K_s (cm/s)
7A	0.377	0.0404	0.029	1.825	1.04E-03
10A	0.413	0.0279	0.1161	1.784	2.95E-03
12A	0.363	0.0309	0.065	1.755	2.15E-03
14A	0.416	0.0324	0.0445	1.728	1.99E-03
15A	0.38	0.0254	0.0487	1.844	2.09E-03
16A	0.42	0.0228	0.0682	1.71	9.57E-03
17A	0.423	0.0382	0.0689	1.899	1.99E-03
19A	0.444	0.0279	0.201	1.542	4.31E-03
20A	0.419	0.0321	0.0305	2.081	2.54E-03
21A	0.403	0.0276	0.0545	1.926	2.94E-03
22A	0.352	0.0252	0.1078	1.585	5.06E-03
23A	0.371	0.0411	0.0079	1.553	2.65E-04
24A	0.321	0.0413	0.013	1.684	5.69E-04
25A	0.345	0.0267	0.0842	2.158	5.40E-03
27A	0.377	0.0354	0.083	1.532	8.14E-03
29A	0.359	0.0317	0.0784	1.732	3.75E-03
31A	0.418	0.0444	0.0058	2.012	8.21E-04
32A	0.359	0.0401	0.0931	1.703	6.71E-03
34A	0.316	0.0324	0.0819	2.398	1.32E-02
35A	0.299	0.0428	0.0897	2.16	1.06E-02
45L	0.385	0.008	0.1039	1.737	3.24E-02
45U	0.385	0.005	0.088	1.664	3.24E-02
50L	0.42	0.025	0.073	1.71	1.75E-03
50U	0.42	0.013	0.045	1.667	1.75E-03
80L	0.359	0.031	0.0403	2.368	1.05E-03
80U	0.359	0.033	0.0313	2.572	1.05E-03
85L	0.406	0.023	0.1074	1.697	3.84E-02
85U	0.406	0.027	0.0847	1.595	3.84E-02
110L	0.412	0.039	0.0362	2.328	5.16E-04
110U	0.412	0.046	0.0268	3.182	5.16E-04
130L	0.358	0.032	0.094	2.003	1.97E-02
130U	0.358	0.036	0.0674	1.934	1.97E-02
150L	0.431	0.015	0.0992	1.547	7.48E-03
150U	0.431	0.024	0.0703	1.514	7.48E-03
200L	0.41	0.002	0.0995	2.162	4.93E-02
215L	0.37	0.028	0.0448	1.918	2.24E-03
215U	0.37	0.023	0.0333	1.815	2.24E-03
230L	0.309	0.04	0.0472	1.658	3.56E-03
230U	0.309	0.038	0.04	1.658	3.56E-03
251L	0.427	0.032	0.084	1.845	1.43E-02
261L	0.39	0.045	0.0191	2.485	5.54E-04
C3826-171	0.382	0.0226	0.039	1.84	7.96E-03
C3827-63.5	0.444	0	0.0914	1.5	2.23E-02
C3827-221	0.361	0.022	0.066	1.77	7.30E-03

Table 6.4. The van Genuchten Parameters (based on the multistep method) and Saturated Hydraulic Conductivity Data for 25 Borehole Samples Used to Represent the Gravel Sequence

Sample Locations	Sample	θ_s	θ_r	α (1/cm)	n	K_s (cm/s)
100 Area[a]	2-1307	0.236	0.0089	0.013	1.447	1.29E-04
	2-1308	0.12	0.0208	0.0126	1.628	6.97E-05
	2-1318	0.124	0.0108	0.0081	1.496	1.67E-04
	278713	0.135	0.0179	0.0067	1.527	6.73E-05
	279078	0.125	0.0136	0.0152	1.516	1.12E-04
	279809	0.138	0	0.0087	1.284	1.02E-04
	280174	0.094	0	0.0104	1.296	1.40E-04
	3-0570	0.141	0	0.0869	1.195	2.06E-02
	3-0577	0.107	0	0.0166	1.359	2.49E-04
	3-0686	0.184	0	0.0123	1.6	5.93E-04
	3-1702	0.103	0	0.0491	1.26	1.30E-03
	4-1086	0.137	0	0.1513	1.189	5.83E-02
	4-1090	0.152	0.0159	0.0159	1.619	4.05E-04
	4-1118	0.163	0	0.2481	1.183	3.89E-02
	4-1120	0.131	0.007	0.0138	1.501	2.85E-04
300 Area[b]	C6186,18.4-19.4	0.152	0	0.0388	1.378	2.83E-04
	C6197,27-28	0.176	0	0.115	1.324	4.33E-04
	C6197,42-43	0.178	0	0.0929	1.366	2.61E-02
	C6197,51-52	0.214	0	0.0435	1.272	5.43E-05
	C6200,21-22	0.219	0	0.0626	1.383	2.85E-01
	C6203,16-17	0.213	0	0.358	1.195	1.06E-01
	C6203,20-21	0.285	0	0.2286	1.269	3.72E-03
	C6203,35.8-36.8	0.302	0	2.4189	1.299	3.26E-02
	C6203,40-41	0.266	0	0.2733	1.509	1.30E-02
	C6208,23-24	0.246	0	0.1479	1.201	2.13E-02

(a) After Table 4 of Khaleel (2004).
(b) After Table A.2 of Rockhold et al. (2013).

6.6.2   Directional Effective Hydraulic Parameters

The strong stratification of the Hanford formation indicates anisotropy in hydraulic conductivity. Furthermore, the degree of anisotropy is dependent on the wetness of the soil. The PA-TCT method described in Zhang and Khaleel (2010) was used to develop the directional effective hydraulic parameters. The procedures are described below.

1) Conceptual model

The geology of the IDF site was conceptualized as two EHMs, i.e., the sand sequence over the gravel sequence. The hydraulic conductivity of each of the EHMs is assumed to be anisotropic and the anisotropy is dependent on soil wetness.

2) Effective Retention Curve

A linear averaging scheme (Green et al. 1996) was used to calculate the effective soil-water saturation, S^e, at a given pressure head, h:

$$S^e(h) = \frac{1}{N} \sum_{j=1}^{N} S_j(h) \qquad (6.19)$$

The effective soil-water retention characteristics for the two units were evaluated for the pressure-head range of (-1000, 10) cm, which was divided into 15 equal segments of ln|h|. This pressure range represents the field conditions at Hanford. The retention data of individual samples and the effective results are shown in Figure 6.6.
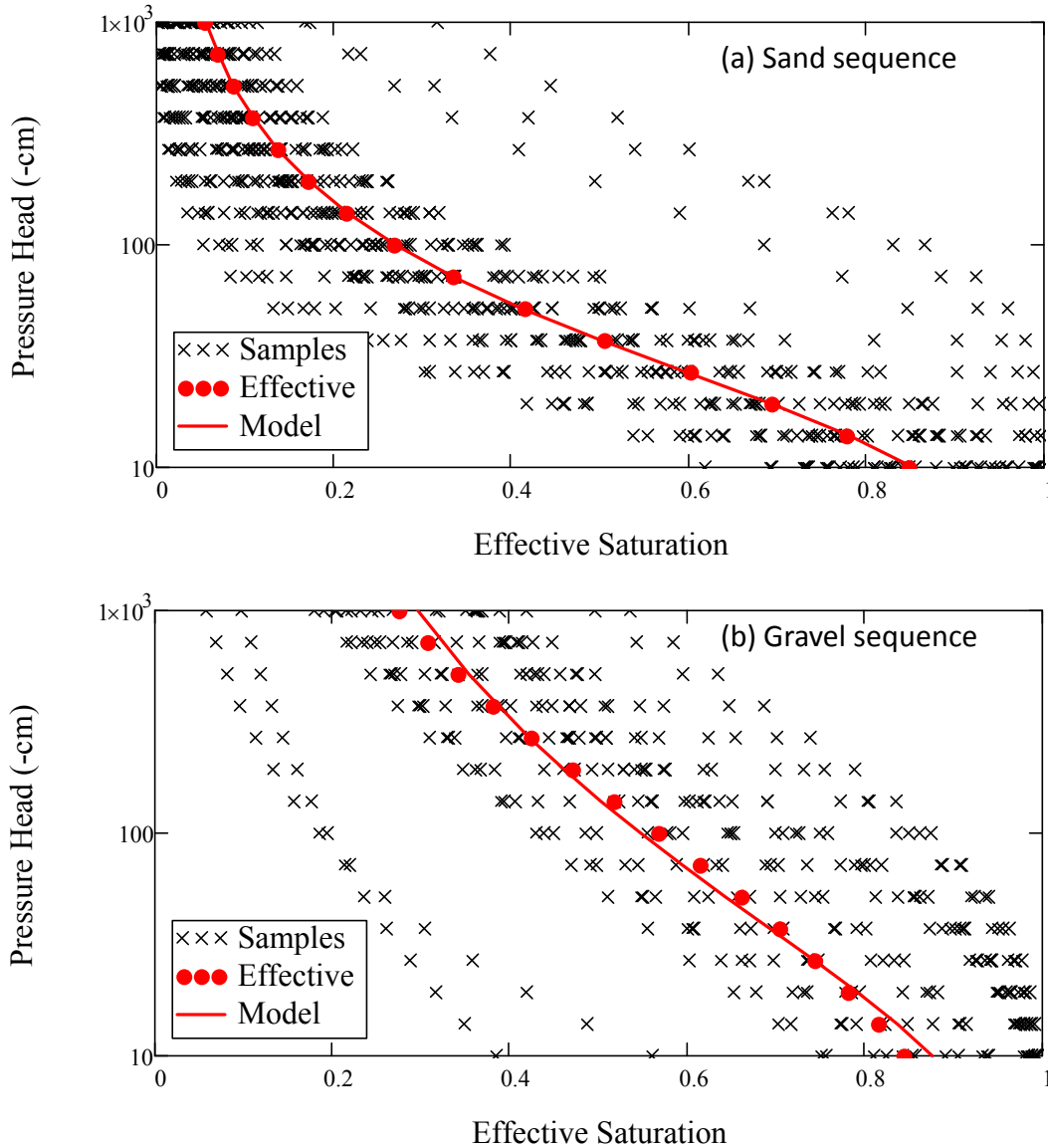
Figure 6.6. The Effective Retention Curves for the (a) Sand Sequence and (b) Gravel Sequence

6.18

3) Directional hydraulic conductivity

The effective unsaturated hydraulic conductivity in the ith principal direction, $K_i^e(h)$, for each of the anisotropic EHMs, as a function of pressure head, h, was estimated with the power-averaging model:

$$K_i^e(h) = \left\{ \frac{1}{N} \sum_{j=1}^{N} \left[K_j(h) \right]^{p_i} \right\}^{1/p_i} \qquad i = 1, 2 \, or \, 3 \tag{6.20}$$

where j denotes the sample index, N is the number of samples, $K_j(h)$ is the hydraulic conductivity of the jth sample as a function of h, and the power p varies between -1 and 1.

With Eq. (6.20), the effective hydraulic conductivities of an EHM corresponding to different pressure heads are obtained as discrete K_i^e vs. h data pairs. The data pairs in the ith principal direction are described by the TCT model (Zhang et al. 2003b):

$$K_i^e(h) = K_{si}^e \left[S^e(h) \right]^{L_i^e} A^e(h, \beta, \gamma) \qquad i = 1, 2 \, or \, 3 \tag{6.21}$$

where K_s^e is the effective hydraulic conductivity of an EHM at full saturation, L^e is effective connectivity-tortuosity coefficient, and $S^e(h) = [\theta^e(h) - \theta_r^e)]/(\theta_s^e - \theta_r^e)$ is the effective saturation of an EHM, $\theta^e(h)$ is the effective soil water content as a function of h, θ_s^e is the effective volumetric water content at full saturation, θ_r^e the effective residual volumetric water content, and $A^e(h, \beta, \gamma)$ is defined by Eq. (6.10).

Before upscaling the hydraulic conductivities, the degree of stratification needs to be defined. Because there are no field data to directly indicate the degree of anisotropy, three anisotropy scenarios, i.e., low, immediate, and high anisotropy, were defined per Zhang and Khaleel (2010) by choosing different combinations of p values in the horizontal and vertical directions. These p values are given in Table 6.5 and the upscaled hydraulic conductivities corresponding to the four values of p are shown in Figure 6.7.

Table 6.5. Definition of the Degree of Anisotropy in Hydraulic Conductivity

Anisotropy Level	p value for the horizontal direction ($i = 1, 2$)	p value for the vertical direction ($i = 3$)
Low Anisotropy	1	$^1/_3$
Intermediate Anisotropy	1	0
High Anisotropy	1	-1
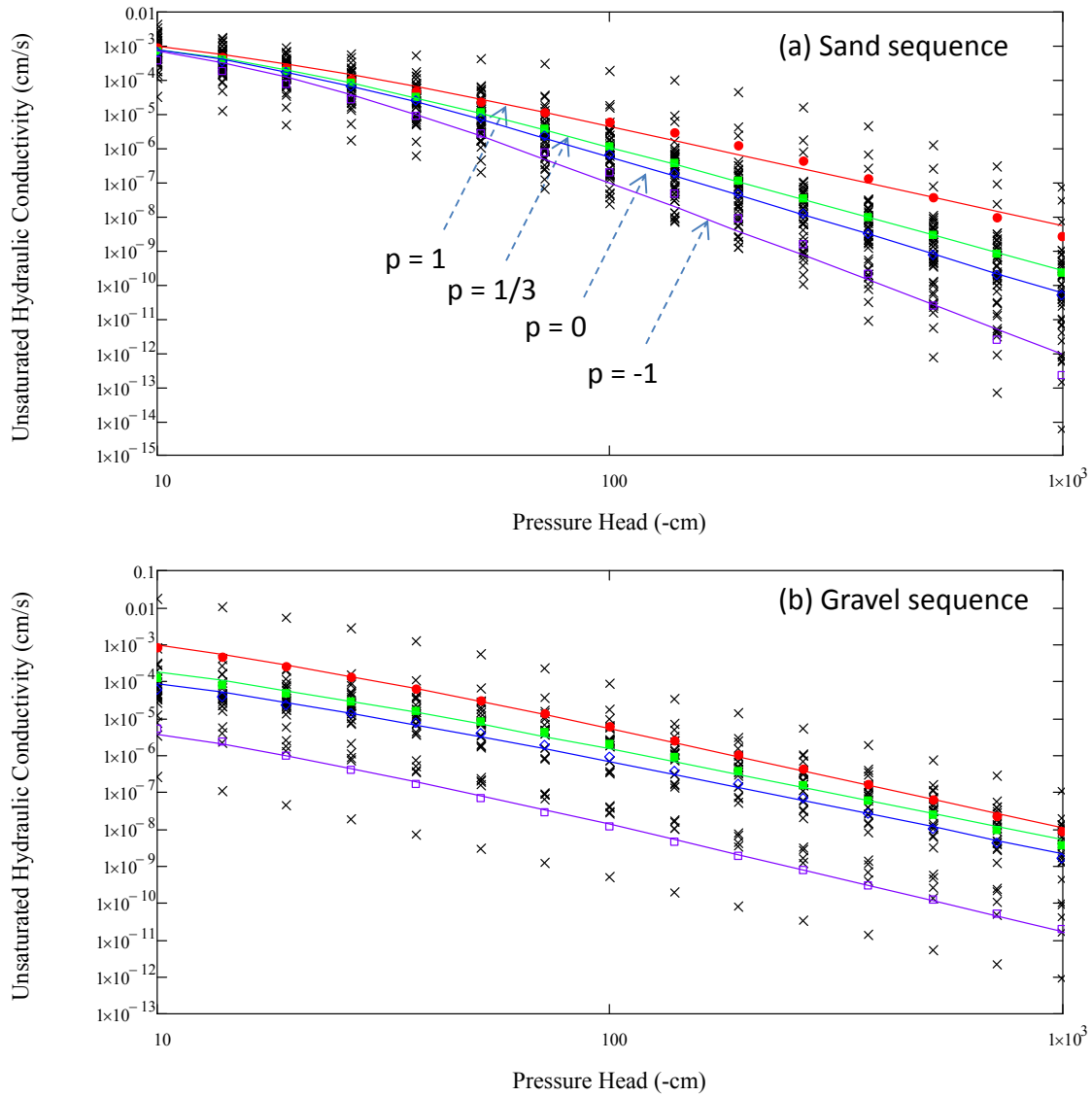
Figure 6.7. The Effective Hydraulic Conductivities for the (a) Sand Sequence and (b) Gravel Sequence

4) Estimate the Upscaled Hydraulic Parameters

The upscaled parameters θ_s^e and θ_r^e for each of the sand and gravel sequences were the simple average of the samples. Parameters α^e and n^e were fitted to the mean retention curves shown in Figure 6.6. Using the obtained values of θ_s^e, θ_r^e, α^e, and n^e, effective parameters K_s^e and L^e corresponding to each of the four values of p were fitted. The upscaled hydraulic parameters are summarized in Table 6.6. Predicted anisotropy coefficients are shown if Figure 6.8.

Note that all the effective parameters except parameter L in Table 6.6 are comparable with those reported in Khaleel (2004). The L parameter for the TCT model, as a replacement for the Polmann (1990) model, is used to describe saturation-dependent anisotropy. According to Zhang and Khaleel (2010), a low anisotropy would best predict the observed flow behavior for the injection experiment at the

Sisson and Lu site. Different K_s^e and L^e are to be used for different levels of anisotropy based on the definitions in Table 6.5.

Table 6.6. Estimated Upscaled Hydraulic Parameters for Different Levels of Anisotropy. Parameters for the low anisotropy case (defined in Table 6.5) are recommended as best-estimate values.

Parameters		Sand Sequence	Gravel Sequence
θ_s^e (cm^3 cm^{-3})		0.384	0.174
θ_r^e (cm^3 cm^{-3})		0.029	0.00380
α^e (cm^{-1})		0.06419	0.08859
n^e (-)		1.698	1.271
K_s^e (cm s^{-1})	$p = 1$	6.196×10^{-3}	4.671×10^{-2}
	$p = {}^1\!/_3$	6.157×10^{-3}	7.714×10^{-3}
	$p = 0$	6.575×10^{-3}	3.790×10^{-3}
	$p = -1$	7.741×10^{-3}	1.959×10^{-4}
L^e (-)	$p = 1$	-0.683	0.637
	$p = {}^1\!/_3$	0.375	-0.225
	$p = 0$	0.916	-0.111
	$p = -1$	2.386	1.471
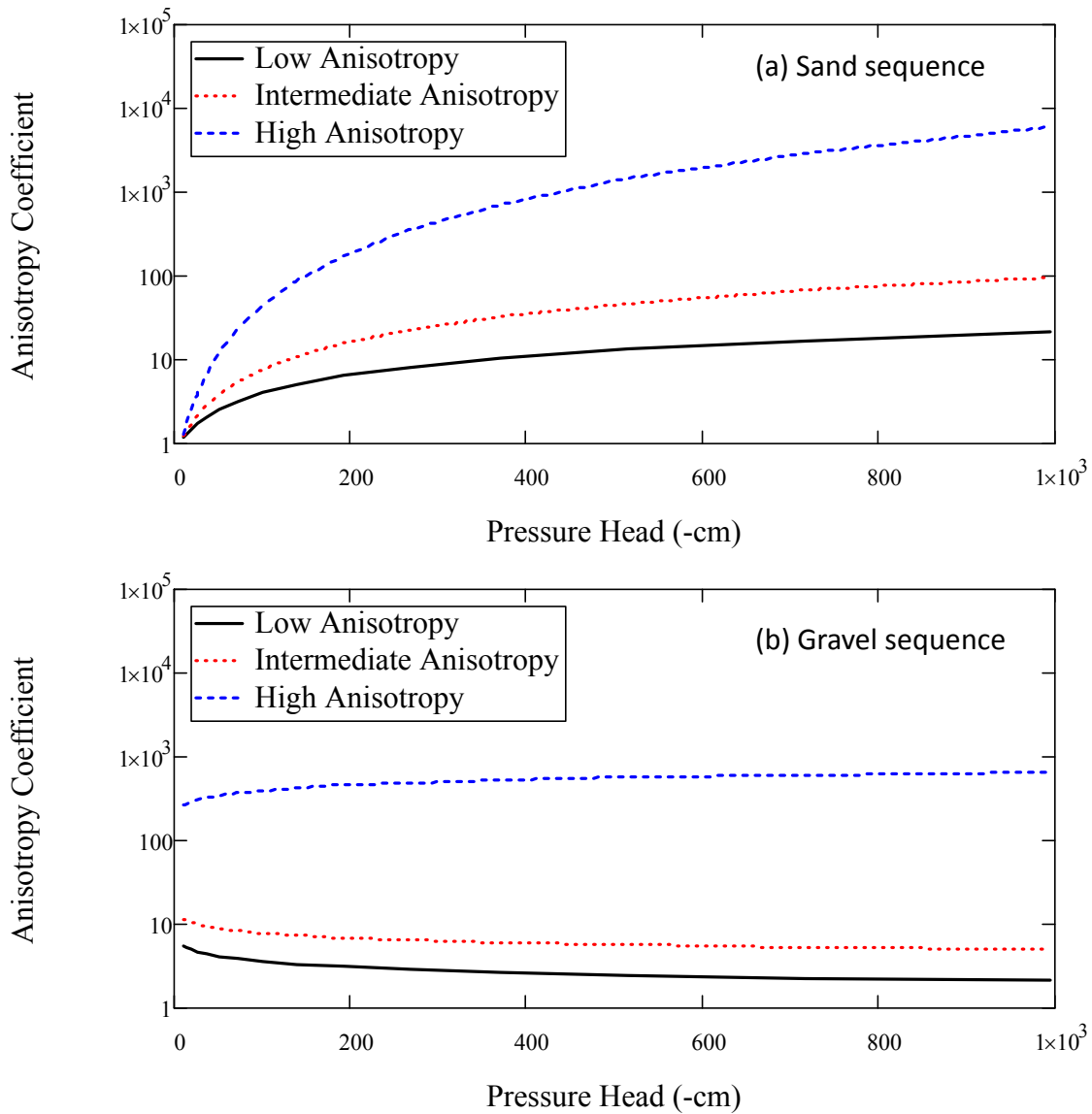
Figure 6.8. The Anisotropy for the (a) Sand Sequence and (b) Gravel Sequence

6.7   Clastic Dike Materials

As noted earlier, clastic dikes are of special interest because they may provide preferential flow paths through the vadose zone to the ground water under certain flux conditions (Murray et al. 2007). These features could also serve to compartmentalize flow and transport behavior in the vadose zone, potentially reducing the lateral spreading that might otherwise occur. As in earlier IDF PAs, addressing the possible effects of clastic dikes on facility performance would likely be through the development and application of special sensitivity cases.

Parameterization of a model that explicitly or implicitly includes clastic dike features requires 1) knowledge of the physical, hydraulic, and transport properties of the dike materials; and 2) knowledge of the spatial distribution and characteristics of dike networks. Both types of information are available to

some extent from previous studies, as described earlier. However, information on 3D characteristics of clastic dike networks at Hanford is lacking. In lieu of new data, we recommend the properties and parameters for clastic dike sediments reported by Khaleel (2004), which are listed in Table 6.7.

Murray et al. (2007) summarize hydraulic property measurements on clastic dike samples from the Army Loop Road site as follows:

"A total of about 450 measurements were made on the three tiers of the excavation, one-third in the dike and two-thirds in the host matrix. The results indicate the median air permeability of the dike is about an order of magnitude lower than the permeability of the matrix. The variability of the data from the dike is much higher than that of the matrix, with a coefficient of variation (i.e., ratio of standard deviation to the mean) of 1.2 in the dike compared with 0.6 in the matrix. The overall variability of air permeability in the dike-matrix system is about four orders of magnitude. This is an important observation because some methods for upscaling permeability data assume the variability of the system is low, about an order of magnitude, which means that applying those methods to the clastic dike and its surrounding sediments is questionable. In addition to the air permeability measurements, K_{fs} (field-saturated hydraulic conductivity) was measured in situ on Tier 2 using the Guelph permeameter (Reynolds and Elrick, 1985). Guelph permeameter measurements showed a mean K_{fs} for the host matrix of 3.24×10^{-2} cm s^{-1} and 2.58×10^{-3} cm s^{-1} for the dike. The mean K_{fs} in an adjacent sill, a dense layer of horizontally laminated fine-textured sediments, was 5.9×10^{-4} cm s^{-1}. Several measurements of K_{fs} were also made every 0.3 m along a 7.5-m transect on Tier 2 using a minidisk infiltrometer using deionized water (Zhang, 1997). Results show an order of magnitude difference between the sandy host matrix (2.29×10^{-2} cm s^{-1}) and the composite dike (fine plus coarse vertical layers) region (2.04×10^{-3} cm s^{-1}). The mean of the measurements made on isolated fine-textured skins within the dike wide enough to fit the minidisk were almost five times smaller (4.68×10^{-3} cm s^{-1}) than the host sand. The mean K_{fs} in the dike (fine plus coarse) material was 1.48×10^{-6} cm s^{-1}, and the coefficient of variation was much higher (2.1) than in the matrix (0.9)."

Ward and Zhang (2007) describe additional field and modeling studies and hydraulic property characterization (including anisotropy) for sediments at the Army Loop Road site.

Table 6.7. van Genuchten Parameters (based on the multistep method), Saturated Hydraulic Conductivity, and Bulk Density for Seven Clastic Dike Samples (Khaleel 2004)

Sample	θ_s (cm^3/cm^3)	θ_r (cm^3/cm^3)	α (1/cm)	n (-)	Saturated Hydraulic Conductivity (cm/s)	Bulk Density (g/cm^3)
1	0.424	0.063	0.0839	1.33	5.97E-04	1.57
2A	0.446	0.019	0.0762	1.98	4.70E-03	1.50
2B	0.443	0.023	0.0741	1.84	3.14E-03	1.51
3A	0.424	0.025	0.0143	2.49	3.41E-03	1.46
3B	0.448	0.050	0.0593	1.54	1.14E-03	1.52
4A	0.454	0.030	0.0092	1.97	1.84E-03	1.49
4B	0.425	0.021	0.0823	2.09	5.43E-03	1.57

7.0 Best-Estimate Values for Transport Parameters of Far-Field Materials

7.1 Dispersivity

Dispersion of solutes in porous media is usually modeled using the well-known advection-dispersion equation (ADE), which is also frequently referred to as the convection-dispersion equation (CDE). The dispersion tensor in the ADE typically includes *dispersivity* terms that account for flow-induced mechanical mixing in both the longitudinal and transverse directions, and a diffusion term that accounts for *molecular diffusion* of the solute in the fluid. In a previous data package for far-field material properties, Khaleel (2004) noted that the apparent longitudinal dispersivity in water-saturated aquifer systems is often observed to increase with increasing transport distance, until some asymptotic limit is reached (Gelhar et al. 1994; Gelhar 1993). This well-known behavior is usually attributed to heterogeneity-induced spreading and mixing until the point at which all of the heterogeneity has effectively been "sampled" by the solute plume such that dispersion becomes constant. Khaleel (2004) also notes that a constant asymptotic value of dispersivity—representing so-called Fickian behavior—is typically reached after a solute pulse has traveled a few tens of correlation scales of the hydraulic conductivity field in saturated aquifer systems.

For an earlier far-field material data package, Khaleel (2004, p.18) stated that "*dispersivity estimates needed for modeling are essentially based on literature values and the available stochastic equations.*" He provided a brief review of literature on the scale dependence of (longitudinal) dispersivity in aquifers (Gelhar et al. 1993; Gelhar and Axness1983; Dagan 1984) and estimated "macro-dispersion" coefficients for non-reactive species in far-field materials—including vadose zone sediments—based on the variance in $\ln(K_s)$, or $\ln(K)$ for unsaturated conditions, using a formula attributed to Gelhar and Axness (1983) which was developed for saturated porous media. Khaleel (2004, Table 9) estimated longitudinal "macro-dispersivities," A_L, for both the "sandy" and "gravelly" sequences of sediments underlying the IDF site using the following equation:

$$A_L(h) = \sigma_{LnK}^2 \lambda \tag{7.1}$$

where the first term on the right side is the variance of the natural log of *unsaturated* hydraulic conductivity, $K(h)$, computed for a soil moisture tension, h, of 100 cm, and the second term is the correlation length in the direction of flow. Khaleel (2004) assumed that for application to (unsaturated) vadose zone sediments the λ term in Eq. (7.1) represents the vertical direction. He used a vertical correlation length of 0.3 m for both the sandy and gravelly sediments and estimated longitudinal and transverse dispersivity values of ~2 m and 0.2 m, respectively, for the sandy sequence, and ~0.3 m and 0.03 m, respectively, for the gravelly sequence. The formula in Eq. (7.1) was actually used only for the longitudinal dispersivity. Khaleel (2004) cites Gelhar et al. (1993) as the basis for assuming a longitudinal to transverse dispersivity ratio of 10X, which was assumed to also be applicable to unsaturated vadose zone materials. Note that both the tension value (100 cm) used by Khaleel (2004) for computing σ_{LnK}^2 and the vertical correlation length (30 cm) used for λ in Eq. (7.1) differ from the tension range (150-200 cm) and the vertical correlation length (50 cm) used by Khaleel (2004) for computing Polmann (1990) model parameters.

There are several issues of concern when applying results from stochastic theories derived for saturated aquifer materials to estimate dispersivities for IDF site PA modeling. Gelhar et al. (1994, p.15) state, *"There is no scientific consensus about how to characterize dispersion in unsaturated flow,"* and, *"Clearly there is a need for carefully designed field tracer experiments extending over tens of meters with measurements of spatially variable hydraulic parameters in order to evaluate the predictive capabilities of the unsaturated stochastic transport theory."* Although these statements were made more than 20 years ago, they remain true today. It has not yet been clearly demonstrated that dispersivity estimates based on stochastic theories developed for saturated aquifer systems, in which solute transport is predominantly parallel to stratification, are applicable to variably saturated systems in which the principal transport direction is usually normal (perpendicular) to stratification. Evidence to the contrary is provided by the results of a number of experimental and modeling studies, some of which are reviewed below.

7.1.1   Vadose Zone Field Studies

Figure 7.1 shows computed values of dispersivity versus depth (or vertical transport distance) from four vadose zone field experimental studies (Butters and Jury 1989; Porro et al. 1993; Khaleel 2004), including one performed in surficial Hanford sediments near the IDF site (see appendix by Ward et al. 1998 in Khaleel, 2004). None of these data sets show dispersivity values reaching asymptotic (constant) values with increasing transport distance. The reported transport distances represented by these vadose zone data sets are, however, relatively short compared to saturated aquifer systems.

It should be reemphasized that in saturated aquifer systems, solute transport typically occurs in a direction parallel to stratification, whereas in unsaturated sediments, transport typically occurs in a direction perpendicular to stratification, which can result in dramatically different behavior. For example, the data shown in Figure 7.1 from Porro et al. (1993, Table 5) are from unsaturated flow and tracer transport experiments performed in two large, 0.95 m diameter × 6 m deep sediment-filled lysimeters, using tritium as a tracer. One of the lysimeters (labeled "uniform") was packed uniformly with Berino loamy fine sand (fine-loamy, mixed thermic Typic Haplargid), composed of 92.8% sand, 2.5% silt, and 4.7% clay (Porro et al. 1993). The other lysimeter (labeled "layered") was packed with alternating 20-cm-thick layers of the Berino loamy fine sand and Glendale silty clay loam (fine-silty, mixed (calcareous), thermic, Typic Torrifluvent), composed of 15.4% sand, 62.5% silt, and 22.1% clay. Steady vertical flow conditions were established in the lysimeters prior to addition of tracers, with flow rates of 1.84 and 2.06 cm/d used for the uniform and layered lysimeters, respectively. The CDE was fit to observed tritium breakthrough curves monitored at multiple depths to estimate dispersion coefficients. Dispersivities were then calculated from the fitted dispersion coefficients and pore water velocities.

The dispersivity values shown in Figure 7.1 for the lysimeter packed with uniform sediment of Porro et al. (1993) are significantly <u>larger</u> than for the lysimeter packed with layered (more heterogeneous) sediment. This result is the opposite of what has been observed in saturated aquifers, where more heterogeneity leads to more dispersion. Porro et al. (1993) attributed the behavior observed in their lysimeter experiments to increased mixing of solute in wetter areas of the layered column, more uniform passage of solutes through the finer-textured, silty clay loam layers, and the inhibiting effect of layering on preferential flow. It is important to note that in the experiments of Porro et al. (1993) flow was effectively one-dimensional (vertical): water flow and solute transport were forced in the direction normal to layering. In a layered vadose zone system with no lateral boundaries, some lateral flow would also likely occur. However, Ellsworth and Jury (1991) report a similar front sharpening effect, or reduced

dispersion in the direction normal to soil layering, for a three-dimensional field study in unsaturated, layered soils for the same field site used by Butters and Jury (1989).

For 2D modeling of water flow and tracer transport for a field experiment performed at the Las Cruces Trench Site in New Mexico, Hills and Wierenga (1994) used *isotropic* dispersivity values of 0.05 m and 0.03 m for models with uniform and heterogeneous property fields, respectively, and grid block sizes of 0.05×0.05 m. Rockhold et al. (1996) used an *isotropic* dispersivity value of 0.03 m for modeling the same Las Cruces Trench experiment using models with heterogeneous property fields and with uniform grid block sizes of 0.1×0.1 m. In both cases, selection of dispersivity values was based on the results of Porro et al. (1993) for the uniform Berino sand-filled lysimeter (Figure 7.1).

Rockhold et al. (1996) report values of σ^2_{lnKfs} [cm/d] = 1.47 for a sample size of 444 measurements of field-saturated hydraulic conductivity (K_{fs}) made with a borehole permeameter at the Las Cruces Trench Site, and λ=45 cm (for the vertical direction) for scaling factors representing the K_{fs} data. Using these values in the expression of Gelhar and Axness (1983), shown in Eq. (7.1), yields a dispersivity estimate of ~66 cm (0.66 m). This value is >10X larger than the dispersivity values determined by Porro et al. (1993) from the large-scale lysimeter experiments with the Berino loamy fine sand, which were used successfully by both Hills and Wierenga (1994) and Rockhold et al (1996) for modeling the field-scale flow and tracer transport experiments performed at the Las Cruces Trench Site. If σ^2_{lnK} (the variance of the natural log of the *unsaturated* hydraulic conductivity at some prescribed flux) was used instead of σ^2_{lnKfs}, as suggested by Khaleel (2004) for the Hanford IDF PA calculations, the estimated dispersivity would be even higher.

To the best of our knowledge, aside from the experiments performed at the Las Cruces Trench Site, no other large-scale field experimental studies of unsaturated flow and transport have been performed and documented <u>anywhere</u> that could be used to test or validate the use of these stochastic transport theories applied to unsaturated conditions. The total vertical transport distance in the field experiments at the Las Cruces Trench Site was also less than 6 m, or less than 1/10 the thickness of the vadose zone underlying the Hanford IDF site. The bottom line is that it is much more difficult to estimate large-scale asymptotic dispersivity values from field experimental data for vadose zone sediments—if such a thing even exists for highly stratified vadose zone sediments—compared to aquifer materials. Additional, larger-scale vadose zone experimental and/or carefully designed modeling studies are needed for testing the validity of these stochastic transport theories, or for developing alternative methods, for application to the very-large-scale unsaturated flow and transport modeling required for Hanford Site PA calculations.

The longitudinal dispersivity value of 2 m estimated by Khaleel (2004) for the sandy sequence of unsaturated sediments underlying the IDF is significantly larger than any known experimentally derived vadose zone results that have been reported in the literature. Extrapolation of the trend line shown in Figure 7.1 for the data of Ward et al. (1998) (see appendices of Khaleel, 2004) suggests that this value could be reasonable if the character of heterogeneity at the field site investigated by Ward et al. (1998) is similar to that of the sandy sediments underlying the IDF site, and if the entire sandy sequence of the Hanford formation is treated as an EHM. On the other hand, the data from Porro et al. (1993) indicate that strong stratification of vadose zone sediments, which is typical of some areas at Hanford, may actually lead to smaller dispersivities relative to uniform sediments for the flow direction normal to stratification. The calculations noted above for soils at the Las Cruces Trench Site also suggest that Eq. (7.1) may overestimate dispersivities for vadose zone sediments. For IDF PA calculations, overly

diffusive vadose zone transport results stemming from the use of excessively large macro-dispersivities would result in earlier predicted arrivals and longer tailing, but lower predicted peak concentrations of contaminants at the water table.
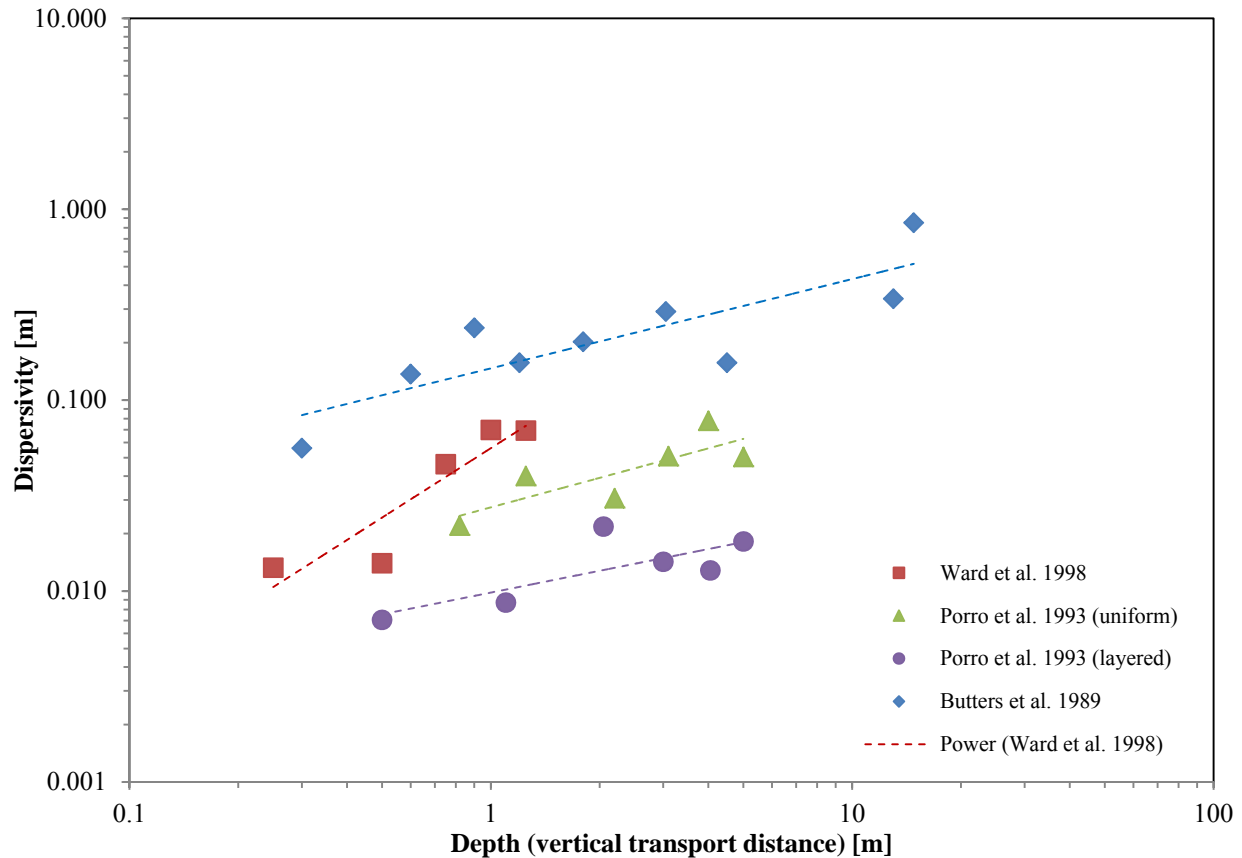
Figure 7.1. Dispersivity versus Depth (vertical transport distance) Computed for Selected Vadose Zone (unsaturated) Flow and Transport Field Experimental Studies

Several numerical issues should also be considered. For large-scale modeling of unsaturated flow and transport, variable grid spacings are typically used for the horizontal and vertical directions, with the horizontal discretization generally being much larger than the vertical. Although this fact is usually overlooked, differences between the horizontal and vertical spatial discretization generate anisotropic behavior in flow and transport simulation results, even if permeability and dispersion tensors are specified as being isotropic. For example, a point source injection into a grid block that is 10 × 10 m (x-y) × 1 m (z) immediately results in water and solute spreading that is 10 times greater in the horizontal direction than in the vertical direction, simply because of the spatial discretization. Standard numerical methods for solving the ADE usually also exhibit some degree of numerical dispersion, which is typically not quantified but may add a significant amount of spreading to simulated solute plumes beyond that which is generated via the user-specified dispersivity values.

7.1.2   Laboratory Studies in Saturated Porous Media

It is not the transport distance per se but rather the character of heterogeneity encountered along the transport path, and the resultant variations in velocity of the transporting fluid, that leads to solute

dispersion. The basic premise behind the development of the stochastic transport theories noted above is that we will never know the details of subsurface heterogeneity, but we can estimate the mean and variance of $Ln(K_s)$ [or $Ln(K)$ for unsaturated conditions] and its correlation lengths based on limited characterization data. If we then assume the porous media is stationary, such that the statistics based on the limited characterization data are applicable anywhere in the field of interest, then the stochastic transport theory may be applicable (assuming other assumptions used in its development are also met). One additional assumption, generally not stated but implied by the use of the stochastic perturbation method, is that the variance of $ln(K)$ is relatively "small" (<1). This assumption is rarely satisfied but is typically not worried about.

If other information on physical heterogeneity is available, such as grain size distribution data or other metrics that are known to be related to solute dispersion, it may also be possible to estimate dispersivity from more fundamental data. Geostatistical conditional simulation methods can then be used to infer properties at unsampled locations. Development of correlation functions based on more fundamental physical property data is usually accomplished using data obtained from laboratory experiments, typically performed in columns.

As noted by Han et al. (1985) "*if the column is too short one can measure a dispersion coefficient that is significantly lower than the final asymptotic value.*" Asymptotic refers to the so-called *Fickian* behavior that was mentioned earlier in the context of macro-dispersion coefficients estimated using stochastic theories. Han et al. (1985) also note that the more heterogeneous the porous media, the longer a column needs to be to achieve asymptotic results. Therefore, when developing correlations between dispersion coefficients or dispersivities and other physical properties, laboratory experimental data require careful screening to avoid using results with experimental artifacts, or mixing pre-asymptotic and asymptotic data. There is an enormous amount of literature on dispersion of solutes in packed beds of porous media (Delgado 2006). A few select studies are reviewed here.

7.1.2.1   Longitudinal Dispersion

Harleman et al. (1963) describe the results of 60 experiments performed using seven different types of spherical particles and three different types of angular sands with different mean grain diameters and size distributions to estimate longitudinal dispersion coefficients. Although a total of 10 different types of particles were used, each was either uniform, or nearly uniform, with uniformity coefficients, $C_u = d_{60}/d_{10}$, ranging from 1 to 1.15, and porosities ranging from 0.36 to 0.4. Their results show that (dimensionless) dispersion coefficients for packed columns of both uniform spherical particles and the relatively uniform non-spherical sands of different sizes were well-described by power functions of (dimensionless) Reynolds numbers computed using either the mean grain size (d_{50})

$$R_{d_{50}} = \frac{|u|d_{50}}{\upsilon} \tag{7.2}$$

or the square root of permeability ($\sqrt{k}$)

$$R_k = \frac{|u|\sqrt{k}}{\upsilon} \tag{7.3}$$

as characteristic length scales. In Eqs. (7.2) and (7.3), $|u|$ is the pore water velocity [cm/s] and υ [cm^2/s] is the kinematic viscosity, defined by

$$\upsilon = \frac{\mu}{\rho} \qquad\qquad (7.4)$$

where μ is the dynamic viscosity [g/(cm s)], and ρ is the fluid density [g/m^3]. Figure 7.2 and Figure 7.3 show experimental results and fitted correlation functions relating longitudinal dispersion coefficients, D_1/υ, to Reynolds numbers.

As shown in Figure 7.2 and Figure 7.3, the leading constants in the power function expressions developed by Harleman et al. (1963) differed (by a factor of <1.6) for spherical particles versus non-spherical sands, and depending on whether a grain-size-based or permeability-based Reynolds number was used. However, the exponent in their expressions was the same constant value (~1.2) for all cases. For a given value of the Reynolds number, more dispersion was observed for the angular sands than for the spherical particles, even when the mean particle diameters and uniformity coefficients were the same for both types of particles. This is clearly a particle shape or surface roughness effect. They noted that the leading constants in their equations were dependent on particle shape and size distributions, and speculated that the exponent in their expressions was also a function of the particle-size distribution. To the best of our knowledge this latter conjecture has not been tested systematically.

The inside diameter of the column used by Harleman et al. (1963) was reported to be 9.78 cm. A schematic diagram of the experimental apparatus shown in their paper suggests that the length of the porous media-packed region of column was 4 to 5 times greater than the column diameter, or ~43 cm. However, the actual length of the column was not reported. Solute breakthrough was measured only near the outflow end of the column, so the extent to which these results might represent asymptotic behavior is unknown.
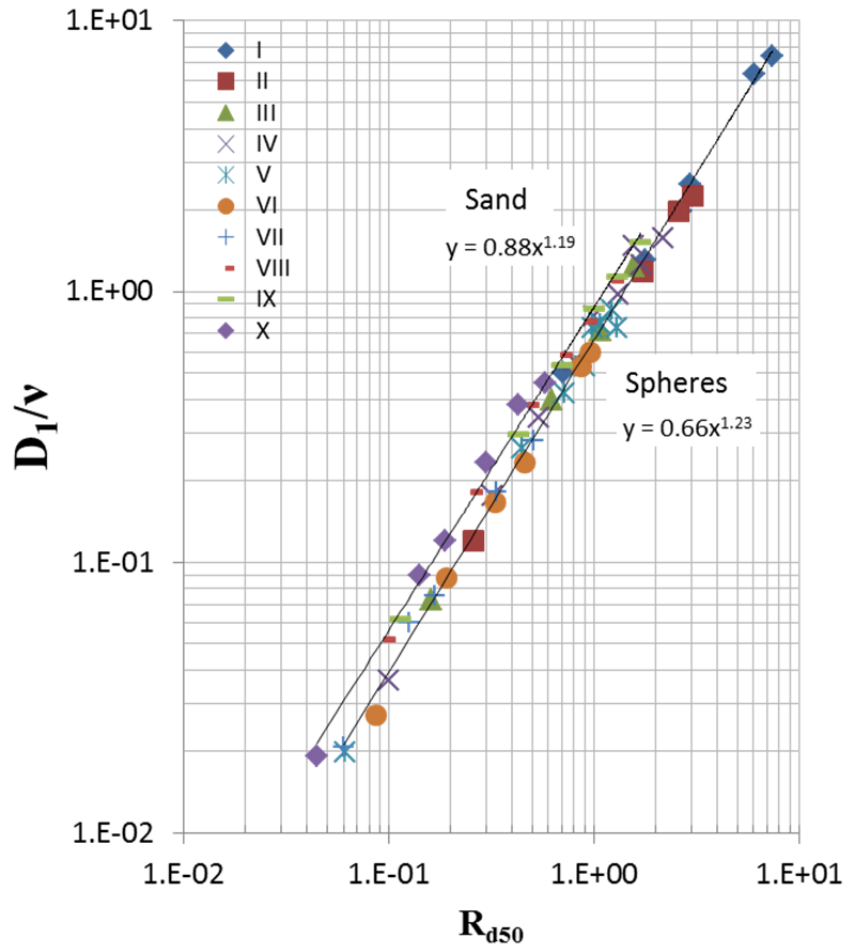
Figure 7.2. Relationships Between Dispersion Coefficients and Particle-size-based Reynolds Numbers for Angular Sands and Spherical Particles (from Harleman et al. 1963)
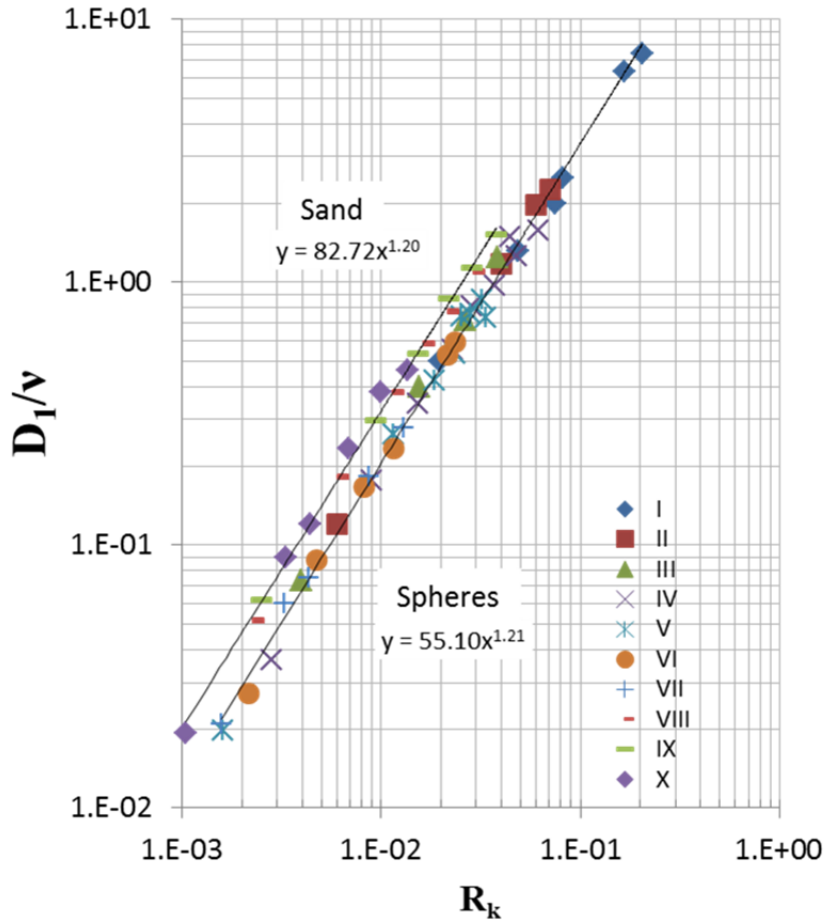
Figure 7.3. Relationships Between Dispersion Coefficients and Permeability-based Reynolds Numbers for Angular Sands and Spherical Particles (from Harleman et al. 1963)

   Han et al. (1985) conducted an extensive literature review and performed an experimental study of longitudinal and transverse dispersion in packed beds in which the effects of column length and PSDs were carefully evaluated. They paid particular attention to the use of experimental data sets with length and time scales that were long enough so that asymptotic values of dispersivity were achieved. They also used 150-cm-long columns instrumented at five different locations along their lengths for their own experiments so that they could determine when asymptotic behavior was reached. The dispersion coefficients computed using the data for the largest transport distance (~150 cm) in their experiments were used in the development of correlation functions. Figure 7.4, modified from Han et al. (1985) to include a trend line, shows selected results for seven different sets of experiments, including their own work, which used spherical particles. A strong log-log relationship is shown between the (dimensionless) Peclet number, Pe_p, and the (dimensionless) ratio $D_{xx}*/D_m$, where Pe_p is defined as

$$Pe_p = \frac{|u|d_p}{D_m}\left(\frac{\theta}{1-\theta}\right) \tag{7.5}$$

where d_p is the (presumed mean, d_{50}) particle diameter [cm], D_m is the coefficient of molecular diffusion for the solute in the fluid [cm^2/s], and θ is the void fraction (porosity or volumetric fluid content)

[dimensionless]. The term $D_{xx}*$ in Figure 7.4 is the longitudinal component of the dispersion tensor. The trend line overlain on the data from Han et al. (1985) in Figure 7.4 delineates what appears to be a very robust relationship between Peclet numbers and dispersion coefficients for a wide range of conditions, albeit with particles of either uniform or very narrow size distributions. The exponent of the trend line (~1.2) is of particular interest since it is essentially the same as the exponent determined some 22 years earlier by Harleman et al. (1963). To the best of our knowledge, this correspondence has not been previously noted. However, we speculate that this similarity in exponents is a result of these studies all using uniform (or nearly uniform) and spherical (or nearly spherical) particles. The curvature in the trend of the data shown in Figure 7.4 for larger Peclet numbers was attributed to experiments for which the columns were not quite long enough to achieve asymptotic results, while the constant values of dispersivity at low Peclet numbers represent the regime where diffusion dominates.

The Peclet number used by Han et al. (1985) is the product of a particle-based Reynolds number, like that used by Harleman et al. (1963), a Schmidt number,

$$S_c = \frac{\mu}{\rho D_m} \tag{7.6}$$

and the ratio of the fluid-to-solid volume fractions. The dimensionless dispersion coefficient used by Han et al. (1985) is the longitudinal dispersion coefficient divided by the molecular diffusion coefficient. Given the similarities in variables, the favorable correspondence between the results from Han et al. (1985) and Harleman et al. (1963) is not unexpected.

Han et al. (1985) also looked at the relationships between Pe_p and $D*_{xx}/D_m$ for packed columns containing uniform particles, and columns containing particles with two different size distributions, specifically to examine the influence of PSDs on dispersion. These relationships, shown in Figure 7.5, also yield exponents of ~1.2. Size distribution 1 had a ratio of maximum to minimum particle diameter of 2.2. Size distribution 2 had a small percentage of very large particles where the ratio of maximum to minimum particle diameter was 7.3. The large particles in size distribution 2 made up ~11% of the total solid volume.
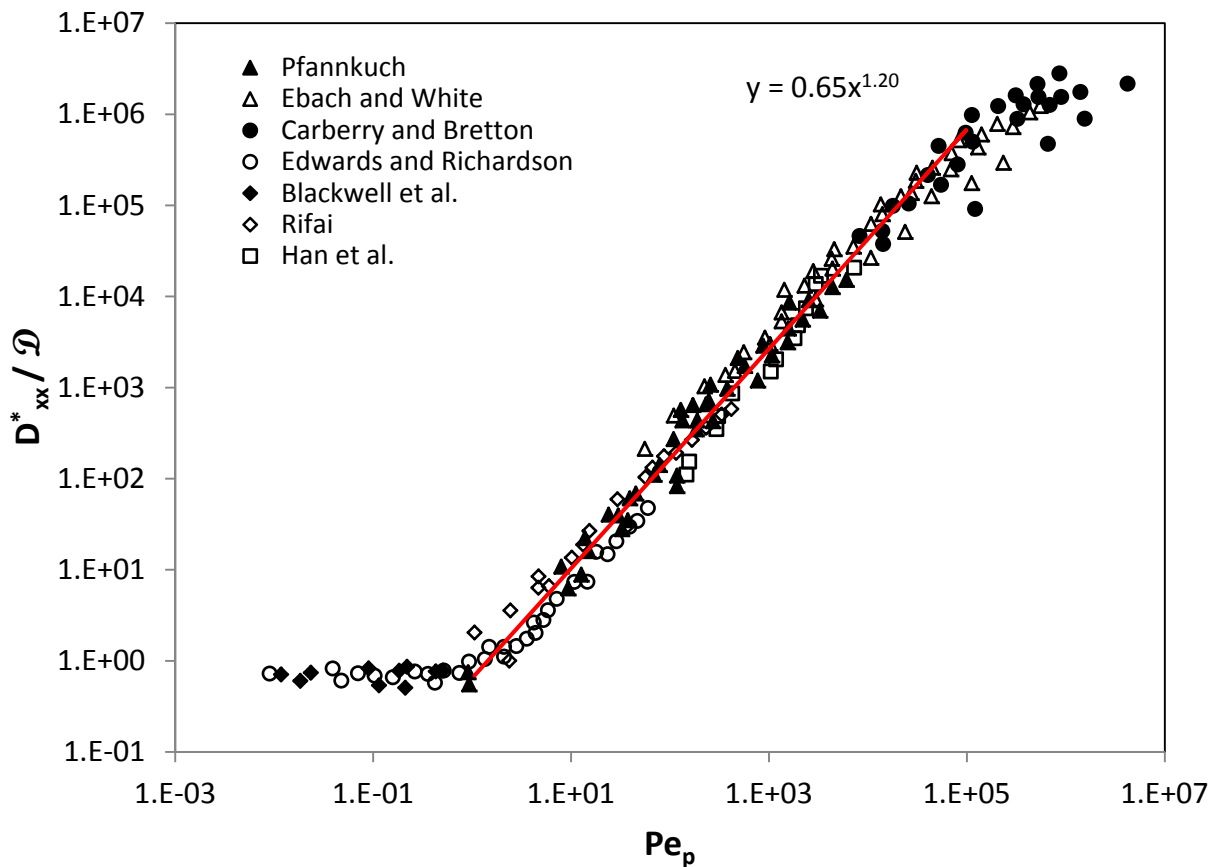
Figure 7.4. Dimensionless Longitudinal Component of Hydrodynamic Dispersion Tensor versus Dimensionless Peclet Number (modified from Han et al. 1985)

The differences in the leading coefficients of the power functions fit to the results for size distributions 1 and 2 clearly suggest that the value of this coefficient is related to the width of the PSD. However, the similarity of results shown in Figure 7.5 for the size distribution 1 and the uniform size distribution also suggests that there is a threshold of grain size non-uniformity below which dispersion is essentially unaffected. As shown earlier by the results from Harleman et al. (1963), these leading coefficients are also related to particle shape or surface roughness. It would appear that increasing the angularity of particle shapes and/or surface roughness has essentially the same effect on dispersion as increasing the width of the PSD.

Xu and Eckstein (1997) evaluated relationships between dispersivity and other physical properties including porosity, hydraulic conductivity, median grain size, and grain size uniformity coefficient based on 113 experiments performed in 31-cm-long, water-saturated columns packed with glass beads. They found that porosity and uniformity of particle sizes were the two most important factors influencing dispersivity, with dispersivity values being directly proportional to the uniformity coefficient, $C_u = d_{60}/d_{10}$, and inversely proportional to porosity. Porosity and uniformity coefficient were shown to be correlated, as expected, with porosity declining rapidly from about 0.5 to 0.3 as C_u increased from 1 to 10. For uniform materials, dispersivity values increased with increasing median particle size, d_{50}. However, interestingly the median particle size was reported to have a significant influence on dispersivity values

only for relatively uniform materials ($C_u < 3$). Also, contrary to some other studies (Harleman et al. 1963), the dispersivity values computed by Xu and Eckstein (1997) were reported to not be strongly related to the average hydraulic conductivity, K, of the porous media.
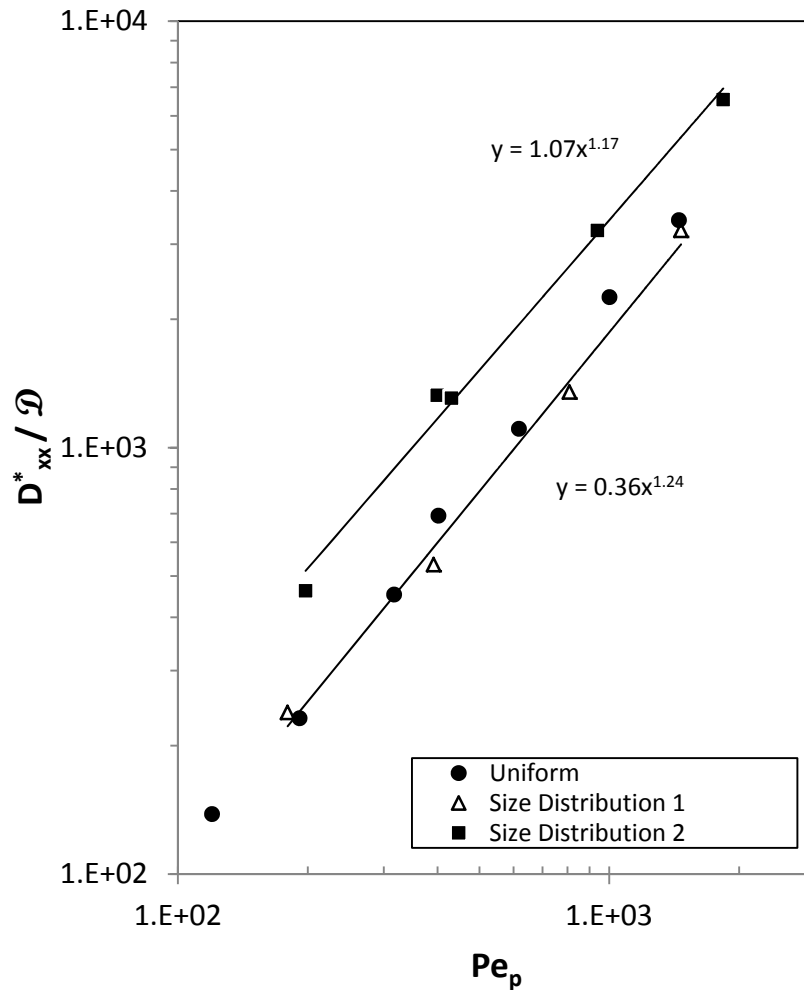
Figure 7.5. Dimensionless Longitudinal Component of Dispersion Tensor versus Dimensionless Peclet Number for a Uniform Particle Size and for Two Different PSDs (modified from Han et al. 1985)

One point of caution with the study of Xu and Eckstein (1997) is that their columns were only 31 cm long, so the extent to which their results may have been affected by column length is unknown. Recall that earlier work has shown that the less uniform the particle size, the longer the column must be to obtain asymptotic dispersion results (Han et al. 1985). The maximum longitudinal dispersivity value reported by Xu and Eckstein (1997) for all 113 of their experiments was 4.6 cm for a bead pack with $C_u = 7.5$.

Xu and Eckstein (1997) report that dispersivities were most strongly correlated with porosity and particle uniformity coefficient, C_u. Returning to the data of Han et al. (1985, Table 2), the PSDs 1 and 2 (whose dispersion results are shown in Figure 7.5) are depicted in Figure 7.6. The computed values of C_u for PSDs 1 and 2 are ~1.59 and ~1.50, respectively. These two PSDs were clearly constructed in such a way that C_u is not a useful metric for distinguishing between them.
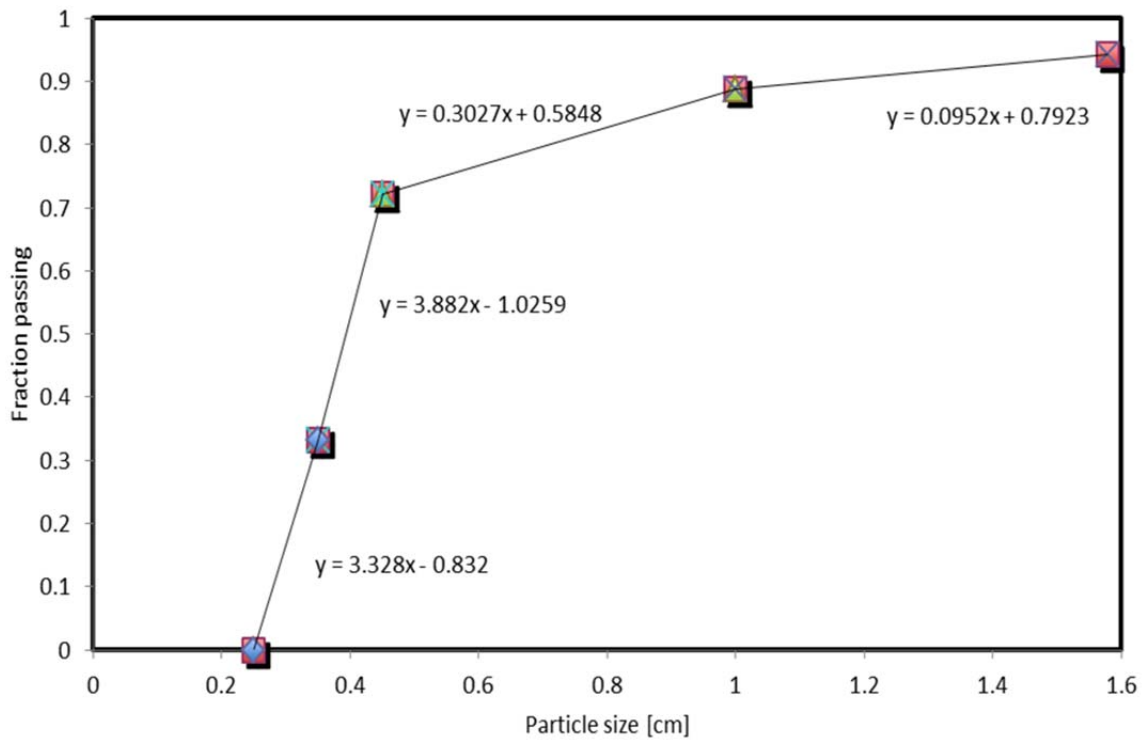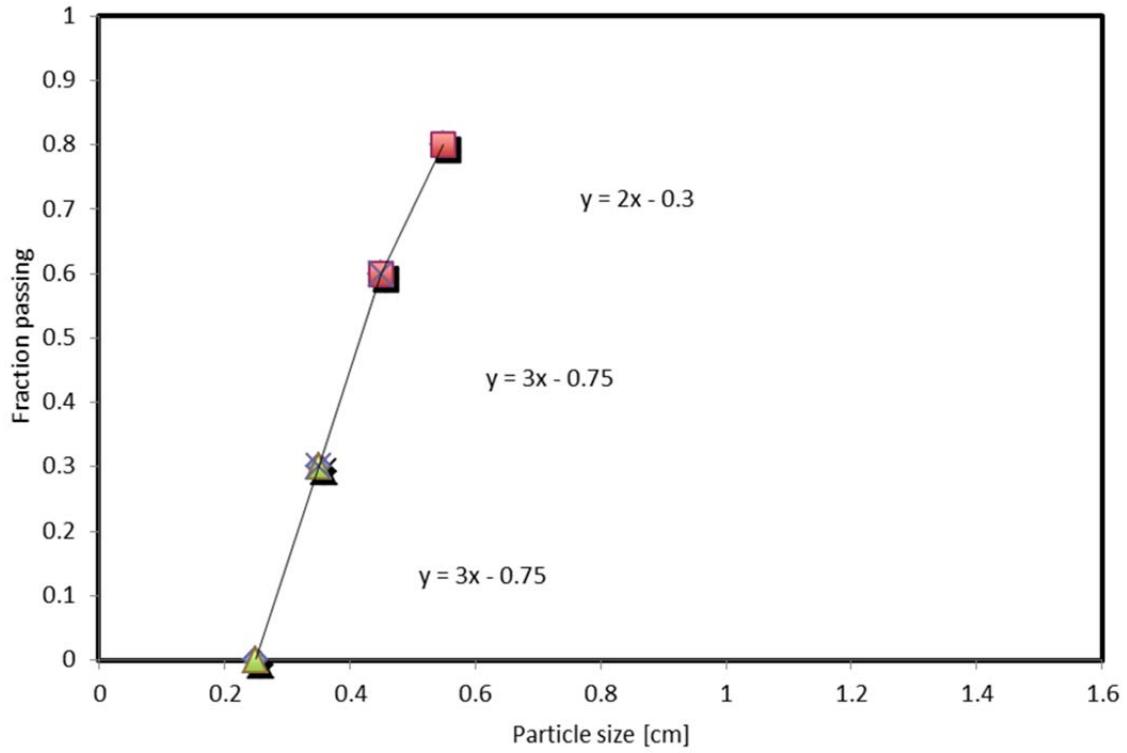
Figure 7.6. Cumulative PSDs for Size Distribution 1 (top) and 2 (bottom) from Han et al. (1985, Table 2)

However, the differences between the computed values of particle size for the 84th and 16th percentiles of the cumulative distribution, d_{84}-d_{16}, may provide a more useful alternative metric. The computed values of d_{84}-d_{16} for particle distributions 1 and 2 of Han et al. (1985, Table 2) are 0.247 cm and 0.545 cm, respectively.

For the evaluation of any given laboratory transport experiment, dispersion coefficients and dispersivities are typically estimated directly by fitting tracer breakthrough curve results to the ADE. However, ultimately we would like to be able to estimate dispersivity from more fundamental and easily measured physical property data. Scheidegger (1961) postulated that the longitudinal component of the dispersion tensor is related to the pore water velocity by

$$D_{xx}^* = \alpha_L |u_{xx}| \tag{7.7}$$

where α_L is a pore system geometry factor known as the longitudinal dispersivity [cm]. The molecular diffusion coefficient, D_m, is sometimes added the right side of Eq. (7.7). The results of Harleman et al. (1963) and Han et al. (1985) suggest a slightly different form

$$D_{xx}^* = \alpha_L |u_{xx}|^{b_L} \tag{7.8}$$

Equating the correlation function used by Han et al. (1985),

$$D_{xx}^* = a_L D_m \left[\frac{|u_{xx}| d_{50}}{D_m} \left(\frac{\theta}{1 - \theta} \right) \right]^{b_L} \tag{7.9}$$

with Eq. (7.8) yields the following expression for estimating longitudinal dispersivity

$$\alpha_L = exp\left\{ ln(a_L) + (1 - b_L)ln(D_m) + b_L ln(d_{50}) + b_L ln\left(\frac{\theta}{1 - \theta} \right) \right\} \tag{7.10}$$

where $b_L \approx 1.2$ for this data set. Equating the correlation function of Harleman et al (1963),

$$D_{xx}^* = a_L \upsilon \left(\frac{|u_{xx}| d_{50}}{\upsilon} \right)^{b_L} \tag{7.11}$$

with Eq. (7.8) yields a similar expression

$$\alpha_L = exp\{ ln(a_L) + (1 - b_L)ln(\upsilon) + b_L ln(d_{50}) \} \tag{7.12}$$

where again $b_L \approx 1.2$. Note that the kinematic viscosity of water at 20 °C is, $\upsilon = 0.01004$ cm^2/s.

Inspection of Eqs. (7.10) and (7.12) shows that both of these equations include the a_L and b_L parameters, which are both likely to be a function of the spread of the PSD. Both equations also contain a d_{50} term, representing the mean particle size—a measure of central tendency. Eq. (7.12), based on the form of the dispersivity correlation function developed by Harleman et al. (1963), includes a kinematic viscosity term, whereas Eq. (7.10), based on the form of the correlation function used by Han et al. (1985), includes terms for the molecular diffusion coefficient, D_m, and the porosity or water content, θ.

As noted by Xu and Eckstein (1997), porosity and uniformity coefficient are correlated. Therefore, including both the a_L term (which like C_u is also a measure of the particle size uniformity), and a porosity term in Eq. (7.10) may provide somewhat redundant information. Eq. (7.10) also shows dispersivity being proportional to porosity, while Xu and Eckstein (1997) report that dispersivity is inversely proportional to porosity. Nützmann et al. (2002) and Padilla et al. (1999), whose results are discussed in more detail later, report that dispersivity increases with decreasing water content.

7.1.2.2   Transverse Dispersion

Harleman and Rumer (1963) performed experiments in a water-saturated, 3.02-m-long Lucite box packed with relatively uniform spherical particles (C_u=1.14; d_{10}=0.86 mm; d_{50}=0.96 mm). The porosity of the sphere pack was 0.36 and the average hydraulic conductivity was 0.8 cm/s. The box was instrumented with conductivity probes placed at three locations along its length (5 cm, 151.5 cm, and 273.5 cm) for measurement of electrical conductivity, from which concentrations of the NaCl tracer were determined. Longitudinal dispersion coefficients were calculated from these results. The vertical positions of the probes were also adjustable to allow for measurement of electrical conductivity at different lateral distances, from which transverse dispersion coefficients were calculated. Although longitudinal dispersion is known to increase with travel distance until some asymptotic limit is reached, Harleman and Rumer (1963) stated that there was no noticeable variation of the transverse dispersion coefficients with transport distance. Han et al. (1985) also calculated transverse dispersion coefficients from their experiments and reported results that were very similar to the results generated by Harleman and Rumer (1963).

Figure 7.7 shows the longitudinal (D_1=D_L) and transverse (D_2=D_T) dispersion coefficients reported by Harleman and Rumer (1963). Figure 7.7 shows that the difference between the longitudinal and transverse dispersion coefficients increases as the Reynolds number increases. Following the development of Eq. (7.12), and using the coefficients reported in Figure 7.7, the longitudinal and transverse dispersivities can be estimated from

$$\alpha_L = exp[ln(0.66) - 0.2ln(\upsilon) + 1.2ln(d_{50})] \tag{7.13}$$

$$\alpha_T = exp[ln(0.036) + 0.3ln(\upsilon) + 0.7ln(d_{50})] \tag{7.14}$$

Calculation of α_L and α_T using Eqs. (7.13) and (7.14), respectively, yields an anisotropy ratio $\alpha_T/\alpha_L \cong 0.01$ for this porous medium.
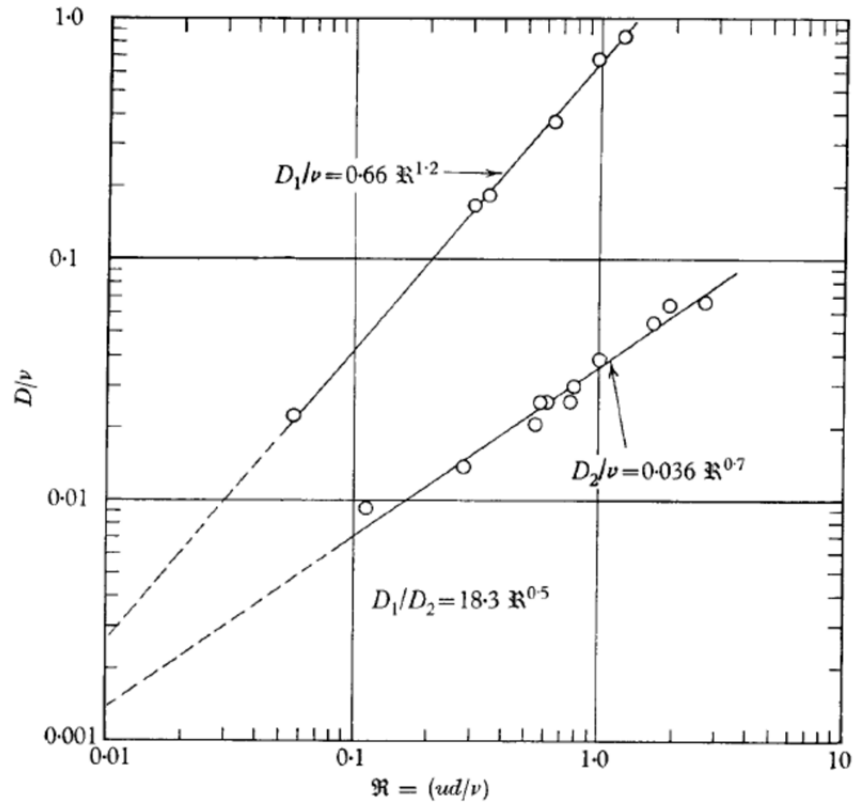
Figure 7.7. Correlation of Longitudinal (D_1) and Transverse (D_2) Dispersion Coefficients with Reynolds Number (from Harleman and Rumer 1963)

7.1.2.3   Generalized Correlations

Delgado (2006) provides a review of more than 50 years of research on dispersion in packed beds. Through dimensional analysis, he suggests that the functional dependence of longitudinal dispersion can be expressed generally as

$$\frac{D_L}{D_m} = Pe_L = \Phi\left(\frac{L}{D}, \frac{D}{d}, \frac{ud}{D_m}, \frac{\mu}{\rho D_m}\right) \tag{7.15}$$

where L is column length, D is column diameter, d is particle diameter, u is pore-water (a.k.a. interstitial) velocity in the longitudinal direction, and other parameters have been defined previously. For columns that are large compared to the particle size, such that wall effects are negligible and asymptotic or near-asymptotic results can be assumed, only the last two terms on the right side of Eq. (7.15) are important. Delgado (2006) developed empirical correlation functions for both longitudinal and transfer dispersion coefficients based on these dimensionless groups for random packings of "isometric" spherical particles that are well-packed. Note that the last two terms in Eq. (7.15) can be recognized as a particle-size-based Peclet number, $Pe_m = ud_{50}/D_m$, and the Schmidt number, Sc. Harleman et al. (1963), Harleman and Rumer (1963), and Han et al. (1985) used slightly different variations of these dimensionless parameter groups in their dispersion correlations.

The previously reviewed experimental work and correlations did not explicitly consider diffusive and convective components of dispersion to be additive, since molecular diffusion was likely small or

negligible for most of the experimental conditions that were evaluated. Others (Gunn 1968; Guedes de Carvalho and Delgado 2000; Delgado 2006) have suggested that if diffusive and convective components of dispersion are additive then both the longitudinal and transverse dispersion coefficients for fluid-saturated porous media can be expressed more generally as

$$\frac{D_{L,T}}{D_m} = \frac{1}{\tau} + a_{L,T} Pe_m{}^{b_{L,T}} \tag{7.16}$$

where the subscript L or T stands for the longitudinal or transverse direction, respectively, the tortuosity factor, $\tau = \sqrt{2}$ (Delgado 2006), and a and b are empirical parameters that depend on the direction (L or T) and the characteristics of the PSD (Harleman and Rumer 1963; Han et al. 1985). For variably-saturated conditions, empirical tortuosity factors are often used (Millington, 1959; Meyer et al. 2004).

7.1.3   Laboratory Studies in Unsaturated Porous Media

Most of the laboratory results discussed thus far represented porous media saturated with a single fluid (typically water). The effect of unsaturated or variably saturated conditions on dispersivity is also obviously of interest. Several studies have suggested that more tortuous flow paths result at lower water contents, which leads to more dispersion (Maraqa et al. 1997; Padilla et al. 1999; Nützmann et al. 2002). An open question is whether or not the estimated values of dispersivity generated using the type of power function expression developed above based on Reynolds or Peclet numbers can be adapted or similar expressions developed to apply to unsaturated flow conditions. Some laboratory experimental studies on transport in unsaturated conditions are reviewed to investigate this question.

Maraqa et al. (1997) measured tritium breakthrough curves under both saturated and unsaturated conditions for ground samples of the A and B horizons of the Oakville sand (mixed mesic Typic Udipsaments) and the B horizon of the Pipestone sand (mixed mesic, Entic Haplaquods), packed into 30.2-cm-long glass cylinders. All three ground samples had very similar grain size distributions, ranging from 94.5% to 95% sand, 3.1% to 4% silt, and 1.5% to 2% clay. They fit the ADE and the mobile-immobile (MIM) pore water models (van Genuchten and Wierenga 1976; Wierenga and van Genuchten 1989) to their experimental results and found that calculated values of dispersivity for unsaturated conditions were about two times greater than for saturated conditions.

Padilla et al. (1999) performed 16 experiments in 25-cm-long columns to investigate the effect of water content on transport of NaCl through unsaturated quartz sand. The particle sizes of the very fine to medium sand that was used in all experiments are reported to have ranged from 53 to 425 μm (0.053 to 0.425 mm), with an average particle size of 250 μm (0.25 mm). This gives a ratio of largest to smallest particle sizes of 8.02. This sand, which we will refer to in subsequent discussion simply as *fine sand*, is reported to have been fairly homogeneous and well sorted, with over 80% of the particles falling between 149 and 300 μm size range. The sand was uniformly packed to a dry bulk density of 1.49 g/cm^3 and total porosity of 0.45.

Padilla et al. (1999) note that the ADE is widely accepted but strictly valid only when the transport of the solute has reached the Fickian regime (discussed earlier). For unsaturated (and saturated) conditions in short columns, which are typically used in laboratory experiments, the time and distance required to reach asymptotic conditions may not be sufficient, and hence solute breakthrough may exhibit multiple peaks, early initial arrival, and long tails that cannot be adequately described by the ADE. Consequently

alternative models such as the dead-end pore model (Coats and Smith 1964) and MIM model (van Genuchten and Wierenga 1976; Wierenga and van Genuchten 1989) have been developed to make up for the shortcomings in the ADE and/or the experimental setup (depending on your perspective). Padilla et al. (1999) modeled their experiments using both the ADE and the MIM model, and developed the following empirical power law model to describe their experimental results, which they claim is applicable to both the ADE and MIM equations

$$D_{xx} = \frac{\eta}{\theta_m^n} v_m^n = \xi(\theta_m) v_m^n \tag{7.17}$$

where (using their notation) v_m is the mobile pore water velocity, η is the dispersivity under water-saturated conditions, $\xi(\theta_m)$ is a water content-dependent dispersivity, and θ_m is the mobile region water content for the MIM model, which is simply the water content, θ, for the ADE. Note the similarity of the form of this equation with that of Eq. (7.8). Best-fit values of n and η were 1.5 and 0.022, respectively, for the MIM model ($r^2=0.98$), and 1.99 and 0.085 for the CDE ($r^2=0.94$) (Padilla et al. 1999). These results clearly indicate that dispersivity is not just a characteristic of the porous media, but also depends on water content or saturation.

Padilla et al. (1999) cite Bear (1971) for a discussion on the role of the *n* parameter applied to the velocity term in Eq. (7.17). With reference to the MIM model, Padilla et al. (1999) state that in pore systems in which mixing results from the combined effect of velocity distribution and transverse molecular diffusion, *n* is close to 2, but when mixing occurs only at junctions connecting pore channels, *n* is near 1. They also note that their results for the η parameter (dispersivity) are consistent with earlier results showing η to increase with mean particle size (De Smedt and Wierenga 1984; Maraqa et al. 1997), and that dispersion in general increases as the width of the PSD increases (Harleman et al. 1963; Harleman and Rumer 1963). Finally, it is interesting to note that Padilla et al. (1999) also postulated that the necessity of using the MIM model may diminish as the solute travels over greater distances because solute concentrations in the mobile and immobile zones may approach equilibrium (i.e., the Fickian regime) due to better mixing.

Nützmann et al (2002) performed experiments with glass beads and *coarse sand* to evaluate the dependence of longitudinal dispersion on water content for unsaturated conditions. Their experiments with glass beads and coarse sand were conducted in 100- and 150-cm-long columns, respectively, which were significantly longer than those used by Padilla et al. (1999). The particle sizes of the glass beads ranged from 0.36 to 0.71 mm in diameter, which gives a ratio of largest to smallest particle sizes of 1.97. The particle sizes of the coarse sand ranged from 0.45 to 0.82 mm, which gives a ratio of largest to smallest particle sizes of 1.82. The bead-packed column had an average porosity of 0.347 and a saturated hydraulic conductivity of 0.0794 cm/s. The sand-packed column had a mean porosity of 0.375 and a saturated hydraulic conductivity of 0.0623 cm/s. The particle densities of the glass beads and sand were 2.57 and 2.62 g/cm^3, respectively.

The empirical expressions reported by Padilla et al. (1999) and Nützmann et al. (2002) to relate dispersivity to water content are shown in Figure 7.8 (top plot). The results from both studies were also re-expressed in terms of saturation versus relative dispersivity to lend more generality to these results.

Recall that Harleman et al. (1963) showed that the dispersion coefficients determined for transport experiments in water-saturated angular sands were larger than for spherical glass beads of approximately

the same diameter. The results reported by Nützmann et al (2002) for glass beads and coarse sand under saturated flow conditions are consistent with Harleman's results. Han et al. (1985) showed that larger dispersion coefficients were obtained for porous media with wider PSDs relative to narrower size distributions. The saturated-column results reported by Padilla et al. (1999) for fine sand and by Nützmann et al. (2002) for coarse sand appear to be consistent with Han's results. These observations all suggest that increasing the angularity of grain shape or surface roughness affects dispersion in the same way as increasing the spread of the PSD, all resulting in increased dispersion under water-saturated flow conditions.

Figure 7.8 (bottom plot) suggests the opposite effect may be true for unsaturated conditions. The rate of increase in relative dispersivity for the coarse sand is lower than for the glass beads, in spite of the fact that the two PSDs have very similar size ranges and ratios of maximum to minimum particle size. The rate of increase of relative dispersivity for the fine sand, which at first glance would appear to have a wider PSD relative to the coarse sand, is lower than for the coarse sand. Additional dispersion data for transport under unsaturated conditions using porous media with wider ranges of measured PSDs are needed.
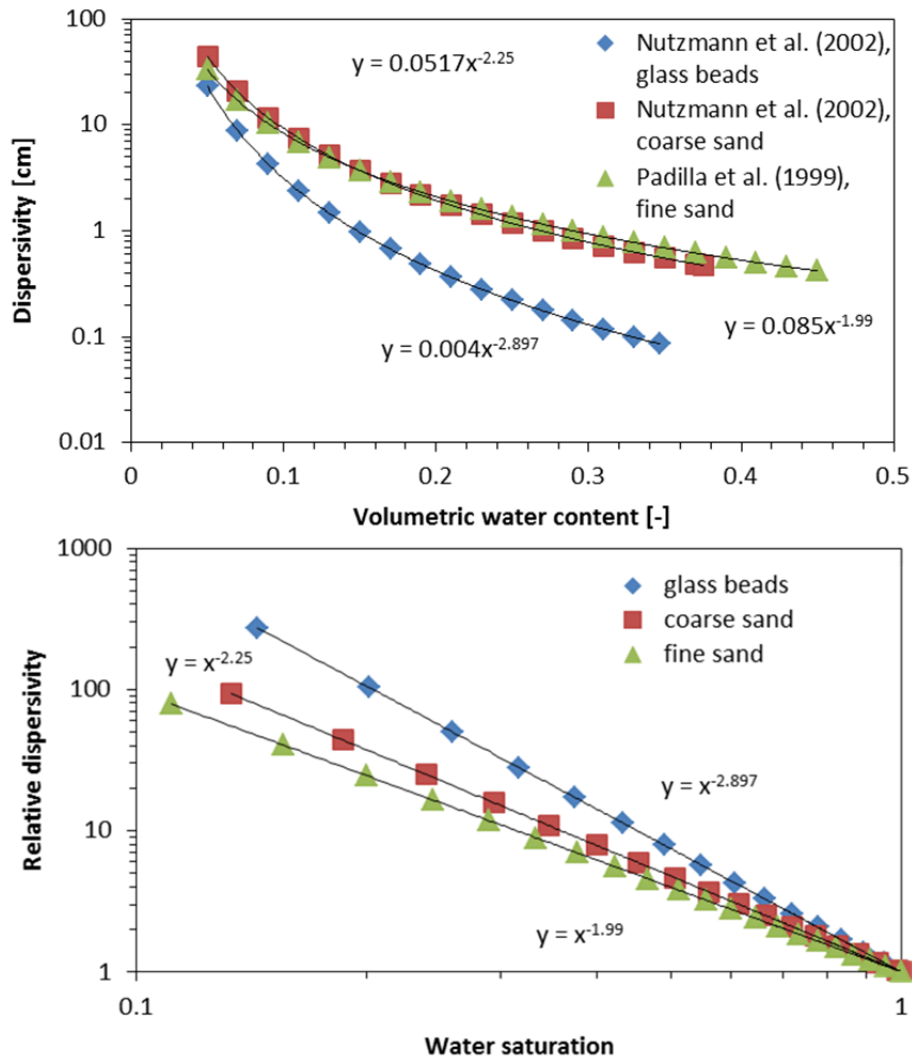
Figure 7.8. Dispersivity as a Function of Water Content (top) and Relative Dispersivity as a Function of Water Saturation (bot). Note that displayed points are computed rather than measured.

7.1.4   General Methodology for Variably Saturated Porous Media

The dispersion results described in this section for laboratory experiments performed in saturated or unsaturated porous media, suggest an equation of the following form for estimating longitudinal dispersivity values for variably saturated porous media

$$\alpha_L(S) = \frac{\alpha_L(1)}{S^n} \tag{7.18}$$

where S is the water saturation, n is an exponent describing the change in relative dispersivity as a function of water saturation, and $\alpha_L(1)$ is the longitudinal dispersivity for water-saturated conditions. For the purpose of estimating $\alpha_L(1)$, if we assume that the first term on the right side of Eq. (7.16), $1/\tau$, is small (negligible) relative to the second term, we can estimate $\alpha_L(1)$ as

$$\alpha_L(1) = exp[ln(a_L) + (1 - b_L)ln(D_m) + b_L ln(d_{50})] \tag{7.19}$$

which follows from Eq. (7.16). Note that Eq. (7.19) is similar to Eq. (7.10), except that the water content or porosity term has been dropped. The longitudinal direction to which $\alpha_L(1)$ and $\alpha_L(S)$ are applied for numerical modeling is taken as the principal coordinate direction that has the maximum pore water velocity. Directions orthogonal to it are the transverse directions to which $\alpha_T(1)$ and $\alpha_T(S)$ are applied.

The experimental data of Harleman et al. (1963), Harleman and Rumer (1963), and Han et al. (1985) suggest that transverse dispersivity for fluid-saturated uniform (or nearly uniform) and spherical (or nearly spherical) particles should be estimated as $\alpha_T = 0.01 \cdot \alpha_L$ [see Figure 7.7 and Eqs. (7.12) and (7.13)]. In the absence of direct experimental measurements for transverse dispersion in unsaturated conditions, it may be reasonable to assume that the same anisotropy ratio applies to unsaturated conditions (e.g., $\alpha_T(S) = 0.01 \cdot \alpha_L(S)$). Note, however, that Khaleel (2004) previously suggested that $\alpha_T = 0.1 \cdot \alpha_L$, based on results from Gelhar and co-workers for aquifer systems. We will also use this assumption but recommend that additional experimental and/or numerical work be performed to clarify these differences.

We postulate that the a_L and b_L terms in Eq. (7.19) are both functions of the PSD. These parameters are related by

$$a_L = exp\left[ln\left(\frac{D_{xx}}{D_m}\right) - b_L ln(Pe_m)\right] \tag{7.20}$$

An application of this dispersivity-estimation methodology is now developed.

The first data set used in this analysis represents sediments from the Hanford formation. Liu et al. (2008) performed a bromide tracer and uranium reactive transport experiment in a 0.8-m-long, water-saturated column, packed with field-textured sediments from the Hanford 300 Area to evaluate scaling relationships between sediment texture and reaction rate parameters. The reported grain size distribution data for the sediments used in this experiment is depicted in Figure 7.9 (see Table 1 of Liu et al. 2008). They did not report an actual size for which 100% of the particles were smaller, so a maximum grain size diameter of 30 mm was assumed based on photographic evidence (see Figure 1 of Liu et al. 2008). The reported porosity was 0.32. For this experiment, they report values for the dispersion coefficient and pore water velocity of 46.52 cm^2/hr and 3.52 cm/hr, respectively, which yields a dispersivity value of 13.2 cm.

We now return to the experimental observations of Porro et al. (1993) for the two field lysimeters described previously—one packed with uniform Berino loamy fine sand and the other packed with alternating layers of Berino loamy fine sand and Glendale silty clay loam. The grain size distribution data for these sediments are shown in Figure 7.10. The reported water contents for the Berino and Glendale soils under the applied flux conditions were 0.18 and 0.44, respectively (Porro et al. 1993). The reported porosities for the Berino and Glendale sediments are 0.3658 and 0.4686, respectively (Hills et al. 1989; Rockhold et al. 1997). These water content and porosity values yield saturation values of 0.4921 and 0.939 for the Berino and Glendale soils. Porro et al. (1993) reported dispersivity values of 5.04 cm and 1.82 cm at the 5-m-depth for the Berino-packed lysimeter and for the lysimeter packed with alternating layers of the Berino and Glendale soils, respectively.

The calculated values of the d_{16}, d_{50}, and d_{84} particle size metrics for the Hanford sediment and for the Berino loamy fine sand, and the reported values of dispersion coefficients, water contents, and porosities for these materials, were used in conjunction with Eqs. (7.18), (7.19), and (7.20) to calculate values of the "b" parameter that would result in matches to the experimentally determined values of $\alpha_L(S)$. Units of length and time are [cm] and [s], respectively, and a value of $n = 2$ in Eq. (7.18) was assumed based on the results of Padilla et al. (1999) and others. A value of $D_m = 2.0 \times 10^{-5}$ cm/s was also assumed. The resulting "a" and "b" parameters were regressed against the d_{84}-d_{16} metrics to yield the following equation which can be used with Eq. (7.18) and Eq. (7.19) for estimating longitudinal dispersivity in variably-saturated porous media

$$a_L = \max[1, 53.192 - 23.529 \times (d_{84}\text{-}d_{16})] \tag{7.21}$$

$$b_L = \min[1.027, 0.8274 + 0.0884 \times (d_{84}\text{-}d_{16})] \tag{7.22}$$
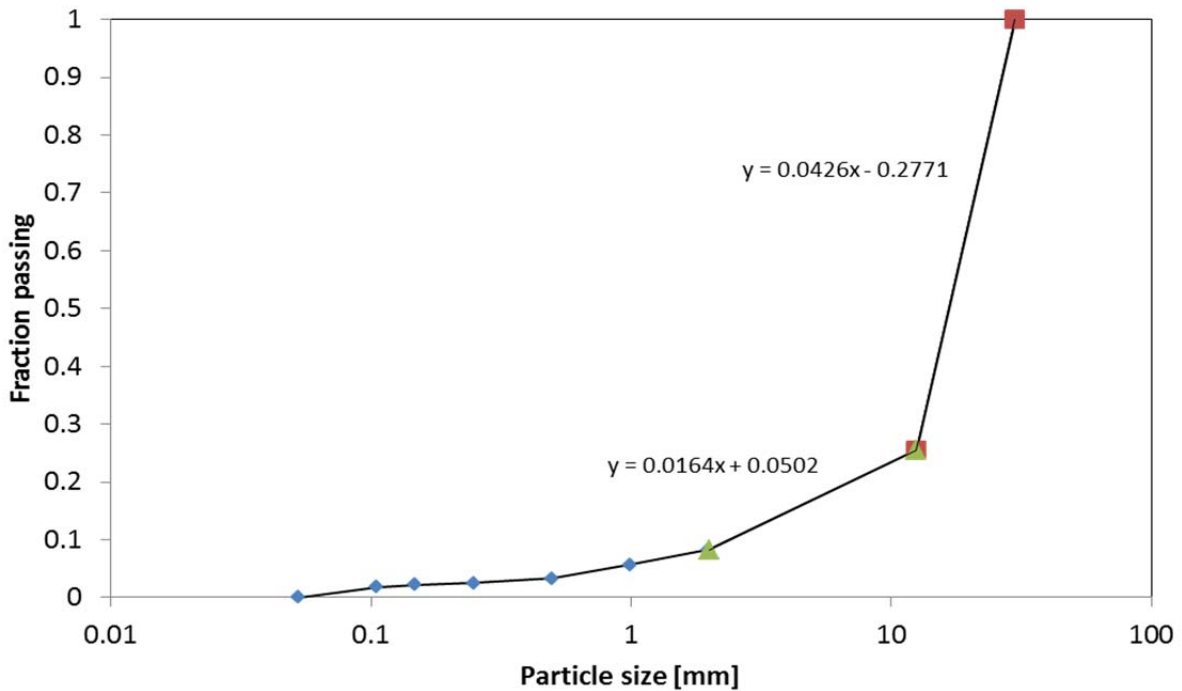
Figure 7.9. Grain Size Distribution Data for Field-textured Sediments from the Hanford 300 Area Used in a Large (0.8-m-long) Column Transport Experiment by Liu et al. (2008)
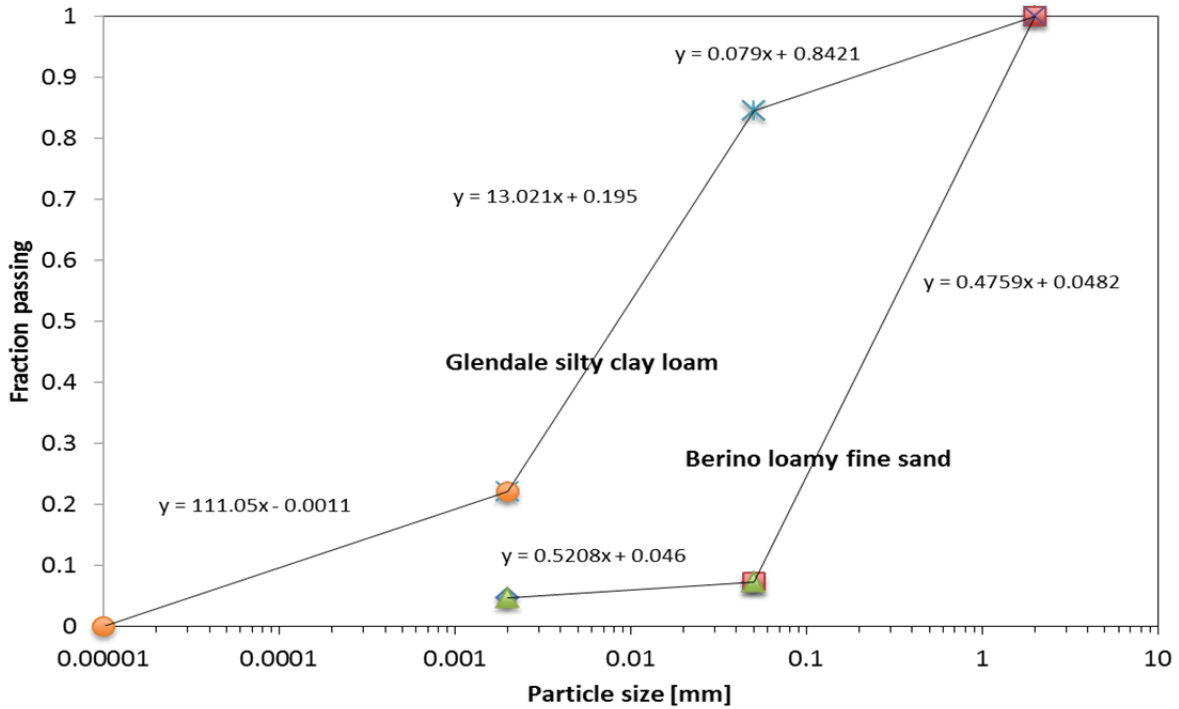
Figure 7.10. PSD Data Reported by Porro et al. (1993) for the Berino Loamy Fine Sand and Glendale Silty Clay Loam Used in Field Lysimeter Experiments

The d_{16}, d_{50}, and d_{84} grain size metrics for the Glendale clay loam were then used to estimate $\alpha_L(S) = 0.0658$ cm. The layered field lysimeter used by Porro et al. (1993) had equal-thickness, alternating layers of the Berino and Glendale soils, so the arithmetic mean value of $\alpha_L(S) = 2.55$ cm computed for these two soils was used as an estimate for the layered lysimeter. In comparison, Porro et al. (1993) reported a dispersivity value of 1.82 cm at the 5 m depth for the layered lysimeter. Dispersivity values were also estimated from the coarse sand data reported by Nützmann et al. (2002).

Experimentally determined dispersivities and dispersivities estimated from particle size distribution data are shown in Figure 7.11. The results based on the data of Nützmann et al. (2002) provide an independent test of the dispersivity estimation methodology. The results for the layered lysimeter experiment of Porro et al. (1993) suggest that reasonable estimates of block-effective (meter-scale) dispersivity values for variably saturated porous media may be obtained as the arithmetic mean of the values determined from grain size distribution metrics calculated for individual core samples. However, additional dispersion data for Hanford sediments are desirable to provide more confidence in these results.

PSD data for 34 core samples from the sandy sequence underlying the IDF site (Khaleel 2004) were used to estimate d_{50} and d_{84}-d_{16} size metrics. These values were then used to compute $\alpha_L(S)$ for different water saturation values using the described methodology. Figure 7.12 shows the calculated (arithmetic) average values of dispersivity as a function of saturation. The average porosity of core samples from the sandy sequence that were used in the calculation of TCT model parameters (described previously) was 0.384. Based on this porosity value, a saturation value of 0.25 corresponds to a volumetric water content of 0.096, which is a reasonable estimate of average water content of the sandy sediments underlying the

IDF site at depth. The computed dispersivity value for this water saturation is $\alpha_L(0.25) = 10.3$ cm. Note that Meyer et al. (2004) previously recommended a dispersivity value of 10 cm for near-field backfill materials surrounding the ILAW. This correspondence is purely coincidental.
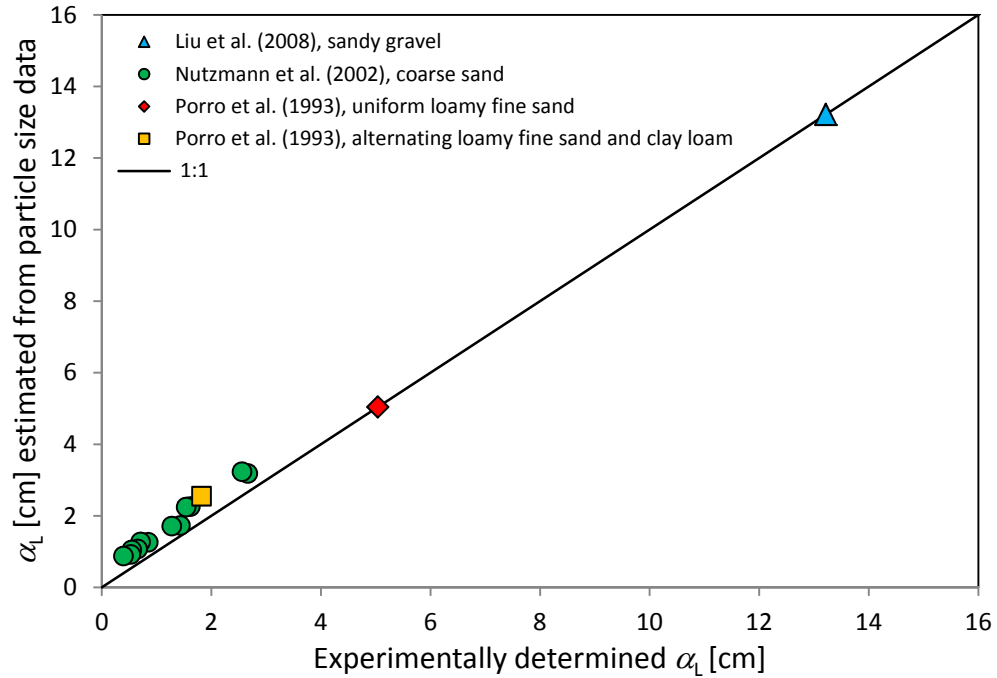
Figure 7.11. Experimentally Determined Dispersivity Values versus Dispersivity Values Calculated from Particle Size Distribution Metrics
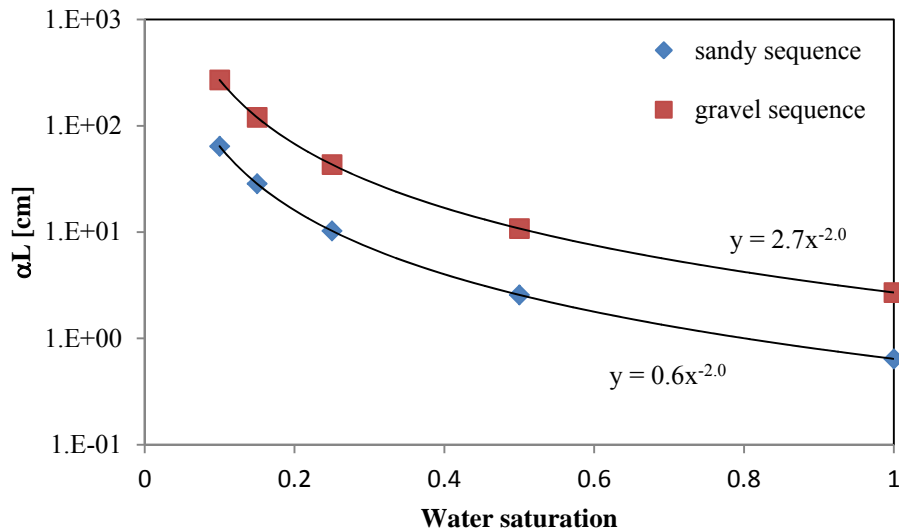
Figure 7.12. Computed Dispersivity Values as a Function of Saturation Based on Particle Size Distribution Metrics for the Sand and Gravel Sequences Underlying the IDF Site

Also shown in Figure 7.12 are the average calculated $\alpha_L(S)$ values determined from the PSD metrics for 10 gravel-dominated core samples from the 300 Area (Rockhold et al. 2013), whose hydraulic

properties were used together with data from fifteen 100 Area samples for estimating TCT model parameters for the gravel sequence under the IDF, described previously. PSD data for the 100 Area samples were not available so those data were not included in the dispersivity calculations. The computed average dispersivity value for these gravel-dominated sediments at a saturation of 0.25 is $\alpha_L(0.25) = 43.3$ cm.

Based on these calculations, we recommend that $\alpha_L(S)$ values of 10 cm and 43 cm be used for the sand- and gravel-dominated facies, respectively, underlying the IDF site. For transverse dispersivity in water-saturated systems, Gelhar and Axness (1983, p 169-170) state that for some special cases (e.g., flow parallel to strata) transverse (macro) dispersivities will be several orders of magnitude lower than longitudinal dispersivities, but when the stratification is at an angle to the mean flow, transverse dispersivities may be from 1 to 10% of the longitudinal dispersivity. In the absence of experimental data on transverse dispersion in variably saturated porous media, we tentatively recommend that $\alpha_T(S) = 0.1 \cdot \alpha_L(S)$, which is the same recommendation made by Khaleel (2004). These recommendations are subject to the following caveats.

It should be recognized that the dispersivity values estimated here from particle size distribution metrics are local values applicable to the model grid block (meter+) scale. Given the experimental observations and calculations based on vadose zone field studies cited at the beginning of this section, and numerical issues related to grid block sizes and numerical dispersion, we suggest that use of local block-effective dispersivity values should provide more conservative transport estimates for large-scale vadose zone modeling than using very large macro-dispersivities estimated from stochastic theory that was originally developed for saturated aquifer systems. Again the key difference here is that flow and transport through the vadose zone is generally normal (perpendicular) to stratification as opposed to parallel to stratification in saturated aquifer systems. This difference can lead to dramatically different results, as discussed earlier.

It may also be of interest to note that Gelhar and Axness (1983, Table 1) report "asymptotic constraints" that are applicable to their results for three-dimensional general orientations in anisotropic systems (see Item Number 4 in their Table 1) of α_L/λ_1, $\alpha_T/\lambda_1 \ll 1$, where λ_1 is the correlation scale (assumed here to be for the vertical direction when applied to the vadose zone) and α_L and α_T are the local dispersivities. The computed local values of $\alpha_L(S)$ of 10 cm and 43 cm for the sand- and gravel-dominated facies, respectively, are very close to or greater than the vertical correlation length of 30 cm that was estimated for these sediments by Khaleel (2004). This suggests that the equation for longitudinal macro-dispersivity suggested by Khaleel (2004) for application to the vadose zone at the IDF site may not be valid since in the development of this equation (Gelhar and Axness, 1983) local dispersivities were assumed to be small (negligible). It appears that local dispersivities for the IDF site may not be negligible and thus the constraints used in the development of the asymptotic results may not be satisfied. This issue may not have been given previous consideration because there were no methods available for independently estimating local dispersion coefficients.

The saturation-dependence of dispersivity illustrated here and elsewhere (Padilla et al. 1999; Nützmann et al. 2002) suggests that dispersivity should actually be calculated dynamically by numerical simulators rather than using constant values, which are strictly applicable only if the porous medium is fully water-saturated. If the saturation state is constant in time (steady-state flow conditions) then the use of constant, but saturation-dependent, values of dispersivity may be warranted. This is an assumption we

have used here as a basis for the recommendations above, but it should be recognized that this assumption will not be valid for all modeling scenarios of interest (e.g., a water-line leak scenario). Although saturation-dependent dispersivities are not currently implemented in the STOMP simulator, the power-function-type relationships shown in Figure 7.12 would be very easy to implement in STOMP and is recommended.

Although the methodology described here for estimating local, block-effective dispersivities has clear and compelling experimental support, data for estimating dispersivities over large transport distances in variably saturated porous media are sorely lacking. We therefore recommend the following activities:

- The saturation-dependence of dispersivity suggests that it should be computed dynamically by flow and transport simulators, instead of being assumed constant for each type of porous media. Implementation of generalized forms of the saturation-dependent dispersivity estimation equations described herein to use as an option in the STOMP simulator (White and Oostrom 2006) would be straightforward and is recommended.

- Perform a limited number of carefully controlled tracer transport experiments in large columns under both saturated and variably saturated conditions using Hanford sediments with different grain size distributions to provide additional data for testing and/or refining the proposed dispersivity-estimation methodology. The experimental equipment and expertise are available through PNNL's Subsurface Flow and Transport Experimental Laboratory, located within the Environmental Molecular Sciences Laboratory.

- Design and perform a limited number of numerical experiments to evaluate the development of macro-dispersion in variably-saturated porous media on the scale of the vadose zone underlying the IDF site. This work would involve the use of existing particle size distribution and borehole geophysical logging data with geostatistical stochastic simulation methods for estimating local-scale flow and transport parameters.

- Ultimately, additional large-scale field experimental studies of flow and transport in the Hanford vadose zone, spanning length scales of 10's of meters are needed, together with detailed characterization data for estimating physical and hydraulic parameters. This reiterates the same suggestion made 20 years ago by Gelhar et al. (1994).

The physical, hydraulic, and transport properties and parameters recommended herein are considered to be directly applicable for IDF PA calculations. Other suggested data collection and analysis work may be considered for future PA maintenance activities.

8.0   Issues and Uncertainties

A unique feature of the Hanford Site is the very thick (~100 m) sequence of heterogeneous, unsaturated, flood-deposited sediments overlying the unconfined aquifer. Characterization of such a thick sequence of mostly coarse sediments is very challenging. In 1998 the U.S. General Accounting Office (USGAO) conducted an audit of vadose zone activities at the Hanford Site and determined that DOE was not adequately performing its mission of protecting human health and the environment (USGAO 1998). They emphasized the need for characterization of the vadose zone as an essential step toward understanding groundwater contamination and providing more confidence in DOE's ability to handle contamination issues at the site (Murray et al. 2007). Since that time a number of different projects have been supported by the DOE Office of Science, Office of Environmental Management, and Richland Operations Office to better characterize and understand the possible influence of heterogeneities and features such as clastic dikes on flow and transport in the vadose zone. Although several field characterization and experimental studies have been performed, these efforts have typically involved relatively shallow investigations, covering a vertical extent of <20 m. Consequently, much is still unknown regarding the characteristics of the deep unsaturated zone underlying the Hanford Site and its influence on contaminant transport behavior over the very large spatial scales that are involved.

A number of boreholes and wells were drilled in and around the IDF site to obtain characterization data and to provide access for groundwater monitoring. Detailed measurements of physical and hydraulic properties were performed on a total of 44 core samples collected from IDF boreholes for the sand-dominated facies of the Hanford formation, and 8 core samples of clastic dike materials collected from elsewhere, both on and off the Hanford Site. No core data were collected or characterized from the IDF site for the gravel-dominated facies underlying the sand-dominated sequence of the Hanford formation. The relatively small number of core samples that were collected and analyzed for physical and hydraulic properties reflects the belief that the engineered portion of the IDF system will perform very well in limiting the release of contaminants, such that transport in the far-field environments is of less importance. Some potential issues and uncertainties are now discussed, following Meyer et al. (2004).

8.1   Changes in Parameter Values Over Time

A number of the near-field materials may undergo significant changes over time, potentially affecting the performance of the IDF. These changes will be caused by natural processes and in response to chemical changes in the near-field environment resulting from degradation of the waste forms. The materials for which hydraulic property changes over time are expected to most significantly impact the transport of contaminants are the surface cover materials, the steel and concrete overpacks, and the waste forms themselves. In addition, changes in backfill material are potentially important.

Changes in recharge through the surface cover either as a result of subsidence or in response to expansion of the waste containers due to steel corrosion are not discussed here. While these processes will not produce changes in the small-scale hydraulic properties of the surface cover materials (with the exception of the low-permeability asphaltic concrete layer), they may significantly affect the overall performance of the cover. Potential variations in the recharge rate over time are discussed in the recharge data package (Fayer and Szecsody 2004).

Steel will corrode over time and concrete will gradually degrade. Meyer and Serne (1999) provided unsaturated hydraulic parameter values for fully corroded steel and completely degraded concrete. They recommended sensitivity simulations to examine the impact of the change in these material properties on the performance of the facility. With the potential addition of significant amounts of steel in the form of the WTP melter overpacks, the issue of volume expansion during steel corrosion should be revisited.

Of the expected waste forms in the IDF, the ILAW glass has been the most extensively studied to develop models of its corrosion over time and consequent release of contaminants. In laboratory experiments the glass matrix has been shown to exhibit a propensity for dissolution and secondary mineral precipitation (McGrail et al. 2000). The resulting aqueous environment in the trench is marked by significant excursions in many of the physico-chemical parameters that influence its geochemistry, such as pH, ionic strength, and solution composition. In controlled laboratory experiments, McGrail et al. (2000) established that the concentrations of Si, Na, K, and Al register such dramatic excursions and obtained evidence of significant precipitation of secondary mineral phases. Precipitation of such minerals can cause a significant reduction in porosity and permeability by plugging pore throats of porous materials. Changes in these two basic properties of the medium also result in significant changes in the related properties (i.e., relative permeability, fluid-fluid and fluid-solid interfacial areas, and pore and particle size distributions) and the constitutive relationships among these properties (Saripalli et al. 2001). This fact, coupled with the very long time frames of interest (thousands of years) during which temporal changes in the near-field hydrology and geochemistry are to be expected, suggests that such changes may impact IDF performance.

Experiments and modeling research have been conducted to quantitatively characterize the hydraulic properties of representative ILAW glass media and the effect of physico-chemical reactions (especially secondary mineral precipitation) on these properties. In this context, it should be noted that the ILAW glass is expected to progressively fracture due to the combined effects of mechanical fracturing and glass corrosion reactions. Such disintegration is likely to reduce the initial glass monolith into increasingly fractured, rubblized, and granular material, over many (hundreds of) years. As such, the experimental and modeling investigations were designed to evaluate the effect of chemical reactions on the hydraulic properties of single-fracture, rubblized, and granular ILAW glass media. Results from these experiments and modeling indicated that the hydrologic properties of ILAW and the surrounding backfill can change significantly due to glass corrosion reactions (Freedman et al. 2003, 2004).

Mechanically fractured glass blocks, prepared as discussed in Section 4.4.1, were subjected to accelerated corrosion using a modified vapor hydration test (VHT) procedure.[1] A reduction in porosity ranging from 33% to 51% was measured in three blocks (one of HAN-28 glass and two of LAWBP1 glass) due to a reaction precipitate deposited as a layered film on the glass surfaces. Measured saturated hydraulic conductivity also decreased in general as a result of the VHT reaction. The observed decrease ranged from none to almost an order of magnitude. In general, the effect of the reaction on the saturated hydraulic conductivity was more significant for the HAN-28 glass (the more reactive glass).

A critical component of reactive transport modeling to determine the suitability of disposing of ILAW glass is the identification of key mineral assemblages affecting the porosity and permeability of both the

---

[1] Saripalli KP, MJ Lindberg, JV Crum, MJ Schweiger, and PD Meyer. 2002. *Effect of Chemical Reactions on the Hydraulic Properties of ILAW Near-field Materials: Experimental Investigation*. Letter Report to CH2MHill Hanford Group, Inc., September 30, 2002, Pacific Northwest National Laboratory, Richland, Washington.

glass and near- and far-field materials. In Freedman et al. (2003), two different classes of geochemical models were used to identify mineral precipitation and dissolution potentials for the disposal of ILAW. The first was a static geochemical model that did not consider the effects of transport. The second model was dynamic, and combined geochemical reactions with hydrogeological processes such as advection, diffusion, and dispersion. This reactive transport model also included an innovative application of a depositional film model for determining changes in permeability due to mineral precipitation and dissolution reactions. Although both models described solid-aqueous phase reactions kinetically, the two models identified two different sets of mineral assemblages affecting the porosity and permeability of the media. These markedly different results were due to transport considerations, the most significant of which were the spatial variability in aqueous concentrations, and advection and diffusion of dissolved glass constituents into the backfill materials. This work showed that, for the prediction of geochemical behavior of engineered system, such as the IDF, the traditional reaction path modeling approach using static (batch) models alone was not sufficient for an accurate assessment of the precipitation of key mineral assemblages and their effect on the geochemical and hydraulic behavior of the geomedia. Reactive transport modeling improved this assessment significantly. The static model was useful in identifying potential minerals to be included in the reactive transport simulations. The dynamic model, however, ultimately determined the key mineral assemblages affecting both the geochemical behavior and the hydraulic properties of the geomedia in the presence of a flowing aqueous phase.

In Freedman et al. (2004), a film depositional modeling approach was developed for modeling changes in permeability due to mineral precipitation and dissolution reactions in unsaturated porous media. This model is appropriate for describing ILAW glass dissolution and secondary mineral precipitation in the IDF. The model is based on the assumption that the mineral precipitate is deposited on the pore walls as a continuous film, which may cause a reduction in permeability. Previous work in saturated media has used continuous pore-size distributions to represent the pore space. In Freedman et al. (2004), the film depositional model was developed for a discrete pore-size distribution, which was determined using the unsaturated hydraulic properties of the porous medium. This facilitated the process of dynamically updating the unsaturated hydraulic parameters used to describe fluid flow through the media. Single mineral test simulations were conducted to test both the Mualem (1976) and Childs and Collis-George (1950) permeability models. Results from simulation of the simultaneous dissolution of ILAW glass and secondary mineral precipitation showed that the film depositional models yielded physically reasonable predictions of permeability changes due to solid-aqueous phase reactions. The film depositional model may need to be implemented or tested in eSTOMP (the parallel counterpart of the STOMP simulator), which is intended for use in future ILAW PA modeling efforts.

8.2 Uncertainty Assessment

Meyer and Serne (1999) discussed uncertainty in parameter values and provided recommendations for upper and lower bounds on hydraulic parameters for a number of near-field materials. These bounding values were not used in the 2001 ILAW PA (Mann et al. 2001), however, and are therefore not updated here. The approach to uncertainty assessment that was taken in the previous ILAW PAs has been to identify a small number of sensitivity cases for which simulations are conducted to identify the impact of individual parameters or processes on the facility performance. The assessment of uncertainty in complex modeling is an active area of research. An example of such an assessment for a waste disposal application comparable to the IDF is the uncertainty assessment conducted for the Waste Isolation Pilot Plant (Helton et al. 2000 and related papers). Even if the sensitivity of model results to parameter values

is the only interest, there are a number of systematic methods that can be used to explore model sensitivities in a comprehensive manner (Saltelli et al. 2000, 2004). Some of these methods are designed for application to complex models that require significant computational time for a single run, such as the IDF PA models. Campolongo et al. (2000) provide a summary of such screening methods. The availability of eSTOMP should facilitate the application of more rigorous sensitivity and uncertainty analysis, if necessary, because more simulations can be run in a shorter period of time than was previously possible using STOMP.

9.0 Summary

This report provides a summary and update of information associated with three data packages that have been used in earlier performance assessments of the Hanford IDF site: 1) the site conceptual model data package by Reidel (2005), 2) the near-field physical and hydraulic properties data package by Meyer et al. (2004), and 3) the far-field physical and hydraulic property data package by Khaleel (2004). The information provided herein is considered to be complete for use in IDF PA calculations. Any recommendations for development or use of new data are applicable only to PA maintenance activities.

The conceptual model of the site remains largely unchanged from Reidel (2005). Additional information from more recent studies on clastic dikes is provided to update the knowledge base. Recent work at other Hanford locations suggests that grain size distribution and spectral gamma log data, which are available for the IDF site, may be used to generate more detailed and realistic models of subsurface heterogeneity (Freedman et al. 2014). However, the use of such data for development of alternative conceptual models of the subsurface would be considered a PA maintenance activity.

Previous estimates of near-field physical and hydraulic parameters by Meyer et al. (2004) are unchanged and recommended as best-estimate values for current IDF PA modeling. One possible exception is that the glass waste forms being evaluated currently are different formulations than the glasses that were used in previous analyses. Testing of these new glasses is ongoing. When these new data sets become available, some of the analyses described herein and in Meyer et al. (2004) should possibly be repeated to generate updated parameter estimates for the new glasses, again as a PA maintenance activity.

The recommended approaches for estimating far-field material properties and parameters differ from those used previously by Khaleel (2004). We recommend that the Polmann (1990) model of anisotropy for unsaturated hydraulic conductivity, which was used previously, be replaced with a more recent TCT model, described by Zhang et al. (2003b). Recommended TCT model parameters for the sand- and gravel-dominated facies underlying the IDF site are presented in Section 6. Previous estimates of dispersivities for unsaturated far-field materials were based on an equation developed from stochastic transport theory for aquifer systems. A review of relevant literature for field studies in unsaturated porous media suggests that this approach may overestimate dispersivities. An alternative method and associated parameter estimates that are recommended for IDF site modeling are presented in Section 7.

10.0 References

Ababou R. 1996. "Random Porous Media Flow on Large 3D Grids: Numerics, Performance, and Application to Homogenization." In *Environmental Studies Mathematical, Computational, and Statistical Analysis,* ed. MF Wheeler. Springer-Verlag, New York.

Arya LM and JF Paris. 1981. "A Physicoempirical Model to Predict the Soil Moisture Characteristic from Particle-Size Distribution and Bulk Density Data." *Soil Sci. Soc. Am. J.* 45:1023-1030.

Arya LM, FJ Leij, and MT van Genuchten. 1999a. "Scaling Parameter to Predict the Soil Water Characteristic from Particle-Size Distribution Data." *Soil Sci. Soc. Am. J.* 63(3):510-519.

Arya LM, FJ Leij, and PJ Shouse. 1999b. "Relationship between the Hydraulic Conductivity Function and the Particle-Size Distribution." *Soil Sci. Soc. Am. J.* 63(5):1063-1070.

ASTM D6527-00. *Standard Test Method for Determining Unsaturated and Saturated Hydraulic Conductivity in Porous Media by Steady-State Centrifugation*. American Society for Testing and Materials, Philadelphia, Pennsylvania.

Bear J. 1972. *Dynamics of Fluids in Porous Media,* Dover, New York.

Bouwer H and RC Rice. 1983. "Effect of stones on hydraulic properties of vadose zones." In *Proceedings of the characterization and monitoring of the vadose (unsaturated) zone*. National Water Well Association, Worthington, Ohio.

Brooks RH and AT Corey. 1964. "Hydraulic Properties of Porous Media." Hydrol. Pap. 3, Colo. State Univ., Fort Collins.

Brooks RH and AT Corey. 1966. "Hydraulic Properties of Porous Media Affecting Fluid Flow." *Proc. ASCE J. Irrig. Drain. Div.* 92:61-68.

Buchwald A. 2000. "Determination of the ion diffusion coefficient in moisture and salt loaded masonry materials by impedance spectroscopy." In *3rd Int. PhD Symposium*, Oct. 11-13, 2000, Vienna, 2:475-482.

Burbank DA. 2002. *Preliminary Closure Plan for the Immobilized Low-Activity Waste Disposal Facility Project*. RPP-69111, Rev. 1, CH2MHILL Hanford Group, Inc., Richland, Washington.

Burdine NT. 1953. "Relative Permeability Calculation from Size Distribution Data." *Trans. AIME* 198:71-78.

Butters GL and WA Jury. 1989. "Field Scale Transport of Bromide in an Unsaturated Soil. 2. Dispersion Modeling." *Water Resources Research* 25(7):1583-1589.

Campbell GS. 1985. "Soil Physics with BASIC." In *Developments in Soil Science 14*, Elsevier Science Publishers B.V., New York, New York.

Campolongo F, J Kleinen, and T Andres. 2000. "Screening Methods." In *Sensitivity Analysis*, A Saltelli, K Chan, and EM Scott (eds.), John Wiley & Sons, Ltd., West Sussex, England.

Cedergren HR. 1989. *Seepage, Drainage, and Flow Nets*, Third Edition. John Wiley and Sons, Inc., New York, New York.

CHG. 2003a. *Integrated Mission Accelerated Plan*. RPP-13678, CH2M HILL Hanford Group, Inc., Richland, Washington.

CHG. 2003b. *Integrated Disposal Facility (IDF) Phase I Critical Systems Design Report*. RPP-18486, CH2M HILL Hanford Group, Inc., Richland, Washington.

CHG. 2003c. *Integrated Disposal Facility (IDF) Detailed Design: Specifications (DOE/CHG Review Draft, December 2003)*. RPP-18489, CH2M HILL Hanford Group, Inc., Richland, Washington.

Childs EC and N Collis-George. 1950. "The permeability of porous materials." *Proc. Roy. Soc. London A* 201:392-405.

Coats KH and BD Smith. 1964. "Dead-end pore volume and dispersion in porous media." Soc. Pet. Eng. J. 4:73-84.

Conca JL and JV Wright. 1990. "Diffusion coefficients in gravel under unsaturated conditions." *Water Resources Research* 26(5):1055-1066.

Conca JL and JV Wright. 1991. "Aqueous diffusion coefficients in unsaturated materials." *Mat. Res. Soc. Symp. Proc.* 212:879-884.

Dagan G. 1984. "Solute Transport in Heterogeneous Porous Formations." *J. Fluid Mech*. 145:151-177.

Dane JH and JW Hopmans. 2002. "Pressure Cell." In *Methods of Soil Analysis: Part 4 - Physical Methods*, JH Dane and GC Topp (eds.). Soil Science Society of America, Madison, Wisconsin.

Dane JH and GC Topp (eds.). 2002. *Methods of Soil Analysis: Part 4 - Physical Methods*. Soil Science Society of America, Madison, Wisconsin.

Delgado JMPQ. 2006. "A Critical Review of Dispersion in Packed Beds." Heat Mass Transfer 42:279-310, doi 10.1007/s00231-005-0019-0.

De Smedt F and PJ Wierenga. 1984. "Solute Transfer through Columns of Glass Beads." *Water Resources Research* 20:225-232.

DOE. 1993a. *Focused Feasibility Study of Engineered Barriers for Waste Management Units in the 200 Areas*. DOE/RL-93-33, Rev. 1, U.S. Department of Energy, Richland Operations Office, Richland, Washington.

DOE. 1993b. *Hanford Site Solid Waste Landfill Permit Application*. DOE/RL-90-38, Rev. 1, U.S. Department of Energy, Richland, Washington

DOE. 2004. *Final Hanford Site Solid (Radioactive and Hazardous) Waste Program Environmental Impact Statement Richland, Washington*. DOE/EIS-0286F, U.S. Department of Energy, Richland Operations Office, Richland, Washington.

Durner W, B Schultze, and T Zurnul. 1999. State-of-Art in Inverse Modeling of Inflow/Outflow Experiments. In MT van Genuchten.and.FJ Leij *Proceedings of Intl. Workshop, Characterization and Measurements of the Hydraulic Properties of Unsaturated Porous Media,* Univ. of California Riverside, Riverside, CA.

Ecology. 1987. *Solid Waste Landfill Design Manual, No. 87-13*. Parametrix, Inc., Bellevue, WA, for Washington State Department of Ecology, Olympia, Washington.

Ellsworth TR and WA Jury. 1991. "A Three Dimensional Field Study of Solute Transport Through Unsaturated, Layered Porous Media. 2. Characterization of Vertical Dispersion." *Water Resources Research* 27(5):967-981.

EPA. 1989. *Technical Guidance Document: Final Covers on Hazardous Waste Landfills and Surface Impoundment*. EPA 530-SW-89-047, U.S. Environmental Protection Agency, Washington, D.C.

Fayer MJ and CS Simmons. 1995. "Modified soil water retention functions for all matric suctions." *Water Resources Research* 31(5)1233-1238.

Fayer MJ and TB Walters. 1995. *Estimated Recharge Rates at the Hanford Site*. PNL-10285, Pacific Northwest Laboratory, Richland, Washington.

Fayer MJ, EM Murphy, JL Downs, FO Khan, CW Lindenmeier, and BN Bjornstad. 1999. *Recharge Data Package for the Immobilized Low-Activity Waste 2001 Performance Assessment*. PNNL-13033, Pacific Northwest National Laboratory, Richland, Washington.

Fayer MJ and JE Szecsody. 2004. *Recharge Data Package for the Integrated Disposal Facility 2005 Performance Assessment*. PNNL-14744, Pacific Northwest National Laboratory, Richland, Washington.

Fecht KR, KA Lindsey, BN Bjornstad, DG Orton, GV Last, and SP Reidel. 1998. *Clastic Injection Dikes of the Pasco Basin and Vicinity*. BHI-01103, Draft A. Bechtel Hanford, Richland, WA.

Flint AL and LE Flint. 2002a. "Particle Density." In *Methods of Soil Analysis: Part 4 - Physical Methods*, JH Dane and GC Topp (eds.). Soil Science Society of America, Madison, Wisconsin.

Flint AL and LE Flint. 2002b. "Porosity." In *Methods of Soil Analysis: Part 4 - Physical Methods*, JH Dane and GC Topp (eds.). Soil Science Society of America, Madison, Wisconsin.

Flury M and TF Gimmi. 2002. "Solute Diffusion." In *Methods of Soil Analysis: Part 4 - Physical Methods*, JH Dane and GC Topp (eds.). Soil Science Society of America, Madison, Wisconsin.

Folk RL. 1980. *Petrology of Sedimentary Rocks*. Hemphill Publishing Co., Austin, Texas.

Freedman VL, KP Saripalli, and PD Meyer. 2003. "Influence of mineral precipitation and dissolution on hydrologic properties of porous media in static and dynamic systems." *Applied Geochemistry* 18:589-606.

Freedman VL, DH Bacon, KP Saripalli, and PD Meyer. 2004. "A film depositional model of permeability for mineral reactions in unsaturated media." *Vadose Zone Journal* (3):1414-1424.

Freedman VL, X Chen, S Finsterle, MD Freshley, I Gorton, LJ Gosink, EH Keating, CS Lansing, WAM Moeglein, CJ Murray, G SH Pau, E Porter, S Purohit, M Rockhold, KL Schuchardt, C Sivaramakrishnan, VV Vessilonov, and SR Waichler. 2014. "A high-performance workflow system for subsurface simulation." *Environmental Modeling and Software* 55:176-189.

Gardner WR. 1958. "Some Steady-State Solutions of the Unsaturated Moisture Flow Equation with Application to Evaporation from a Water Table." *Soil Science* 85:228-232.

Gee GW and D Or. 2002. "Particle Size Analysis." In *Methods of Soil Analysis: Part 4 - Physical Methods*, JH Dane and GC Topp (eds.). Soil Science Society of America, Madison, Wisconsin.

Gelhar LW. 1993. *Stochastic Subsurface Hydrology*. Prentice-Hall, Inc.

Gelhar LW and CL Axness. 1983. "Three-Dimensional Stochastic Analysis of Macrodispersion in Aquifers." *Water Resources Research* 19(1):161-180.

Gelhar LW, MA Celia, and D McLaughlin. 1994. *Modeling Field Scale Unsaturated Flow and Transport Processes*. NUREG/CR-5965, U.S. Nuclear Regulatory Commission, Washington, D.C.

Grathwohl P. 1998. *Diffusion in Natural Porous Media: Contaminant Transport, Sorption/Desorption and Dissolution Kinetics.* Kluwer Academic Publishers, Boston, Massachusetts.

Green TR, JE Constantz, and EJ Freeman. 1996. "Upscaled Soil-Water Retention Using Van Genuchten's Function," *J of Hydrologic Engineering*, 1(1):123-130.

Guedes de Carvalho JRF and JMPQ Delgado. 2000. "Lateral Dispersion in Liquid through Packed Beds at Pem < 1,400." *AIChE J*. 46(5):1089-1095.

Gunn DJ. 1968. "Mixing in Packed and Fluidized Beds." *Chem. Eng. J*. CE153-CE172.

Hajek BF. 1966. *Soil Survey Hanford Project in Benton County Washington*. BNWL-243, Pacific Northwest Laboratory, Richland, Washington.

Hall C and WD Hoff. 2002. *Water Transport in Brick, Stone, and Concrete.* Spon Press, New York, New York.

Han N-W, J Bhakta, and RG Carbonell. 1985. "Longitudinal and Lateral Dispersion in Packed Beds: Effect of Column Length and Particle Size Distribution." *AIChE J*. 32(2):277-288.

Harleman DRF and RR Rumer. 1963. "Longitudinal and Lateral Dispersion in an Isotropic Porous Medium." *Fluid Mech*. 16:385-394.

Harleman DRF, PF Mehlhorn, and RR Rumer. 1963. "Dispersion-Permeability Correlation in Porous Media." J. Hydraulics Division, Proc. Amer. Soc. Civil Eng., Vol. 89, No. HY2, 67-89.

Helton JC, DR Anderson, G Basabilvazo, H-N Jow, and MG Marietta. 2000. "Conceptual structure of the 1996 performance assessment for the Waste Isolation Pilot Plant." *Reliability Engineering and System Safety* 69:151-165.

Hendrayanto, K Kosugi, T Uchida, S Matsuda, and T Mizuyama. 1999. "Spatial Variability of Soil Hydraulic Properties in a Forested Hillslope." *Journal of Forest Research*, 4:107-114.

Hillel D. 1980. *Applications of Soil Physics.* Academic Press, San Diego, California, 385 pp.

Hills RG, DB Hudson, I Porro, and PJ Wierenga. 1989. "Modeling One-Dimensional Infiltration into Very Dry Soils. 2. Estimation of Soil Water Parameters and Model Predictions." *Water Resources Research* 25:1271-1282.

Hills RG and PJ Wierenga. 1994. INTRAVAL Phase II Model Testing at the Las Cruces Trench Site. NUREG/CR-6063, U.S. Nuclear Regulatory Commission, Washington, D.C.

Hoffmann-Riem, H, MT van Genuchten, and H Fluhler. 1999. A General Model of the Hydraulic Conductivity of Unsaturated Soils. In M.T. Van Genuchten, L.J. Leij and L. Wu, *Proceedings of Int. Workshop, Characterization And Measurements Of The Hydraulic Properties of Unsaturated Porous Media*, University of California Riverside, Riverside, CA.

Hoitink DJ, KW Burk, JV Ramsdell, Jr, and WJ Shaw. 2003. *Hanford Site Climatological Data Summary 2002 with Historical Data*. PNNL-14242, Pacific Northwest National Laboratory, Richland, Washington.

Hopmans JW, J Simunek, N Romano, and W Durner. 2002. "Inverse Methods." In *Methods of Soil Analysis: Part 4 - Physical Methods*, JH Dane and G. Topp (eds.). Soil Science Society of America, Madison, Wisconsin.

Johnson V, TE Jones, SP Reidel, and MI Wood. 1999. *Subsurface Physical Conditions Description of the S-SX Waste Management Area*. HNF-4936, Rev. 0, Lockheed Martin Hanford Corp., Richland, Washington.

Kemper WD. 1986. "Solute Diffusivity." In *Methods of Soil Analysis, Part 1, Physical and Mineralogical Methods*, A Klute (ed.), pp. 1007-1024. American Society of Agronomy, Madison, Wisconsin.

Kemper WD and JC van Schaik. 1966. "Diffusion of salts in clay-water systems." *Soil Sci. Soc. Amer. Proc.* 30:534-540.

Khaleel R, T-C Yeh, and Z Lu. 2002. "Upscaled flow and transport properties for heterogeneous unsaturated media." *Water Resources Research* 38. doi:10.1029/2000WR000072.

Khaleel R and JF Relyea. 2001. "Variability of Gardner's α for course-textured sediments." *Water Resources Research* 37(1):1567-1575.

Khaleel R, JF Relyea, and JL Conca. 1995. "Evaluation of van Genuchten-Mualem relationships to estimate unsaturated hydraulic conductivity at low water contents." *Water Resources Research* 31(11):2659-2668.

Khaleel R, TE Jones, AJ Knepp, FM Mann, DA Myers, PM Rogers, RJ Serne, and MI Wood. 2000. *Modeling Data Package for S-SX Field Investigation report (FIR)*. RPP-6296, Rev. 0, CH2M Hill Hanford Group, Inc. Richland, Washington.

Khaleel R. 2004. *Far-Field Hydrology Data Package for Integrated Disposal Facility Performance Assessment*. RPP-20621, Rev. 0, CH2MHill Hanford Group, Richland, Washington.

Klute A. 1986. "Water Retention: Laboratory Methods." In *Methods of Soil Analysis: Part 1 - Physical and Mineralogical Methods*, A Klute (ed.), pp. 635-660. American Society of Agronomy, Madison, Wisconsin.

Krupka KP, DI Kaplan, and RJ Serne. 2004. *Geochemical Data Package for the 2005 Integrated Disposal Facility Performance Assessment*. PNNL-13037, Rev. 2, Pacific Northwest National Laboratory, Richland, Washington.

Last GV, EJ Freeman, KJ Cantrell, MJ Fayer, GW Gee, WE Nichols, BN Bjornstad, and DG Horton. 2006. *Vadose Zone Hydrology Data Package for Hanford Assessments*. PNNL-14702, Rev. 1, Pacific Northwest National Laboratory, Richland, Washington.

Last GV, CJ Murray, DA Bush, EC Sullivan, ML Rockhold, RD Mackley, and BN Bjornstad. 2007. "Standardization of Borehole Data to Support Vadose Zone Flow and Transport Modeling." *Vadose Zone Journal* 6:906-912.

Lenhard RJ and JC Parker. 1988. "Experimental validation of the theory of extending two-phase saturation-pressure relations to three-fluid phase systems for monotonic drainage paths." *Water Resources Research* 24(3):373-380.

Lenhard RJ and JC Parker. 1987. "A model for hysteretic constitutive relations governing multiphase flow, 2. Permeability-saturation relations." *Water Resources Research* 23(12):2197-2206.

Lenhard RJ, JC Parker, and S Mishra. 1989. "On the correspondence between Brooks-Corey and van Genuchten models." *ASCE J. Irrigation and Drainage Engineering* 115(4):744-751.

Liu C, JM Zachara, NP Qafoku, and Z Wang. 2008. "Scale-dependent Desorption of Uranium from Contaminated Subsurface Sediments." *Water Resources Research* 44, W08413, doi:10.1029/2007WR006478.

Luckner L, MT van Genuchten, and DR Nielsen. 1991. "Reply." *Water Resources Research* 27(4):663-664.

Mann FM and RJ Puigh. 2001. *Data Packages for the Hanford Immobilized Low-Activity Tank Waste Performance Assessment: 2001 Version*. HNF 5636, Rev. 2, prepared by Fluor Federal Services for Fluor Daniel Hanford Company, Richland, Washington.

Mann FM, KC Burgard, WR Root, RJ Puigh, SH Finfrock, R Khaleel, DH Bacon, EJ Freeman, BP McGrail, SK Wurstner, and PE LaMont. 2001. *Hanford Immobilized Low-Activity Waste Performance Assessment: 2001 Version*. DOE/ORP-2000-24, Rev. 0, Office of River Protection, Department of Energy, Richland, Washington.

Mann FM, RJ Puigh, SH Finfrock, R Khaleel, and MI Wood. 2003a. *Integrated Disposal Facility Risk Assessment*. RPP-15834, CH2M Hill Hanford Group, Inc., Richland, Washington.

Mann FM, BP McGrail, DH Bacon, RJ Serne, KM Krupka, RJ Puigh, R Khaleel, and S Finfrock. 2003b. *Risk Assessment Supporting the Decision on the Initial Selection of Supplemental ILAW Technologies*. RPP-17675, Rev. 0, CH2M Hill Hanford Group, Inc., Richland, Washington.

Mann FM. 2002. *Performance Objectives for the Hanford Immobilized Low-Activity Waste (ILAW) Performance Assessment*. RPP-13263, CH2M Hill Hanford Group, Inc., Richland, Washington.

Mann FM. 2003. *Annual Summary of the Integrated Disposal Facility Performance Assessment for 2003*. DOE/ORP-2000-19, Rev. 3, Office of River Protection, Department of Energy, Richland, Washington.

Mantoglou A and LW Gelhar. 1987a. "Capillary Tension Head Variance, Mean Soil Moisture Content, and Effective Specific Soil Moisture Capacity of Transient Unsaturated Flow in Stratified Soils." *Water Resources Research* 23(1):47-56.

Mantoglou A and LW Gelhar. 1987b. "Effective Hydraulic Conductivities of Transient Unsaturated Flow in Stratified Soils." *Water Resources Research*, 23(1):57-67.

Mantoglou A and LW Gelhar. 1987c. "Stochastic Modeling of Large-Scale Transient Unsaturated Flow Systems." *Water Resources Research* 23(1):37-46.

Maraqa MA, RB Wallace, and TC Voice. 1997. "Effects of Degree of Water Saturation on Dispersivity and Immobile Water in Sandy Soil Columns." *J. Contam. Hydrol.* 25:199-218.

Mayes MA, PM Jardine, TL Mehlhorn, BN Bjornstad, JL Ladd, and JM Zachara. 2003. "Transport of Multiple Tracers in Variably Saturated Humid Region Structured Soils and Semi-Arid Region Laminated Sediments." *Journal of Hydrology*, 275(3-4):141-161. 10.1016/s0022-1694(03)00039-8.

McCord JT, DB Stephens, and JL Wilson. 1991. "Hysteresis and State-Dependent Anisotropy in Modeling Unsaturated Hillslope Hydrologic Processes." *Water Resources Research* 27(7):1501-1518.

McGrail BP, DH Bacon, JP Icenhower, WL Ebert, PF Martin, HT Schaef, and EA Rodgriguez. 2000. *Waste Form Release Data Package for the 2001 Immobilized Low-Activity Waste Performance Assessment*. PNNL Report 13043, Rev. 1., Pacific Northwest National Laboratory, Richland, Washington.

Meyer PD and RJ Serne. 1999. *Near Field Hydrology Data Package for the Immobilized Low-Activity Waste 2001 Performance Assessment*. PNNL-13035, Rev. 1, Pacific Northwest National Laboratory, Richland, Washington.

Meyer PD, KP Saripalli, and VL Freedman. 2004. *Near-Field Hydrology Data Package for the Integrated Disposal Facility 2005 Performance Assessment.* PNNL-14700, Pacific Northwest National Laboratory, Richland, Washington.

Millington RJ. 1959. "Gas diffusion in porous media." *Science* 130:100-102.

Mualem Y. 1976. "A New Model for Predicting the Hydraulic Conductivity of Unsaturated Porous Media." *Water Resources Research* 12:513-522.

Murray CJ, AL Ward, and JL Wilson. 2003. *Influence of Clastic Dikes on Vertical Migration of Contaminants in the Vadose Zone at Hanford.* PNNL-14224, Pacific Northwest National Laboratory, Richland, Washington.

Murray CJ, AL Ward, and JL Wilson. 2007. "Influence of Clastic Dikes on Vertical Migration of Contaminants at the Hanford Site." *Vadose Zone Journal* 6(4):959-970.

Neitzel DA (ed.). 1998 . *Hanford Site National Environmental Policy Act (NEPA) Characterization.* PNNL-6415, Rev. 10, Pacific Northwest National Laboratory, Richland, Washington.

Nimmo JR. 1991. "Comment on the treatment of residual water content in 'A consistent set of parametric models for the two-phase flow of immiscible fluids in the subsurface' by L. Luckner et al." *Water Resources Research* 27(4):661-662.

Nützmann G, S Maciejewski, and K Joswig. 2002. "Estimation of Water Saturation Dependence in Unsaturated Porous Media: Experiments and Modeling Analysis." *Adv. Water Resour.* 25:565-576.

Oostrom M, ML Rockhold, PD Thorne, GV Last, and MJ Truex. 2006. *Carbon Tetrachloride Flow and Transport in the Subsurface of the 216-Z-9 Trench at the Hanford Site: Heterogeneous Model Development and Soil Vapor Extraction Modeling.* PNNL-15914, Pacific Northwest National Laboratory, Richland, Washington.

Padilla IY, T–CJ Yeh, and MH Conklin. 1999. "The Effect of Water Content on Solute Transport in Unsaturated Porous Media." *Water Resources Research* 35(11):3303-3313.

Papendick RI and GS Campbell. 1980. "Theory and Measurement of Water Potential." In *Water Potential Relations in Soil Microbiology.* Am. Soc. of Agron. Spec. Publication No. 9, Soil Science Society of America, Madison, Wisconsin, pp. 1-22.

Parker JC and RJ Lenhard. 1987. "A model for hysteretic constitutive relations governing multiphase flow, 1. Saturation-pressure relations." *Water Resources Research* 23(12):2187-2196.

Pierce EM, BP McGrail, EA Rodriguez, HT Schaef, KP Saripalli, RJ Serne, KM Krupka, PF Martin, SR Baum, KN Geiszler, LR Reed, and WJ Shaw. 2004. *Waste Form Release Data Package for the 2005 Integrated Disposal Facility Performance Assessment.* PNNL-14805, Pacific Northwest National Laboratory, Richland, Washington.

Polmann DJ. 1990. "Application of Stochastic Methods to Transient Flow and Transport in Heterogeneous Unsaturated Soils." PhD, Massachusetts Institute of Technology, Cambridge, Massachusetts.

Porro I, PJ Wierenga, and RG Hills. 1993. "Solute Transport Through Uniform and Layered Soil Columns." *Water Resources Research* 29(4):1321-1330.

Porter LK, WD Kemper, RD Jackson, and BC Stewart. 1960. "Chloride diffusion in soils as influenced by moisture content." *Soil Sci. Soc. Am. Proc.* 24:460-463.

Puigh R. 2004. *Disposal Facility Data for the Hanford Integrated Disposal Facility Performance Assessment.* RPP-20691, CH2MHill Hanford Group, Inc., Richland, Washington.

Raats PAC, ZF Zhang, AL Ward, and GW Gee. 2004. "The Relative Connectivity–Tortuosity Tensor for Conduction of Water in Anisotropic Unsaturated Soils." *Vadose Zone Journal* 3:1471-1478.

Reidel SP, KD Reynolds, and DG Horton. 1998. *Immobilized Low-Activity Waste Site Borehole 299-E17-21.* PNNL-11957, Pacific Northwest National Laboratory, Richland, Washington.

Reidel SP. 2005. *Geologic Data Package for 2005 Integrated Disposal Facility Waste Performance Assessment*. PNNL-14586, Pacific Northwest National Laboratory, Richland, Washington.

Reidel SP and KR Fecht. 2005. *Geology of the Integrated Disposal Facility Trench*. PNNL-15237, Pacific Northwest National Laboratory, Richland, Washington.

Rockhold ML, CS Simmons, and MJ Fayer. 1997. "An Analytical Solution Technique for One-dimensional, Steady Vertical Water Flow in Layered Soils." *Water Resources Research* 33(4):897-902.

Rockhold ML, DH Bacon, VL Freedman, KR Parker, SW Waichler, and MD Williams. 2013. *System-Scale Model of Aquifer, Vadose Zone, and River Interactions for the Hanford 300 Area – Application to Uranium Reactive Transport*. PNNL-22886, RPT-DVZ-AFRI-019, Pacific Northwest National Laboratory, Richland, Washington.

Rockhold ML, DL Saunders, CE Strickland, SR Waichler, and RE Clayton. 2009a. *Soil Water Balance and Recharge Monitoring at the Hanford Site – FY09 Status Report.* PNNL-18807, Pacific Northwest National Laboratory, Richland, Washington.

Rockhold ML, GV Last, and LA Middleton. 2009b. *A Long-Term Strategic Plan for Hanford Sediment Physical and Hydraulic Property and Vadose Zone Hydraulic Parameter Databases*. PNNL-18836, Pacific Northwest National Laboratory, Richland, Washington.

Rockhold ML, LA Middleton, and GV Last. 2010. *Prototype Data Models and Data Dictionaries for Hanford Sediment Physical and Hydraulic Properties.* PNNL-19817, Pacific Northwest National Laboratory, Richland, Washington.

Rockhold ML, MJ Fayer, and GW Gee. 1988. *Characterization of Unsaturated Hydraulic Conductivity at the Hanford Site.* PNL-6488, Pacific Northwest Laboratory, Richland, Washington.

Rockhold ML, RE Rossi, and RG Hills. 1996. "Application of Similar Media Scaling and Conditional Simulation for Modeling Water Flow and Tracer Transport at the Las Cruces Trench Site." *Water Resources Research* 32(3):595-609.

Romano N, JW Hopmans, and JH Dane. 2002. "Suction Table." In *Methods of Soil Analysis: Part 4 - Physical Methods*, JH Dane and GC Topp (eds.). Soil Science Society of America, Madison, Wisconsin.

Rossi C and J R Nimmo. 1994. "Modeling of soil water retention from saturation to oven dryness." *Water Resources Research* 30(3):701-708.

Saltelli A, K Chan, and EM Scott (eds.). 2000. *Sensitivity Analysis*. John Wiley & Sons, Ltd., Chichester, England.

Saltelli A, S Tarantola, F Campolongo, and M Ratto. 2004. *Sensitivity Analysis in Practice: A Guide to Assessing Scientific Models.* John Wiley & Sons, Ltd., Chichester, England, 232 pp.

Saripalli KP, PD Meyer, DH Bacon, and VL Freedman. 2001. "Changes in Hydrologic Properties of Aquifer Media due to Chemical Reactions: A Review." *Critical Reviews in Environmental Science and Technology* 31(4):311-349.

Schaap MG, PJ Shouse, and PD Meyer. 2003. *Laboratory Measurements of the Unsaturated Hydraulic Properties at the Vadose Zone Transport Field Study Site.* PNNL-14284, Pacific Northwest National Laboratory, Richland, Washington.

Schaap MJ and FJ Leij. 2000. "Improved prediction of unsaturated hydraulic conductivity with the Mualem-van Genuchten model." *Soil Sci. Soc. Am. J.* 64:843-851.

Scheidegger AE. 1961. "General theory for dispersion in porous media." *J. Geophys. Res.* 66:3273-3278.

Schuh WM and RL Cline. 1990. "Effect of Soil Properties on Unsaturated Hydraulic Conductivity Pore-Interaction Factors." *Soil Science Society of America Journal*, 54:1509-1519.

Shinomiya Y, K Takahashi, M Kobiyama, and J Kubota. 2001. "Evaluation of the Tortuosity Parameter for Forest Soils to Predict Unsaturated Hydraulic Conductivity." *Journal of Forest Research*, 6:221-225.

Stephens DB and S Heermann. 1988. "Dependence of Anisotropy on Saturation in a Stratified Sand." *Water Resources Research* 24(5):770-778.

Ursino N and T Gimmi. 2004. "Combined Effect of Heterogeneity, Anisotropy and Saturation on Steady State Flow and Transport: Structure Recognition and Numerical Simulation." *Water Resources Research*, 40(1):n/a-n/a. doi:10.1029/2003wr002180.

Ursino N, T Gimmi, and H Fluhler. 2001. "Combined Effects of Heterogeneity, Anisotropy, and Saturation on Steady State Flow and Transport: A Laboratory Sand Tank Experiment." *Water Resources Research* 37(2):201-208.

U.S. General Accounting Office (USGAO). 1998. Nuclear Waste, Understanding of Waste Migration at Hanford is Inadequate for Key Decisions. GAO/RCED-98080, U.S. General Accounting Office, Washington, D.C.

van Genuchten MT. 1980. "A Closed-Form Equation for Predicting the Hydraulic Conductivity of Unsaturated Soils." *Soil Science Society of America Journal* 44:892-898.

van Genuchten MT and PJ Wierenga. 1976. "Mass Transfer Studies in Sorbing Porous Media. I. Analytical Solutions." *Soil Science Society of America Journal* 40:473-480.

Ward AL, ME Conrad, WD Daily, JB Fink, VL Freedman, GW Gee, GM Hoverston, MJ Keller, EL Majer, CJ Murray, MD White, SB Yabusaki, and ZF Zhang. 2006. *Vadose Zone Transport Study Summary Report*. PNNL-15443, Pacific Northwest National Laboratory, Richland, Washington.

Ward AL and ZF Zhang. 2007. "Effective Hydraulic Properties Determined from Transient Unsaturated Flow in Anisotropic Soils." *Vadose Zone Journal*, 6(4):913. 10.2136/vzj2006.0174.

WDOT. 1991. *Specification for Road, Bridge, and Municipal Construction*. Washington State Department of Transportation, Olympia, Washington.

White MD and M Oostrom. 2006. STOMP – Subsurface Transport over Multiple Phases, Version 4.0, User's Guide. PNNL-15782, Pacific Northwest National Laboratory, Richland, Washington.

White MD, M Oostrom, MD Williams, CR Cole, and MP Bergeron. 2001. *FY00 Initial Assessments for S-SX Field Investigation Report (FIR): Simulations of Contaminant Migration with Surface Barriers.* PNWD-3111, Battelle--Pacific Northwest Division, Richland, Washington.

Wierenga PJ and MT van Genuchten. 1989. "Solute Transport through Small and Large Soil Columns." *Ground Water* 27:35-42.

Wood MI, R Khaleel, PD Rittmann, AH Lu, SH Finfrock, RJ Serne, and KJ Cantrell. 1995. *Performance Assessment for the Disposal of Low-Level Waste in the 200 West Area Burial Grounds*. WHC-EP-0645, Westinghouse Hanford Company, Richland, Washington.

Wood MI, R Khaleel, PD Rittmann, SH Finfrock, TH DeLorenzo, and DY Garbrick. 1996. *Performance Assessment for the Disposal of Low-Level Waste in the 200 East Area Burial Grounds.* WHC-EP-0875, Westinghouse Hanford Company, Richland, Washington.

Wosten JHM and MT van Genuchten. 1988. "Using Texture and Other Soil Properties to Predict the Unsaturated Soil Hydraulic Functions." *Soil Science Society of America Journal*, 52:1762-1770.

Xu M and Y Eckstein. 1997. "Statistical Analysis of the Relationships Between Dispersivity and Other Physical Properties of Porous Media." *Hydrogeology Journal* 5(4):4-20.

Yates SR, MT van Genuchten, AW Warrick, and LJ Leij. 1992. "Analysis of Measured, Predicted, and Estimated Hydraulic Conductivity Using the Retc Computer Program." *Soil Science Society of America Journal*, 56:347-354.

Yeh T-CJ, LW Gelhar, and AL Gutjahr. 1985a. "Stochastic Analysis of Unsaturated Flow in Heterogeneous Media, 3. Observations and Applications." *Water Resources Research* 21:465-471.

Yeh T-CJ, LW Gelhar, and AL Gutjahr. 1985b. "Stochastic Analysis of Unsaturated Flow in Heterogeneous Soils, 1. Statistically Isotropic Media." *Water Resources Research* 21:447-456.

Yeh T-CJ, LW Gelhar, and AL Gutjahr. 1985c. "Stochastic Analysis of Unsaturated Flow in Heterogeneous Soils, 2. Statistically Anisotropic Media with Variable A." *Water Resources Research* 21:457-464.

Zaslavsky D and G Sinai. 1981. "Surface hydrology: IV. Flow in sloping layered soil." *J. Hydraul. Div.* Am. Soc. Civ. Eng., 107:1-93.

Zhang ZF and R Khaleel. 2007. *Comparison of Models of Saturation-Dependent Anisotropy in Unsaturated Hydraulic Conductivity.* PNNL-16886, Pacific Northwest National Laboratory, Richland, Washington.

Zhang, ZF and R Khaleel. 2010. "Simulating Field-Scale Moisture Flow Using a Combined Power-Averaging and Tensorial Connectivity-Tortuosity Approach," *Water Resources Research*, 46(9)10.1029/2009wr008595. Zhang ZF, AL Ward, and GW Gee. 2003. "A Tensorial Connectivity-Tortuosity Concept to Describe the Unsaturated Hydraulic Properties of Anisotropic Soils." *Vadose Zone Journal* 2:313-321.

Zhang ZF, CE Strickland, JG Field, and DL Parker. 2011. *T-TY Tank Farm Interim Surface Barrier Demonstration – Vadose Zone Monitoring FY10 Report*. PNNL-20144, Pacific Northwest National Laboratory, Richland, Washington.

Zhang ZF. 2014. "Relationship between Anisotropy in Soil Hydraulic Conductivity and Saturation." *Vadose Zone Journal.* 13(6):1-8. doi:10.2136/vzj2013.09.0172

Distribution*

<u>Washington River Protection Solutions</u>
DJ Swanberg
WRPS Documents – TOCVND@rl.gov

<u>Pacific Northwest National Laboratory</u>
PD Meyer
ML Rockhold
JN Thomle
JH Westsik, Jr.
ZF Zhang
Project File
Information Release (pdf)

*All distribution will be made electronically.